**Development and Product Characterization of Vaginal Progesterone Gel**

by

KaiKai Wang

A dissertation submitted in partial fulfillment
of the requirements for the degree of
Doctor of Philosophy
(Pharmaceutical Sciences)
in the University of Michigan
2026

Doctoral Committee:

Professor Anna S. Schwendeman, Chair
Assistant Professor Ashlee Brunaugh
Professor James Moon
Professor Ariella Shikanov

Kaikai Wang

wangkk@umich.edu

ORCID iD: 0009-0009-4266-5979

© Kaikai Wang 2026

## Dedication

To all mothers around the world, whose love and courage make the miracle of life possible.

**Acknowledgements**

I once heard a Buddhist saying: without others, there is no self. Over these past years, I have come to understand this deeply. I am like a river—countless people have continuously poured water into "me," allowing me to keep flowing toward the sea. Here, I must thank all those who have accompanied and helped me along the way. Without you, I would not be who I am today.

First, I would like to thank my advisor, Dr. Anna Schwendeman. Thank you for giving me research projects that were both challenging and meaningful, and for guiding me to explore the field of pharmaceutical sciences in depth. In you, I have seen an inspiring example of intelligence, capability, and dedication. I have often admired your creativity, passion, and energy in research. I know that in the future I will often think back on the lessons you taught me, both in science and in life. I would also like to thank my dissertation committee: Dr. James Moon, Dr. Ashlee Brunaugh, Dr. Ariella Shikanov. Your feedback, thoughtful suggestions, and insightful questions have greatly improved this thesis and broadened the way I think.

To my parents and family, thank you for supporting me in every way over so many years. As a Chinese son, I have never been good at speaking openly with my parents or expressing my love. Yet through the work and reflection that came with this thesis, I have come to understand more deeply how difficult and extraordinary it is to bring a life into the world and raise it. You are truly great. To my girlfriend, Vivian Du, thank you for always supporting and encouraging me, and for making my life brighter and more beautiful.

I would also like to thank everyone who helped and guided me in the lab: Dr. Adaeze Eneli, Dr. Jingyao Gan, Dr. Ji Li, Dr. Vivian Juang, Yiran Huo, Dr. Mei Lei, Ziyi Lu, Dr. Sergey Solomevich, Dr. Gregory Lautner, Xinyao Wang, Dr. Xingwu Zhou, Dr. Shuying Wang, Dr. Ziyun Xia, Dr. Weiqing Wang, Dr. Chen Wu, Dr. Minzhi Yu, Dr. Tao Zheng, Luke Morrissette, Dr. Yekaterina Fyodorova, May Phoo and Helen Ju. Your help was invaluable, and the many conversations we shared over the long course of research made life more interesting and enjoyable. I would especially like to thank our lab manager, Rose Ackermann, Karl Olsen

and Dr. Brian Shay. Together we set up and repaired many instruments and carried out many memorable experiments. Those experiences remain some of the most unforgettable parts of my PhD journey.

To my friends in China, thank you. Over these years I have missed many of your weddings and countless gatherings, and perhaps I will miss more in the future. But you have always remained dear friends whom I think of often and care about deeply. I am grateful that the internet has allowed our friendships to continue across time and distance, and that we can still bring joy to one another.

I would like to express my special gratitude to McDonald's on Plymouth Road. Over these years, it provided me with countless cheap and hot meals during long days of work. During the pandemic, when I had just arrived in the United States and did not yet have a car, the restaurant was closed for dine-in service and only offered drive-through or curbside pickup. I would order food and stand in the parking spot to pick it up. Now, I have a car, and I can either dine in or use the drive-through. In some small way, it feels like a reflection of how life has gradually become better.

Finally, I would like to thank myself. No matter what unpredictable changes in the future, I hope you will continue to face them with courage and perseverance, and live your life with confidence and grace.

## Table of Contents

Dedication ..... ii

Acknowledgements ..... iii

List of Tables ..... ix

List of Figures ..... xi

List of Appendices ..... xiv

Abstract ..... xv

Chapter 1 Introduction ..... 1

1.1 Current status and future direction of delivery of progesterone (P4) ..... 1

1.1.1 Physiology functions and clinical application of Progesterone (P4) ..... 1

1.1.2 Current status and limitations of P4 delivery ..... 3

1.1.3 Physiology of vagina and how it is related to drug delivery ..... 7

1.1.4 Tendency of next generation vaginal delivery system ..... 8

1.2 Challenges in developing complex generics ..... 10

1.2.1 Introduction to Doxil® and challenges in liposomal generic development ..... 12

1.2.2 Introduction to Crinone® and challenges for generic P4 vaginal gel ..... 14

1.3 Research scope and chapter overviews ..... 16

Chapter 2 Reverse Engineering of Crinone®: Progesterone Vaginal Gel ..... 18

2.1 Abstract ..... 18

2.2 Introduction ..... 19

2.3 Materials and Methods ..... 20

2.3.1 Materials ..... 20

2.3.2 Physical appearance and pH ..... 20
2.3.3 Globule size measurement ..... 21
2.3.4 Polarized light microscope (PLM) ..... 21
2.3.5 Scanning electron microscope (SEM) ..... 21
2.3.6 Solid X-ray diffraction (XRD) ..... 22
2.3.7 Differential Scanning Calorimetry (DSC) ..... 22
2.3.8 Texture analysis ..... 23
2.3.9 Rheology measurements ..... 24
2.3.10 In vitro release test (IVRT) ..... 25
2.3.11 Statistical analysis ..... 26
2.4 Results ..... 27
2.4.1 Appearance and pH measurement ..... 27
2.4.2 Globule size distribution ..... 27
2.4.3 Crystal particle morphology of Crinone® under polarized microscopy and SEM ..... 27
2.4.4 Solid X-ray diffraction (XRD) ..... 29
2.4.5 Differential Scanning Calorimetry (DSC) ..... 30
2.4.6 Texture analysis ..... 31
2.4.7 Rheological characterization ..... 33
2.4.8 In vitro release studies ..... 34
2.5 Discussion ..... 35
2.6 Conclusion ..... 38
Chapter 3 Development of P4-Cyclodextrin Complex Based Gel for Vaginal Delivery ..... 39
3.1 Abstract ..... 39
3.2 Introduction ..... 40
3.3 Materials and Methods ..... 41

3.3.1 Materials ..... 41
3.3.2 Preparation of simulated vaginal fluid (SVF) ..... 42
3.3.3 Solubility test of P4 in common buffer and surfactants solution ..... 42
3.3.4 Cyclodextrin screening by phase solubility study ..... 42
3.3.5 Cyclodextrin progesterone complex preparation ..... 43
3.3.6 Cyclodextrin progesterone complex characterization ..... 43
3.3.7 Preparation of P4-CD hydrogel formation ..... 44
3.3.8 Muco-adhesion test ..... 45
3.3.9 Syringeability test ..... 45
3.3.10 Steady shear viscosity ..... 45
3.3.11 Oscillation measurement ..... 46
3.3.12 In vitro release study ..... 46
3.3.13 In vitro permeation test ..... 47
3.3.14 Pharmacokinetic study ..... 48
3.3.15 Plasma sample pretreatment and LC/MS condition ..... 48
3.4 Results ..... 49
3.4.1 Solubility of P4 in common buffer and surfactants solution ..... 49
3.4.2 Phase solubility of different CDs ..... 50
3.4.3 Characterization for P4-CD complex ..... 52
3.4.4 P4-CD hydrogel characterization ..... 56
3.4.5 Pharmacokinetics of intravaginal single dose in healthy mice ..... 61
3.5 Discussion ..... 62
3.6 Conclusion ..... 67
Chapter 4 Reverse Engineering of Complex Liposomal Injections ..... 68
4.1 Abstract ..... 68

4.2 Introduction ..... 69
4.3 Materials and Methods ..... 72
4.4 Result ..... 78
4.5 Discussion ..... 87
Chapter 5 Conclusions and Future Directions ..... 91
Appendices ..... 94
Bibliography ..... 108

## List of Tables

Table 1-1 Current progesterone products in clinical use ..... 4

Table 2-1 Globule size distribution of Crinone® determined by Mastersizer. (n = 3, mean ± SD) ..... 27

Table 2-2 Mechanical properties of Crinone®. (n = 5, mean ± SD)..... 32

Table 2-3 Muco-adhesiveness and syringeability of Crinone®. (n = 5, mean ± SD)..... 33

Table 3-1 P4 solubility in different buffer/surfactant solution (n=3, mean ± SD) ..... 50

Table 3-2 Phase-solubility analysis and calculated CD:P4 ratios of different cyclodextrins ..... 51

Table 3-3 Comparison of mucoadhesion and syringeability between the P4–CD gel and Crinone®..... 57

Table 3-4 Comparison of steady-state flux ($J_{ss}$) and cumulative permeation at 8 h ($Q_{8h}$) of P4 across sheep vaginal tissue between Crinone® and P4-CD gel..... 61

Table 3-5 Pharmacokinetic parameter of Crinone and P4-CD gel group..... 62

Table 4-1. Sample Inventory..... 71

Table A-0-1 Composition of Crinone® vaginal gel and the functions of its excipients ..... 94

Table A-0-2 Appearance and pH value of three batches of Crinone®. (n = 3, mean ± SD)..... 95

Table A-0-3 The f2 values of in vitro release profiles comparing different batches of Crinone® 96

Table C-0-4 ICH Q2(R1) validation results for the doxorubicin quantitation method..... 100

Table C-0-5 ICH Q2(R1) validation results for the lipid quantitation method for HSPC. ..... 101

Table C-0-6 ICH Q2(R1) validation results for the lipid quantitation method for cholesterol. . 101

Table C-0-7 ICH Q2(R1) validation results for the lipid quantitation method for DSPE-PEG 2000..... 102

Table C-0-8 Size distribution, polydispersity index and zeta potential measurements of different liposomal doxorubicin formulations analyzed by DLS (n ≥ 3, mean ± SD)..... 103

Table C-0-9 Quantification of doxorubicin and lipid content within liposomal doxorubicin formulations by different manufacturers (mean ± SD; n = 3). ..... 104

Table C-0-10 Quantification of doxorubicin purity and identification of USP impurities within liposomal doxorubicin formulations by different manufacturers (mean ± SD; n = 3). ..... 105

Table C-0-11 Quantification of free doxorubicin present in liposomal doxorubicin formulations by different manufacturers (n > 2). ..... 106

## List of Figures

Figure 1-1 Schematic representation of a PEGylated liposomal doxorubicin..... 13

Figure 1-2 Crinone 8% Package and prefilled applicator..... 16

Figure 1-3 Diagram of Crinone® progesterone gel..... 16

Figure 2-1 Microscopic images of three batches of Crinone® under bright field (upper panel) and polarized light (lower panel). The scale bar represents 20 μm. ..... 28

Figure 2-2 SEM images of three batches of Crinone®. The scale bar in the upper panel represents 50 μm and lower panel represents 20 μm. ..... 29

Figure 2-3 X-rays diffraction patterns of progesterone (API) and three different batches of Crinone®. The characteristic peaks of progesterone were identified at 10.55°, 12.70°, 14.55°, 15.35°, and 16.95°..... 30

Figure 2-4 Differential scanning calorimetry curves of different ingredients in Crinone® and formulations. ..... 31

Figure 2-5 Flow curves of different batches of Crinone®: shear stress and viscosity as a function of shear rate. ..... 34

Figure 2-6 Oscillatory rheometry of Crinone®: effect of increasing oscillatory frequency on the elasticity modulus (G', storage modulus) and viscosity modulus (G", loss modulus). ..... 34

Figure 2-7 The release profiles of different batches of Crinone®. (n = 3, mean ± SD)..... 35

Figure 3-1 Phase solubility diagram of different CDs..... 52

Figure 3-2 Structure of progesterone ..... 53

Figure 3-3 Structure of RAME-β-CD..... 53

Figure 3-4 FTIR spectra of progesterone, RAME-β-CD, their physical mixture, and the resulting P4–RAME-β-CD inclusion complex..... 54

Figure 3-5 DSC thermograms of progesterone, RAME-β-CD, their physical mixture, and the P4–RAME-β-CD inclusion complex..... 55

Figure 3-6 X-ray diffraction patterns of progesterone, RAME-β-CD, their physical mixture, and the P4–RAME-β-CD inclusion complex ..... 56

Figure 3-7 Steady shear rheological behavior of the P4–CD gel: shear stress and viscosity as a function of shear rate ..... 58

Figure 3-8 Oscillatory frequency sweep rheology of the P4–CD gel: storage modulus (G′) and loss modulus (G″) as a function of frequency..... 59

Figure 3-9 Result of two different IVRT methods..... 60

Figure 3-10 IVPT comparison of P4 permeation across sheep vaginal tissue between Crinone® and P4-CD gel..... 61

Figure 3-11 *In vivo* plasma P4 concentration–time profiles following single vaginal administration of Crinone® and P4-CD gel in mice..... 62

Figure 4-1. Chapter 4 Graphical Abstract..... 69

Figure 4-2. Size characterization of doxorubicin liposomes in formulation developed by innovator and different generic manufacturers: Baxter Healthcare, Dr. Reddy's Laboratories, Sun Pharmaceuticals and Zydus. a) Particle size, b) polydispersity index, and c) zeta potential was measured using the Malvern Zetasizer (mean ± SD, $n \geq 3$) ..... 79

Figure 4-3. Measured doxorubicin and lipid content present in different liposomal preparations of doxorubicin hydrochloride produced by different manufacturers (mean ± SD, n = 3). a) Doxorubicin content, b) Lipid content for HSPC, DSPE-PEG (MW 2000) and cholesterol. **c**) Chromatographic separation of doxorubicin from lipid components using an UPLC-ELSD assay under a gradient mobile phase..... 80

Figure 4-4. Purity of liposomal doxorubicin formulations quantified as a percentage of peak AUC over cumulative peak AUC in each sample using UPLC-TUV analysis. a) Doxorubicin purity (%), b) daunorubicinone impurity levels (%), c) daunorubicin impurity levels (%), d) doxorubicinone impurity levels (%), e) chromatographic separation of doxorubicin and the respective impurities (mean ± SD, $n = 3$) ..... 82

Figure 4-5. Quantification of lipid impurities in liposomal doxorubicin hydrochloride formulations. a) cumulative lyso-PC (16:0) and (18:0) impurities (mean ± SD, $n \geq 2$). b) Chromatographic separation of lyso-PC (16:0) and (18:0) impurities in a representative, liposomal DOX sample manufactured by Dr. Reddy's Laboratories ..... 83

Figure 4-6. Quantification of free, non-encapsulated doxorubicin present in liposomal doxorubicin hydrochloride formulations produced by different manufacturers (mean ± SD, $n \geq 2$) ..... 84

Figure 4-7. Morphology of the doxorubicin liposome from different formulations: a) Doxil.® (batch no. MDZT300); b) Dr. Reddy's (batch no. 501635); c) Sun Pharmaceuticals (batch no. JX5514A); d) Zydus (batch no. P100084)..... 84

Figure 4-8. SAXS scattering profiles for a) one liposomal DOX formulation representative of each manufacturer (n = 4). b) Structural similarity between generic and reference, liposomal DOX formulations was compared and depicted using the SAXS similarity map (SSM) developed by SIBYLS at the Advanced Light Source (12.3.1), Lawrence Berkeley Laboratory. The Volatility of Ratio, $V_R$, correlation method was used to define similarity and dissimilarity between samples (mean ± SD, $n \geq 2$) ..... 85

Figure 4-9. Characterization and comparison of in vitro dissolution profiles for individual batches of approved generic liposomal doxorubicin hydrochloride formulations with the reference Doxil® formulation (mean ± SD; n = 3) ..... 86

Figure A-0-1 Manufacturing process of Crinone® ..... 95

Figure A-0-2 Schematic diagrams of texture analysis: (A) mechanical test; (B) muco-adhesion test; (C) syringeability test. ..... 95

Figure A-0-3 Histograms of globule size distribution of three batches Crinone®. ..... 96

Figure B-0-4 Specificity of mucoadhesion test assay (P4-CD gel) ..... 97

Figure B-0-5 Specificity of syringeablilty test assay (P4-CD gel) ..... 98

Figure B-0-6 Representative LC/MS chromatography of P4 (red) and P4-d9 internal STD (blue) ..... 98

Figure B-0-7 Schematic diagrams of IVPT using sheep vaginal tissue ..... 99

Figure B-0-8 Visual leakage check after 8hr IVPT ..... 99

Figure C-0-9 Specificity of doxorubicin quantification assay. Blank is in black, doxorubicin in blue. ..... 100

Figure C-0-10 Specificity of the lipid quantification assay. Blank is in black, lipids in blue. ... 102

Figure C-0-11 Chromatographic identification of doxorubicin in a Doxil® formulation using an isocratic mobile phase of deionized water and methanol with 0.1% formic acid (Baxter Healthcare, batch no. MDZT300). ..... 107

## List of Appendices

Appendix A: Supplementary materials for Chapter 2.....94

Appendix B: Supplementary materials for Chapter 3.....97

Appendix C: Supplementary materials for Chapter 4.....100

## Abstract

Progesterone (P4), a naturally occurring endogenous hormone, and its various formulations are widely utilized in assisted reproductive technology (ART) and in vitro fertilization (IVF). Among these, Crinone®, a P4 vaginal gel, has been extensively prescribed for various luteal phase support indications since its approval in 1997, with well-established clinical efficacy via vaginal administration. However, despite the expiration of its patent years ago, Crinone® remains the sole commercialized P4 gel in North America and globally, with no generic equivalents or novel gel formulations currently approved in the North American market. Considering this regard, we developed a comprehensive suite of analytical and characterization methods to evaluate the critical quality attributes (CQAs) of Crinone® to systematically reverse engineer this unique P4 gel. Furthermore, a novel P4 gel delivery system was formulated. A series of systematic *in vitro* and *in vivo* performance evaluations were subsequently conducted to compare the novel delivery system against Crinone®

In Chapter 2 focuses on my work reverse engineering of P4 gel Crinone®. We developed and performed following analytical and characterization methods to evaluate the critical quality attributes (CQAs) of Crinone® from 3 different batches: globule size, crystal particle morphology, progesterone content, crystalline state, thermal properties, texture analysis, rheology behavior and *In vitro* release. Polarized light microscopy (PLM) and scanning electron microscope (SEM) revealed that progesterone is dispersed in the gel matrix in crystalline form, and the globule size distribution of different batches of Crinone® was highly similar. The X-ray diffraction (XRD) analysis confirmed the presence of characteristic peaks of progesterone crystal in Crinone®, while differential scanning calorimetry (DSC) indicated that the thermodynamic properties of progesterone crystals changed upon distribution within the gel matrix. Texture analysis demonstrated that the three different batches of Crinone® exhibited similar mechanical properties, muco-adhesiveness, and syringeability. Rheological evaluation revealed a non-Newtonian, shear-thinning profile, consistent with an elastic, solid-like state. The in vitro release

study highlighted a sustained release profile, with similar release behaviors across all three batches.

Chapter 3 presents my research on the design and characterization of a novel vaginal P4 gel. In this work, we systematically screened cyclodextrin types and preparation approaches to identify an optimal complexation strategy for P4. The resulting P4-cyclodextrin complex is successfully incorporated into a hydrogel platform. To evaluate its performance, we applied the Crinone characterization methods to conduct the head-to-head comparisons between Crinone and novel P4 gel. The new formulation demonstrated rheological behavior similar to Crinone, while achieving superior *ex vivo* tissue permeability and enhanced *in vivo* bioavailability in a mouse model.

Chapter 4 covers my research on reverse engineering of liposomal drugs, including Doxil® and Onivyde®. We developed various analytical methods to analyze Doxil® and its generic drug products for multiple attributes, including liposome size distribution, zeta potential, Doxorubicin (DOX) content, lipid content, purity, non-encapsulated doxorubicin, morphology, nanostructure similarity, and quantified *in vitro* release. Our results showed formulation similarities and minor variation across different attributes assessed in the Q3 evaluation of generic, liposomal DOX products. Lipid purity, and the amount of free non-encapsulated DOX within liposomal formulations are critical to ensure the safety, efficacy, stability, and quality of each liposomal product. Our experimental results show a low prevalence of drug and lipid impurities and acceptable levels of non-encapsulated DOX in each formulation.

# Chapter 1 Introduction

## 1.1 Current status and future direction of delivery of progesterone (P4)

Progesterone (P4) is widely used for vaginal delivery in luteal phase support and prevention of preterm birth. The administration of P4 remains a cornerstone in modern reproductive medicine and hormone therapy. Over the past century, P4 supplement in clinical use has benefited countless patients and newborns. However, can current progesterone formulations meet the increasing standards of patients and address a wider range of therapeutic indications? This section reviews the physiological importance of P4, evaluates the limitations of current delivery modalities, and explores the development of next-generation, targeted delivery systems.

### *1.1.1 Physiology functions and clinical application of Progesterone (P4)*

Progesterone (P4) is a naturally occurring steroid hormone first isolated and characterized by Willard M. Allen and George W. Corner over 90 years ago [1]. While classically recognized for its indispensable role in establishing and maintaining pregnancy, extensive research has illuminated its broader physiological significance. Human endogenous P4 is secreted by the corpus luteum in the ovaries, the placenta during pregnancy, and, in smaller amounts, the adrenal glands. It modulates critical reproductive processes. During the normal menstrual cycle, P4 regulates the transformation of the uterine endometrium from the proliferative phase to the secretory phase, creating a receptive environment for embryo implantation. Following successful implantation, P4 continues to support pregnancy by maintaining endometrial integrity and promoting a stable intrauterine environment. In addition, P4 contributes to maternal immune tolerance toward the semi-allogeneic fetus and suppresses excessive myometrial contractility, thereby reducing the risk of premature uterine contractions and preterm labor [2,3]. P4 actions are not limited to its role in the reproductive system, it also plays some other important role across various physiological systems. In the central nervous system, P4 is local synthesized by neurons and glial cells and is involved in the regulation of various key processes including neurogenesis,

gliogenesis, myelination, neuroprotection, neural circuit maturation, and brain sexual differentiation [4]. Combined with estrogen, P4 also plays a critical role in bone formation. By stimulating the P4 receptor on osteoblast, P4 increases the osteoblastic growth at initial stage of bone modeling [5]. P4 signaling plays an important role in both normal mammary gland biology and breast cancer development. In the breast epithelium, P4 exerts its effects through progesterone receptors (PR), which regulate gene transcription and coordinate complex cell-cell signaling networks. PR signaling is essential for mammary gland development and physiological expansion of epithelial cells during reproductive cycles and pregnancy. However, dysregulation of this pathway has been implicated in breast carcinogenesis. Experimental studies indicate that P4 can stimulate proliferation of mammary epithelial progenitor cells through mediators such as RANKL and Wnt4 signaling pathways, which may contribute to tumor initiation or progression under certain hormonal contexts [6]. Moreover, PR signaling closely interacts with estrogen receptor pathways, adding further complexity to the hormonal regulation of breast cancer biology [7].

P4 has a wide range of clinical applications due to its central role in female reproductive physiology and endocrine regulation. Clinical test of P4 is an useful indicator for successful ovulation (high P4 level) or serious problem correlates with miscarriages [8]. In reproductive medicine, P4 supplement therapy is commonly used for luteal phase support in assisted reproductive technologies (ART), such as *in vitro* fertilization (IVF), as well as for the prevention of recurrent miscarriage and preterm birth. In gynecological practice, P4 and synthetic progestins are also widely utilized in hormonal contraception, the management of dysfunctional uterine bleeding, and the treatment of endometriosis [9]. Beyond reproductive indications, emerging evidence suggests that P4 may also have beneficial effects in other clinical contexts, including osteoporosis treatment, neuroprotection in patients with traumatic brain injury, depression treatment in postpartum women and attenuate the damage in demyelinating lesions or disease [5,10,11]. In addition, P4 is frequently combined with estrogen in menopausal hormone replacement therapy (HRT) to relieve vasomotor symptoms and to protect the endometrium from estrogen-induced hyperplasia in women with an intact uterus.

Hormone replacement therapy (HRT) has historically been associated with increased risks of breast cancer and cardiovascular disease, largely based on findings from the landmark Women's Health Initiative (WHI) randomized clinical trial published in 2002 [12]. These findings

led the U.S. Food and Drug Administration (FDA) to require a 'black box warning' on many menopausal hormone therapy products to inform the potential risk of HRT. However, subsequent reanalysis and additional clinical studies have demonstrated that the risks of HRT are strongly influenced by factors such as patient age, timing of therapy initiation, and hormone formulation. Evidence suggests that initiating HRT within 10 years of menopause onset or before the age of 60 is associated with a more favorable risk–benefit profile [13–15]. Based on a comprehensive review of the accumulated scientific literature, the FDA announced in November 2025 that it would remove several boxed warning statements related to breast cancer, cardiovascular disease, and dementia from menopausal hormone therapy labeling to better reflect current clinical evidence [16].

### *1.1.2 Current status and limitations of P4 delivery*

Currently marketed progesterone products include oral capsules and tablets, vaginal formulations, topical preparations, and parenteral injections. Representative products and their compositions are summarized in Table 1.1-1.

The first pharmaceutical formulation of P4 on the market for medical use is P4 in oil (PIO) intramuscular injection (IM). It was developed right after the first isolation of P4 in 1934 under the brand name Proluton. PIO formulation has been used for over 90 years and has proven its reliable therapeutic efficacy. By dissolving P4 in an oil vehicle, PIO overcomes its poor solubility and forms a natural intramuscular depot that enables sustained release. PIO formulation also avoids the low bioavailability of oral P4 dosage caused by extensive first-pass metabolism. PIO formulation provides another advantage that it allows measurable, stable circulating progesterone levels that can be monitored by clinicians to assess patient requirements—an option not feasible with vaginal administration route. This is why many clinicians across Europe and the United States prefer PIO injections [17]. However, IM injections are associated with several obvious drawbacks, like injection-site pain and leakage, inflammation, and poor patient compliance. In recent years, a water-soluble progesterone formulation, Prolutex®, has been approved for clinical use in Europe. This formulation utilizes hydroxypropyl-β-cyclodextrin as a solubilizer and is administered subcutaneously, an approach that can significantly reduce patient discomfort. Clinical studies have shown that Prolutex® produces a more rapid increase in systemic P4 concentrations compared with intramuscular progesterone in oil.[18]

Table 1-1 Current progesterone products in clinical use

| Formulation type | Product composition | Administration route | Market year | Dosage |
|---|---|---|---|---|
| Capsule (Prometrium) | Peanut oil, gelatin, glycerin, lecithin, titanium dioxide, color | Oral | 1998 (US) | 100/200mg |
| Tablet (Dubagest SR) | NA | Oral | 2012 (India) | 200/300/400 mg |
| Tablet (Luteina) | Mannitol, sorbitol, microcrystalline cellulose, magnesium stearate, and natural flavors. | Sublingual | 2010 (EU) | 100 mg |
| Vaginal gel (Crinone) | glycerin, light mineral oil, polycarbophil, carbomer homopolymer Type B, hydrogenated palm oil glyceride, sorbic acid, purified water | Vaginal | 1997 (US) | 45/90 mg |
| Vaginal ring (Milprosa) | light mineral oil and silicone elastomer | Vaginal | 2020 (US) | 1.78 g |
| Vaginal ring (Fertiring) | Silicone elastomer | Vaginal | 2007 (Chile) | 1.0 g |
| Vaginal ring (Progering) | Silicone elastomer | Vaginal | 1998 (Chile) | 2074 mg |
| Vaginal insert (Lutinus/Endometrin) | Lactose monohydrate, polyvinylpyrrolidone, adipic acid, sodium bicarbonate, sodium lauryl sulfate, magnesium stearate, pregelatinized starch, and colloidal silicon dioxide | Vaginal | 2007 (EU) | 100 mg |
| Intrauterine device (Pregestasert) | Silicone oil, barium sulphate, ethylene vinvy acetate membrane | IUD | 1976 (US)-2001(Discontinues) | 38 mg |
| Vaginal capsule (Utrogestan Vaginal) | sunflower oil, soybean lecithin, gelatin, glycerol, titanium dioxide and water | Vaginal/Oral | 1980 (EU) | 200 mg |

| | | | | |
|---|---|---|---|---|
| Vaginal/rectal suppository (Cyclogest) | Hydrogenated palm kernel oil, hydrogenated palm oil, and glycerol | Vaginal/Rectal | 1976 (UK) | 200/400 mg |
| Topical gel (Progestogel) | Octyldodecanol, carbomer 980, macrogol glycerol hydroxystearate, trolamine, ethanol, and purified water. | Topical | 1972 (EU) | 1% |
| Subcutaneous injection (Protulex) | Hydroxypropylbetadex, water | SC injection | 2014 (EU) | 25 mg |
| Intramuscular Injection | Benzyl alcohol, sesame oil | IM injection | 1934 | 50mg/ml |

During early clinical trial of P4, the significant first pass effect and low bioavailability of oral P4 route has been noticed. A breakthrough was achieved in the late 1970s, with the development of micronized progesterone formulated in oil-filled capsules which significantly enhanced its bioavailability [19]. Finally, nearly half a century after the discovery of P4, the first effective oral formulation, Utrogestan®, was approved in France in 1982 and later introduced in the United States as Prometrium® in 1998. Since then, oral micronized progesterone has been widely adopted and is now widely used worldwide in clinical practice. However, the oral route still cannot overcome the extensive first-pass effect, which results in limited systemic exposure consistency and relatively low P4 levels at the uterine [20]. Consequently, its efficacy in assisted reproductive technologies (ART) remains controversial. In contrast, the higher systemic exposure of oral administration offers lots of advantages for indications requiring systemic P4 effects, such as hormone replacement therapy (HRT). Nevertheless, this systemic exposure is also associated with increased central nervous system (CNS)–related adverse effects, including dizziness and somnolence[21].

Vaginal progesterone formulations represent another important delivery route and are widely used for luteal phase support in *in vitro* fertilization (IVF) and prevention of preterm birth. These include vaginal gels (e.g., Crinone®), vaginal inserts (e.g., Lutinus® and Endometrin®), vaginal capsules (e.g., Utrogestan® and Prometrium®), suppositories (e.g., Cyclogest®), and vaginal rings (e.g., Milprosa®). Vaginal delivery avoids hepatic first-pass metabolism and can provide preferential drug distribution to the uterus through the so-called

'uterine first-pass effect' [22]. Progesterone primarily exerts its physiological effects in the ovary and uterus, where it plays a central role in regulating ovulation and fertilization. In addition, it can avoid CNS side effects like sedation and dizziness caused by systemic exposure following parenteral or oral administration. Moreover, it is self-administered and non-invasive, making it gradually replace PIO injection as the main choice for P4 supplement methods for luteal phase support in IVF [23]. However, currently available vaginal products still suffer from several common limitations, including drug leakage, unpleasant discharge, local irritation, and limited mucosal retention [24].

In addition to these mainstream P4 formulations, several alternative dosage forms have been developed worldwide for specific clinical needs. As early as 1972, a progesterone gel (Progestogel®) was approved in Europe as a local therapy for breast disorder. However, some clinical trial has reported its variable and limited efficacy, which may restrict its further application [25]. In the United States, various compounded P4 creams and gels, as well as over-the-counter (OTC) topical products, are also available. However, due to the lack of strict regulatory oversight and specific characterization, their quality, consistency, and therapeutic effectiveness remain uncertain [26]. In Latin America, P4-releasing vaginal rings have been used for both ART and contraception. For example, Fertiring® is designed to provide sustained 10 mg/day P4 delivery for up to 7 days to support IVF, whereas Progering® is used for postpartum contraception during lactation, also offering a 90-day duration of action [27]. Vaginal rings offer several additional advantages, including high effectiveness, ease of use, and user control. Their ability to local deliver hormones at a nearly constant release rate enables the use of lower doses while maintaining therapeutic efficacy, resulting in improved bioavailability [28]. Intrauterine device (IUD) was also developed for birth control and marketed in 1976 under the name Pregestasert® in United States [29]. Unfortunately, several limitations hindered its clinical use, including a short duration of efficacy (approximately one year), high cost, a relatively high failure rate (2.9%) and insertion-related discomfort that often required local anesthesia [30,31]. Consequently, it was never widely adopted in clinical practice and was discontinued in 2001. Sublingual P4 formulations were first investigated as early as the 1950s to bypass hepatic first-pass metabolism [32]. To date, only a limited number of such products remain on the market, with one formulation Luteina® still approved for sublingual use in Poland and Ukraine.

Overall, the optimal route of P4 administration and dosing regimen remains under debate. Numerous clinical trials and meta-analyses have compared the efficacy of different formulations, but no single approach has been universally established as superior across all patient populations. Nevertheless, a clear trend has emerged: vaginal delivery of P4 is now widely considered the preferred route for luteal phase support in assisted reproductive technology. Traditional PIO injections are gradually being replaced by vaginal formulations due to their improved tolerability, patient convenience, and targeted uterine delivery [23,33].

### *1.1.3 Physiology of vagina and how it is related to drug delivery*

The female reproductive tract is divided into the upper reproductive tract and the lower reproductive tract. The upper reproductive tract includes fallopian tubes, ovaries and uterus. The lower reproductive tract consists of the external genitalia, the vagina and the ectocervix. The vagina is a strong canal of muscle and 6 to 10 cm long extending from the vulva to the cervix with a width of 2-3 cm. Its crosswise folded wall provides it with 80-110 $cm^2$ surface area, which facilitates the local drug delivery [34,35]. In general, vaginal drug delivery refers to the administration of pharmaceutical formulations to the lower female reproductive tract. For example, gels and suppositories are typically applied and maintained on the vaginal wall cavity, whereas vaginal rings and pessaries are positioned near the cervix to enable localized or sustained drug release.

The unique environment of human vagina requires special attention when designing vaginal delivery formulation. First, drug permeation in the vaginal tract is restricted by a formidable dual-layer barrier system. The foundational physical barrier is the vaginal epithelium, a relatively thick (~260 μm) layer of non-keratinized stratified squamous cells that limits the absorption of active pharmaceutical ingredients (API) [1]. The epithelial surface is covered by a mucus layer secreted mainly from the cervix. This cervicovaginal mucus (CVM) has a mesh-like structure with pore sizes averaging 340 ± 70 nm. CVM can effectively trap pathogens such as herpes simplex virus through mucoadhesive interactions, besides purely steric hindrance. This suggests that adhesive interactions between mucus components and foreign particles play a critical role in restricting their mobility and preventing infection [36]. In addition, the vaginal environment is persistently moist, containing both transudates from the vaginal wall and mucosal fluids originating from the upper reproductive tract. These fluids can dilute and facilitate the clearance of administered formulations, thereby limiting their residence time and reducing drug

absorption. Furthermore, the healthy vaginal microbiota is dominated by *Lactobacillus* species, which produce lactic acid to maintain an acidic pH environment (typically 3.5–5.5) [34]. This mildly acidic condition not only provides protection against pathogenic microorganisms but also influences drug solubility, stability, and release behavior. Importantly, drug formulations must be designed to preserve this physiological pH and avoid disrupting the native microbial balance, which is essential for vaginal health.

### *1.1.4 Tendency of next generation vaginal delivery system*

As discussed above, vaginal drug administration represents a unique and underutilized route for drug delivery. By bypassing hepatic first-pass metabolism, it can enhance the systemic bioavailability of certain drugs and, importantly, increase drug concentrations at local target tissues such as the uterus and ovaries. This unique pharmacokinetic advantage makes the vaginal route particularly attractive for therapies targeting the female reproductive system.

However, the development of effective vaginal delivery systems faces two major physiological barriers. First, the continuous secretion of cervical mucus results in a dynamic clearance mechanism that can rapidly remove vaginal administered formulations, leading to poor retention and weakened therapeutic efficacy. Second, the vaginal mucosal layer presents a significant diffusion barrier. This highly hydrated mucus gel restricts the transport of hydrophobic drugs, while the mucin network—characterized by a mesh-like structure with pore sizes on the order of approximately 400–600 nm—can hinder the penetration of larger particles and drug carriers. Overcoming these challenges, while also ensuring compatibility with the mildly acidic vaginal environment, is critical for successful formulation design. Given the relatively large surface area of the vaginal epithelium, an optimized delivery system has substantial potential to achieve both local and systemic therapeutic effects.

In recent years, considerable research efforts have been devoted to the development of advanced vaginal delivery platforms. For example, Farhan et al. systematically evaluated commonly used gel-forming materials, including hydroxypropyl methylcellulose (HPMC), sodium carboxymethyl cellulose (Na-CMC), xanthan gum, guar gum, sodium alginate, Carbopol 971 and polycarbophil, and compared their adhesion, retention and drug release profiles. Their results showed that these conventional gel formulations are compatible with the acidic vaginal environment, while exhibiting distinct mucoadhesive properties and drug release profile, highlighting the potential for further optimization of current vaginal formulations.[37]

Thermosensitive hydrogels have been widely investigated for vaginal drug delivery systems because they combine the ease of administration in its liquids form with enhanced retention time and sustained-release behavior in its gel form. Among these, formulations based on Pluronic F127 are the most commonly used. Pluronic F127 is a triblock copolymer composed of PEO–PPO–PEO segments that exhibits thermosensitive gelation. At low temperature it remains as free polymer chains in solution, whereas at physiological temperature the hydrophobic PPO blocks aggregate into micelles that further pack into a three-dimensional network, leading to rapid gel formation (Figure 1.1-1) [38]. Additional polymers such as hydroxypropyl methylcellulose (HPMC), carbomers, chitosan and related excipients are often incorporated to improve gel strength and mucoadhesive properties [39]. Umme et al. systematically screened F127-based gels containing different combinations of HPMC, sodium carboxymethyl cellulose (NaCMC), Carbopol, and polycarbophil, and evaluated the effects of these polymers on gel strength, viscosity, in vitro drug release, gelation temperature, and gelation time [40]. Cindy et al. further demonstrated that incorporation of HPMC and PEG 400 into F127 gels enhanced in vivo retention and improved drug permeation across vaginal tissues[41]. In addition, a wide range of drugs, including antifungal and antiviral agents, have been explored for vaginal delivery using thermosensitive hydrogels, generally showing improved therapeutic performance [34,42,43].

Liposomes have been also extensively explored as carriers to improve vaginal drug delivery. Current studies primarily involve antiviral and antifungal agents, which are typically formulated in gel-based systems, and have shown enhanced therapeutic efficacy along with sustained drug release profiles [34,44–47]. To address the challenge of mucus penetration, Laura Ensign et al. developed a mucoinert nanoparticle as a PEG-coated progesterone nanosuspension, where dense PEG coating minimizes interactions with mucus. This system improved vaginal absorption and tissue distribution, leading to enhanced local progesterone delivery and efficacy comparable to the reference product Crinone® in a mouse preterm birth model [48]. Claudia et al. introduced cysteine into Carbopol 974P, enabling thiol groups on the polymer to form disulfide bonds with cysteine-rich domains of mucin, thereby enhancing the adhesion of this novel carrier [49]. In addition, innovation in vaginal delivery devices has emerged, like Callavid®. Its patented design integrates a small, tampon-shaped drug delivery component with an integrated absorbent liner (Figure 1.1-2) [50]. After dosing P4 suppository, this absorbent liner can remain in place and

prevent leakage, thereby minimizing mess and absorption variability. A phase I clinical trial is currently ongoing to test the safety and ease of use compared to traditional suppository [51].

In summary, noticeable progress has been made in vaginal drug delivery over recent years, with emerging delivery systems effectively solving key challenges such as local retention, tissue permeation, and sustained release. Nevertheless, despite sustained research efforts over the past few decades, there is no novel progesterone vaginal delivery coming to market and benefiting more patients. This gap highlights the complexity of clinical translation and implies that considerable work still lies ahead.

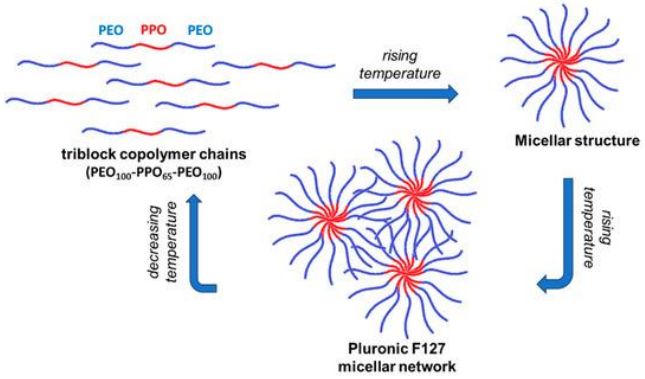


Figure 1.1-1 Schematic presentation of temperature-induced gelation for Pluronic F127

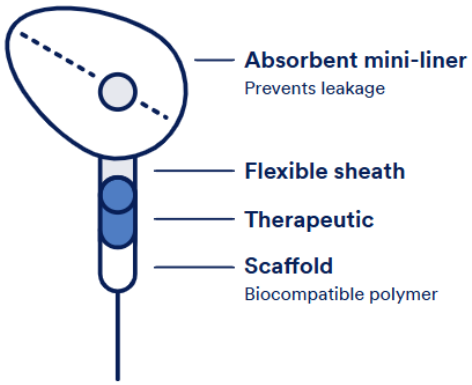


Figure 1.1-2 Structure diagram of Callavid®

## 1.2 Challenges in developing complex generics

Generic drugs currently account for approximately 90% of all prescriptions dispensed in the United States, yet represent only about 13% of total drug spending [52]. Their widespread availability substantially reduces healthcare costs while providing patients with the same therapeutic benefit as the corresponding reference products. Therefore, efficient regulation and approval of generic drugs are critical to maintaining both the accessibility and affordability of healthcare.

A fundamental requirement for generic drug approval is that the generic product contains the same active pharmaceutical ingredient (API) as the reference listed drug (RLD) and demonstrates equivalent pharmaceutical and biological performance. In the United States, generic drugs are generally approved through the Abbreviated New Drug Application (ANDA) pathway, which does not require the extensive nonclinical and clinical studies necessary for a

new drug application[53]. For conventional small-molecule products with simple dosage forms, such as immediate-release oral tablets and capsules, generic approval is typically based on demonstration of pharmaceutical equivalence and bioequivalence. Pharmaceutical equivalence requires the generic product to have the same API, excipients, dosage form, route of administration, and strength as the RLD, often referred to as Q1/Q2 sameness. In most cases, demonstration of pharmaceutical equivalence together with a single clinical bioequivalence study is sufficient for approval. In addition to these conventional products, there is another subset of formulations that cannot be approved through this straightforward pathway. Due to their complex compositions, unique internal structures, or different routes of administration these products are classified as complex generics and they present significant characterization challenges. Typical examples include liposomal formulations, long-acting injectable suspensions, semisolid topical and vaginal formulations, inhalation products, and products containing complex APIs. Because the performance of these products depends not only on their composition but also on their internal structure and manufacturing process, conventional Q1/Q2 sameness and systemic bioequivalence alone are often insufficient to ensure therapeutic equivalence [54,55].

To address these challenges, FDA introduced the concept of Q3 similarity for complex generic products. Q3 similarity refers to equivalence in the physicochemical arrangement of matter within the formulation, namely that the generic product possesses a microstructure comparable to that of the RLD. Attributes such as spatial organization, phase distribution, and particle or droplet characteristics must closely resemble those of the reference product, as they are critical determinants of drug release, local delivery, and overall therapeutic performance. Since critical quality attributes (CQAs) differ among dosage forms, the FDA issues product-specific guidances (PSGs) recommending tailored approaches for demonstrating Q3 similarity. For liposomal drug products, recommended Q3 characterization may include liposome size distribution, lipid composition, internal aqueous environment, encapsulation efficiency, and the physical state of the encapsulated drug. These properties strongly influence drug retention within the carrier, release behavior, and biodistribution [56]. For semisolid gel formulations, FDA commonly recommends characterization of visual appearance, rheological behavior, crystal polymorphism, globule or particle size distribution, and *in vitro* release testing (IVRT). Such

properties affect the microstructure of the formulation and directly affect drug release, permeation, and therapeutic efficacy [57].

Among complex generic products, liposomal formulations and semisolid vaginal gels represent two of the analytically and regulatorily challenging dosage forms. Doxil® liposomal doxorubicin injection is a liposomal product whose therapeutic performance depends on precise control of liposome size, drug encapsulation, and internal physicochemical environment. Crinone® 8% progesterone vaginal gel is a semisolid emulsion-based suspension gel whose performance is governed by its polymer network, oil globule distribution, and progesterone solid-state characteristics. In both cases, small differences in microstructure may lead to substantial changes in drug release and therapeutic outcome, creating significant barriers to generic development. Therefore, this dissertation focuses on Doxil® liposomal doxorubicin injection and Crinone® 8% progesterone vaginal gel as two representative examples of complex generic drug products, with the goal of addressing the analytical and regulatory challenges that hinder the development of therapeutically equivalent generic alternatives.

### *1.2.1 Introduction to Doxil® and challenges in liposomal generic development*

Doxil® is a PEGylated liposomal doxorubicin hydrochloride formulation approved by the U.S. FDA in 1995 and was the first liposomal drug product marketed in the United States [58]. It is indicated for the treatment of ovarian cancer, Kaposi's sarcoma, and multiple myeloma. The clinical success of Doxil® is largely attributed to its ability to overcome the severe dose-limiting cardiotoxicity associated with free doxorubicin. Encapsulation of doxorubicin within long-circulating PEGylated liposomes substantially prolongs systemic exposure while reducing the cardiotoxicity associated with free doxorubicin. Compared with free doxorubicin, Doxil® exhibits a significantly larger area under the plasma concentration-time curve and remains in circulation for approximately six days longer because of its much lower clearance rate [59,60]. Furthermore, its prolonged systemic circulation allows the liposomes to exploit the enhanced permeability and retention (EPR) effect, passively accumulating in tumor tissues and improving the overall therapeutic index [58].

Doxil® consists of liposomes approximately 80–100 nm in diameter composed of hydrogenated soy phosphatidylcholine (HSPC), cholesterol, and MPEG-DSPE (Figure 1.2-1) [61]. Surface PEG chains create a steric barrier that reduces uptake by the reticuloendothelial system, while the rigid HSPC/cholesterol membrane minimizes premature drug leakage [59,62]. The encapsulation of doxorubicin in Doxil® relies on a highly efficient remote loading process driven by a transmembrane ammonium sulfate gradient. During manufacturing, liposomes are first formed containing an aqueous core of ammonium sulfate. As ammonia gas diffuses out across the lipid bilayer, it leaves behind protons, acidifying the internal environment. When unionized doxorubicin is introduced to the external medium, it readily permeates the liposomal membrane. Upon entering the acidic core, doxorubicin becomes protonated and permanently trapped, eventually precipitating with sulfate ions. This active loading process achieves an encapsulation efficiency of over 95% and results in the highly stable, characteristic "coffee bean" internal crystalline structure. [63].

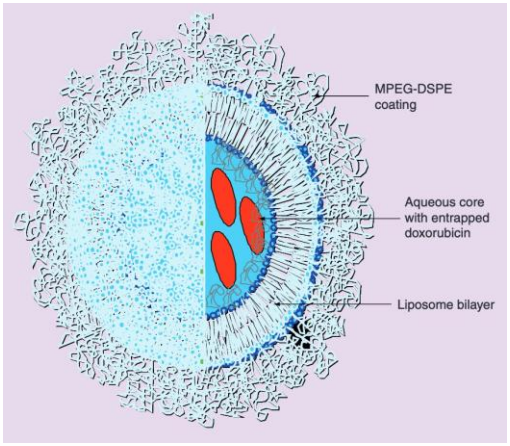


Figure 1-1 Schematic representation of a PEGylated liposomal doxorubicin

Commercial manufacture of Doxil is unusually complex because product performance depends not only on Q1/Q2 composition, but also on the manufacturing process itself. Critical steps include preparation of a narrow-size PEGylated liposome population, establishment of the ammonium sulfate gradient, active drug loading, and tight control of particle size, lamellarity, internal pH, PEG density, and the physical state of encapsulated doxorubicin. Even small changes in lipid composition or process conditions can alter drug leakage, circulation half-life, and biodistribution.

After patent expiration in 2010, development of generic liposomal doxorubicin products accelerated, but only a limited number of products were approved because of the high technical

barrier. In 2010, A manufacturing shutdown at Ben Venue, the sole Doxil manufacturer, caused a global shortage during 2011–2012 and highlighted the market dependence on this product. During the shortage, Lipodox became the first generic approved by the FDA under emergency conditions, and several additional generics were later approved [64].

Development of generic liposomal products remains challenging because conventional bioequivalence approaches are insufficient. Plasma drug levels alone cannot reliably distinguish between free and liposome-encapsulated doxorubicin, nor do they fully reflect tumor delivery. Therefore, regulators require both Q1/Q2 sameness and extensive Q3 equivalence, including comparable particle size distribution, zeta potential, lipid composition, PEG density, internal ion gradient, state of encapsulated drug, in vitro leakage, and release behavior. FDA guidance for generic liposomal doxorubicin further recommends use of the same ammonium sulfate remote-loading process and demonstration of equivalent physicochemical characteristics before in vivo bioequivalence studies can be performed. These requirements make liposomal generics far more difficult to develop than conventional injectable products.

### *1.2.2 Introduction to Crinone® and challenges for generic P4 vaginal gel*

Crinone® (progesterone vaginal gel) is widely utilized for luteal phase support in assisted reproductive technology (ART) and the treatment of secondary amenorrhea. As a locally acting formulation, it offers significant clinical advantages over oral and intramuscular (IM) progesterone therapies. Vaginal administration directly targets the uterus through the "first uterine pass effect," achieving high local tissue concentrations while bypassing hepatic first-pass metabolism. Furthermore, its mucoadhesive properties enable sustained drug release, allowing for convenient dosing and sparing patients the pain and injection-site complications associated with IM therapies. However, the formulation is not without limitations. Patients frequently report formulation-related adverse effects, such as vaginal residue accumulation, local irritation, and discharge—largely attributed to the water-insoluble polycarbophil matrix. Additionally, variations in patient physiological conditions can sometimes lead to erratic drug absorption.

These unique clinical properties are attributed from formulation's complex internal microstructure. Crinone® is not a simple homogeneous gel, instead, it functions as an emulsion-based suspension gel. It consists of a heterogeneous network where micronized progesterone, oil globules, and mucoadhesive polymers coexist within a continuous aqueous phase (Figure 1.2-2). Polycarbophil and carbomer form an interconnected polymeric matrix responsible for the

characteristic rheological behavior and strong vaginal mucoadhesion of the formulation, while mineral oil and hydrogenated palm oil glycerides are dispersed throughout the network as oil droplets. Progesterone is present primarily as suspended solid particles associated with the polymer–oil matrix. Consequently, the *in vitro* and *in vivo* performance of Crinone®—specifically the diffusion path of progesterone, local retention, and release kinetics—is heavily dependent on critical structural attributes such as oil globule size distribution, the degree of polymer crosslinking, and the crystalline state of the drug. [57,65].

The complexity of Crinone® also comes from its manufacturing process, since the microstructure is formed during processing rather than being dictated solely by formulation composition. The preparation of Crinone involves separate manufacture of an aqueous phase and an oil phase (Appendix A-1). First, P4 is mixed with the polymers (polycarbophil and carbomer) and sieved to create a uniform powder blend. At the same time, water, sorbic acid, and glycerin are mixed to form the initial water phase. The powder mixture is then added to this water phase to form a gel-like solution, which is heated to 60 °C. Meanwhile, the oil phase is prepared by melting mineral oil and hydrogenated palm oil glyceride at 75–78 °C, and then cooled to 60 °C. Once both phases reach 60 °C, they are mixed thoroughly to produce a uniform, creamy white product. Finally, sodium hydroxide is added to adjust the pH to about 2.5–3.5. Each step of this process plays a critical role in determining the final microstructure. The initial mixing and sieving steps determine the particle size and distribution of solid progesterone within the gel. The hydration of the polymers determines the strength and mucoadhesion of the gel network. Additionally, the temperature control and mixing intensity at 60 °C determines the size and distribution of oil droplets. The final pH adjustment affects polymer swelling and the overall stability of the gel. Small changes in any of these steps can change the internal structure, which in turn affects how the drug is released and retained in the body.

This strong link between the manufacturing process and the microstructure creates a major barrier for generic drug development. Although the patents for Crinone® expired years ago, and its excipient composition (Q1/Q2) is well known, there are still no FDA-approved generic versions on the market. To help generic developers, FDA drafted a Product-Specific Guidance (PSG) for progesterone vaginal gel that recommends comparative Q3 characterization tests. However, the guidance only lists the required Q3 attributes without providing specific experimental conditions or standard testing methods [57]. Furthermore, there are currently no

published research articles reporting the detailed characterization or *in vitro* release behaviors of Crinone®. Therefore, there is a strong need to establish reliable testing methods to fully characterize this complex semi-solid dosage form. Doing so will not only help in the generic development of Crinone® but also support the design of new progesterone vaginal products.




Figure 1-2 Crinone 8% Package and prefilled applicator

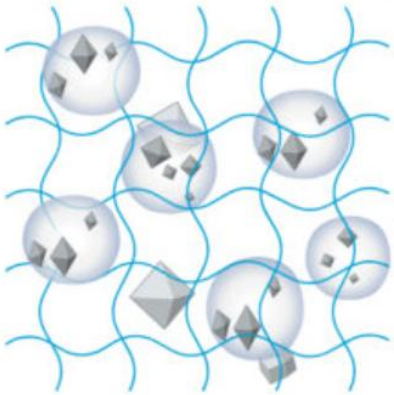

Figure 1-3 Diagram of Crinone® progesterone gel

### 1.3 Research scope and chapter overviews

The scope of this dissertation is to develop and apply physicochemical characterization methods for complex vaginal and liposomal drug products, with particular emphasis on understanding the relationship between formulation microstructure and drug performance. By using both P4 vaginal gel and liposomal anticancer products as model systems, this work seeks to identify the critical quality attributes that affect *in vitro* behavior and to provide a scientific framework for future generic product development. Furthermore, the knowledge and analytical methods established from these reverse engineering studies were subsequently applied to the rational design and evaluation of a novel progesterone vaginal gel, demonstrating how insights from existing products can guide the development of next-generation formulations with improved drug release, tissue permeation, and *in vivo* performance.

Chapter 2 describes the reverse engineering and comprehensive characterization of Crinone. A series of analytical methods were established to evaluate the physicochemical and structural properties of Crinone®, including globule size distribution, morphology, API crystal state, thermal behavior, mechanical properties, mucoadhesion, syringeability, rheology, and *in vitro* release. The results demonstrated that different batches of Crinone® exhibit highly similar physicochemical and functional properties. These findings provide insight into the

microstructure of Crinone® and establish a foundation for the future development of bioequivalent generic vaginal gels. The analytical and characterization methods established in this chapter were subsequently applied in Chapter 3 for the evaluation of our novel P4 gel. The physicochemical and performance data obtained for Crinone® also served as a commercial reference for the design, optimization, and comparison of the novel vaginal gel formulation.

Chapter 3 focuses on the development of a novel P4 vaginal hydrogel based on a P4-CD inclusion complex. Different cyclodextrins were screened to identify the optimal complexation strategy for P4. The resulting inclusion complex was incorporated into a carbomer/polycarbophil gel and systematically compared with Crinone®. The novel P4 formulation exhibited similar rheological properties but improved mucoadhesion, faster drug release, better vaginal tissue permeation, and enhanced systemic exposure following vaginal administration. These results demonstrate the potential of cyclodextrin complexation as a strategy for next-generation vaginal progesterone delivery systems.

Chapter 4 discusses the development and application of analytical methods for the characterization of complex liposomal drug products, with emphasis on liposomal doxorubicin formulations. Methods were established to determine particle size distribution, zeta potential, drug and lipid content, impurity profile, amount of free non-encapsulated doxorubicin, morphology, nanostructure, and *in vitro* release. These approaches were applied to compare reference and generic liposomal doxorubicin products, revealing overall physicochemical similarity together with minor batch-to-batch and manufacturer-to-manufacturer variation. Advanced techniques such as cryo-TEM and SAXs were used to further evaluate liposome morphology and internal structure. The findings contribute to a better understanding of the critical quality attributes governing liposomal drug performance and support future development of complex generic liposomal products.

Chapter 5 of this thesis discusses the conclusion of these chapters and the future context of work and implications for future studies. Chapter 2 was published in *international journal of pharmaceutics*. Chapter 4 was published in the *AAPS Journal.* Chapter 3 is in preparation for publication.

# Chapter 2 Reverse Engineering of Crinone®: Progesterone Vaginal Gel

## 2.1 Abstract

Crinone®, a progesterone-containing vaginal gel, is prescribed in clinical practice for hormone replacement therapy and assisted reproductive technology. Despite its clinical significance, limited studies have delved into its physicochemical properties and release behavior. This study aims to systematically reverse engineer Crinone® by characterizing its structural and functional properties. Key parameters evaluated include globule size, crystal particle morphology, crystalline state, thermal properties, rheological behavior, texture analysis, and in vitro drug release. Polarized light microscopy (PLM) and scanning electron microscope (SEM) revealed that progesterone is dispersed in the gel matrix in crystalline form, and the globule size distribution of different batches of Crinone® was highly similar. The X-ray diffraction (XRD) analysis confirmed the presence of characteristic peaks of progesterone crystal in Crinone®, while differential scanning calorimetry (DSC) indicated that the thermodynamic properties of progesterone crystals changed upon distribution within the gel matrix. Texture analysis demonstrated that the three different batches of Crinone® exhibited similar mechanical properties, muco-adhesiveness, and syringeability. Rheological evaluation revealed a non-Newtonian, shear-thinning profile, consistent with an elastic, solid-like state. The in vitro release study highlighted a sustained release profile, with similar release behaviors across all three batches. These findings provide valuable insights into the formulation design and quality evaluation of Crinone®, offering a robust foundation for developing generic equivalents and optimizing vaginal drug delivery formulations to enhance clinical efficacy.

## 2.2 Introduction

Women's health and reproductive issues represent some of the most pressing challenges in global healthcare today [66]. Conditions such as infertility, recurrent pregnancy loss, and hormonal imbalances not only affect the physical and mental well-being of millions of women but also have profound social and economic implications[67]. Addressing these challenges is of paramount importance, as solutions can significantly improve quality of life, promote gender equity in healthcare, and contribute to broader societal development. Among the various therapeutic approaches, optimizing hormone delivery systems is a critical step in advancing women's reproductive health. However, the development of drug delivery systems targeting diseases and conditions of the female reproductive tract (FRT) remains a relatively underexplored area of research [68].

Progesterone is a critical hormone in maintaining pregnancy, regulating the menstrual cycle, and treating reproductive disorder [9,69]. Vaginal delivery of progesterone offers several advantages, including targeted delivery, reducing hepatic metabolism by partially circumventing the first-pass effect, and sustained local drug release [70,71]. Crinone®, a commercially available progesterone vaginal gel, has been utilized in clinical practice for indications such as luteal phase support during assisted reproductive technology (ART) and hormone replacement therapy (HRT) [9,72]. The effective therapeutic outcomes of Crinone® are primarily attributed to its innovative drug delivery system, which features a unique composition (Appendix A-1). This vaginal gel incorporates bio-adhesive polymers, including carbomer and polycarbophil, which enhance retention at the application site, thereby ensuring sustained release of progesterone. Despite its clinical success and patent expiration, no generic version of Crinone® has been approved in any country to date. The lack of generic alternatives stems from the complex formulation challenges recognized throughout the pharmaceutical industry, particularly since the detailed physicochemical properties that contribute to Crinone®'s unique pharmacokinetic profiles remain underexplored.

To facilitate the development of therapeutically equivalent generic products of Crinone®, the U.S. Food and Drug Administration (FDA) has issued a Draft Guidance on Progesterone Vaginal Gel [73]. This guidance emphasizes the importance of demonstrating equivalence not only in terms of qualitative (Q1) and quantitative (Q2), but also in physicochemical and structural

(Q3) attributes [74]. These Q3 attributes – including globule size, rheology, and microstructure – are critical for ensuring the therapeutic performance and bioequivalence of the generic product to the reference standard [74,75].

Therefore, in this study, we conducted a systematic analysis of Crinone®'s Q3 properties using various analytical techniques to characterize globule size, crystal particle morphology, thermal and crystalline properties, texture analysis, and rheological behavior. Furthermore, the in vitro drug release profile of Crinone® was evaluated to better understand the release kinetics of progesterone from this gel matrix. This research provides critical insights for reverse engineering and development of bioequivalent generic formulations. Moreover, our findings contribute to the broader advancement of vaginal drug delivery systems.

## 2.3 Materials and Methods

### *2.3.1 Materials*

Three batches of 8% Crinone® (Allergan USA, Inc.) were obtained from University of Michigan hospital pharmacy. The lot numbers of 8% Crinone® were: 100046739, 100048963, and 100049672, respectively. Ultrapure deionized water (resistivity ≥ 18.2 MΩ·cm) was prepared using an ultrapure water purification system (Barnstead™ GenPure™ xCAD Plus, Thermo Fisher Scientific, USA). High-Performance Liquid Chromatography (HPLC) grade methanol, acetonitrile and water were purchased from Fisher Chemical (Waltham, MA, USA). Mucin from porcine stomach, sodium acetate (ACS reagent, ≥99.0%) and acetic acid (glacial, ACS reagent, ≥99.7%) were purchased from Sigma-Aldrich (St. Louis, MO, USA). Progesterone (Micronized Powder, USP grade) was purchased from Spectrum® Chemical Manufacture Corporation (New Brunswick, NJ, USA). The Float-A-Lyzers® G2 dialysis device (cellulose ester membrane, molecular weight cut-off (MWCO) of 50 kD) was obtained from Spectrum Labs® (CA, USA). Ethanol (200 proof, USP, Decon™ Labs) was purchased from Fisher Scientific (NH, USA). Carbomer 934P and polycarbophil (Noveon® AA-1 Polycarbophil, USP grade) were kindly provided by Lubrizol (OH, USA).

### *2.3.2 Physical appearance and pH*

The Crinone® gel were visually examined for physical appearance such as color and consistency. The pH of the gel at room temperature was measured by Orion™ Versa Star Pro™ pH benchtop meter. A three-point pH calibration (pH 4.0, 7.0 and 10.0) was performed before

the measurement. Between each sample measurement, residual gel was removed from the electrode surface using Kimwipes, followed by soaking in Dawn dish soap solution to eliminate any oil containing residue. The electrodes were then rinsed several times with deionized water to ensure complete cleanliness before proceeding to the next measurement. Each sample was analyzed in triplicate.

### *2.3.3 Globule size measurement*

Based on the formula of Crinone®, progesterone is primarily present as crystal particles within the oily phase globules. The globule size of Crinone® was determined using laser diffraction analysis with a Mastersizer 2000 system and Hydro 2000s accessory (Malvern Instruments Ltd., Worcestershire, UK) at ambient temperature. A 100 µL aliquot of Crinone® gel was dispersed into 4 mL of deionized water and was vortexed for two minutes to ensure the full dispersion of the colloid. The sample was added to Hydro 2000s sample dispersion unit drop by drop and was further dispersed to achieve a degree of obscuration between 10% and 15%. The stirrer of the accessory was set to 525 rpm, and the ultrasound was set to 20% power to ensure the homogenized dispersion in the system. For progesterone, real refractive index values and imaginary refractive index values (absorption index) were 1.335 and 0.01, respectively. The refractive index of dispersant was 1.33. Regarding the result calculation model, the calculation sensitivity was set to normal, and the particle shape was selected as spherical. The experiment was performed in triplicate.

### *2.3.4 Polarized light microscope (PLM)*

The progesterone crystal in Crinone® matrix was observed using polarized light optical microscopy (PLOM, Olympus IXplore 71 inverted microscope equipped with polarizer, Olympus Corporation, Shinjuku, Tokyo, Japan). A suitable amount of gel was mounted on a clean glass slide and a coverslip was used to pull slowly so that the gel formed a thin film for optimal visualization. The polarizer of the microscope was set at 45°. Images were immediately captured using software. Three sample slides were prepared for each lot, and at least five pictures were taken for each slide. One representative image that best illustrates the typical morphology of the batch was selected for presentation in the figures.

### *2.3.5 Scanning electron microscope (SEM)*

The crystal particle in Crinone® gel was further observed using SEM (TESCAN MIRA3 FEGSEM). Approximately 10 μL of fresh Crinone® gel was directly applied onto a metal stub and spread into a thin layer using a spatula, then air-dried at room temperature for 24 hours before examination. No additional fixation or coating was performed. A 10 kV voltage and a beam intensity of 8 were used for detection. We prepared three samples for each lot, and at least five pictures were taken for each sample. One representative image that best illustrates the typical morphology of the batch was selected for presentation in the figures.

### *2.3.6 Solid X-ray diffraction (XRD)*

The crystalline property of Crinone® gel was analyzed by MINIFLEX 600 XRD (Rigaku, Osaka, Japan) coupled with a Cu Kα radiation. Approximately 0.2 g of Crinone® gel was transferred onto the glass sample holder using a stainless-steel spatula. The sample was spread evenly into a thin layer with the spatula, and then gently compressed with a clean microscope slide to ensure a smooth and uniform surface suitable for diffraction analysis. The voltage was set at 40 kV and the current was 15 mA. The sample was scanned over a 2θ range from 5° to 40° with a step angle of 0.05° and a scanning speed of 2° /min. The experiment was repeated for each lot, with three independent samples prepared per lot. The XRD patterns of the three samples were nearly identical, demonstrating high reproducibility. One representative pattern that best illustrates the typical characteristics of the batch was selected for presentation in the figures.

### *2.3.7 Differential Scanning Calorimetry (DSC)*

The thermal characteristic of Crinone® gel was assessed using DSC (TA INSTRUMENTS DISCOVERY DSC, Waters, USA). For each DSC measurement, a fresh tube of Crinone® gel was opened and approximately 5 mg of gel was carefully transferred into an aluminum DSC pan. The sample was gently spread to ensure even contact with the bottom of the pan. In addition, progesterone and the two polymers (carbomer 934P and polycarbophil) were weighed according to their weight percentage in the Crinone® formulation. The corresponding amounts of materials were thoroughly mixed in a tube using vortex to ensure homogeneity. Approximately 5 mg of the obtained powder mixture was then transferred into the sample pan for DSC analysis. The heating temperature ranged from 50 to 180 °C, with a heating rate of 10 °C/min under the nitrogen atmosphere. An empty aluminum pan was adopted as a reference during the measurements. The

DSC experiment was repeated for each lot, with three independent samples prepared per lot. The thermograms of the three samples were highly consistent, demonstrating reproducibility. One representative thermogram that best illustrates the typical thermal behavior of the batch was selected for presentation in the figures.

### *2.3.8 Texture analysis*

#### *2.3.8.1 Mechanical properties test*

Texture profile analysis (TPA) of the Crinone® gel was performed using a texture analyzer (AMETEK Brookfield CT-3) equipped with 1.5 kg load cell in TPA mode. The experimental setup is shown in Figure S1A. The Crinone® was packed to approximate 20 cm height in McCartney bottles, avoiding the introduction of air bubbles and allowed to sit overnight. The analytical probe (TA-10) was then compressed into sample at a defined rate (2 mm /s) and to a defined depth (15 mm) twice, allowing a delay period of 15 s between consecutive compressions. Mechanical properties such as hardness, compressibility, adhesiveness, and cohesiveness were determined [76]. All analyses were performed at least five times at ambient temperature.

#### *2.3.8.2 Muco-adhesion test*

The mucoadhesive strength of the Crinone® gel was evaluated by measuring the force and work required to detach the gel from a mucin disc under a 1.5 kg load cell in compression mode. The experimental setup is shown in Figure S1B. 0.1M Acetic acid buffer was prepared by dissolving 1.85 g sodium acetate and 1.65 g acetic acid in 400 mL deionized water. Adjust pH to 4.5 using HCl or NaOH then add distill water until the volume is 0.5 L. Filter paper was cut into small discs with a diameter of 3.18 cm. These discs were hydrated by 50 uL of 8% porcine stomach mucin in 0.1 M acetic acid buffer (pH = 4.5) before the measurement. The hydrated discs were attached to the lower end of the probe (TA10) with a double side tape. Crinone® gel (100 uL) were transferred to fixture. The probe holding the mucin disc was lowered to the surface of the gel with a target force of 1 N and kept in contact for 60 s, and then the probe was moved upward with a constant speed (2 mm/s). Maximum detachment force was obtained from the force-distance graph as adhesive force (N) [77]. The area under the curve (AUC) was calculated

from force-distance plot as adhesiveness (mJ) [77]. The tests were conducted at ambient temperature, and each experiment was carried out at least five times.

#### *2.3.8.3 Syringeability test*

The syringeability of Crinone® gel was determined using the texture analyzer (AMETEK Brookfield CT-3) in compression mode. The experimental setup is shown in Figure S1C. 1 mL Air-Tite™ Bulk Unsterile Syringe was filled with 0.5 mL of the Crinone® and held in place with a clamp. The upper probe of the texture analyzer moved downwards until it came in contact with the syringe barrel base. The work required to expel the contents for a distance of 20 mm was measured. The area under the resulting curve was used to determine the work of expulsion (mJ). The tests were conducted at room temperature and each experiment was repeated five times.

### *2.3.9 Rheology measurements*

#### *2.3.9.1 Steady shear viscosity*

The flow curves of the Crinone® gel were determined using a Discovery HR-3 hybrid rheometer (Waters, TA instrument, USA) in flow ramp mode. The measurements were performed in a parallel plate geometry with a diameter of 40 mm and with a solvent trap to limit evaporation during measurement. The geometry gap of the plate was set at 0.5 mm and the running temperature was at 25°C. The gel was applied on to the lower plate, ensuring that formulation shearing was minimized and allowed to equilibrate for at least 1 min before the analysis. The flow curves were measured over a range of shear rates (0.1–100 $s^{-1}$) within 60 seconds. Each data point represents the mean of at least three replicate analyses, with the relative standard deviation (RSD) consistently below 5%. Error bars have been omitted for clarity, as the variation in shear stress and viscosity values across replicates was minimal.

#### *2.3.9.2 Oscillatory rheometry*

The frequency dependence of dynamic viscoelastic parameters in Crinone® was determined using the Discovery HR-3 hybrid rheometer (Waters, TA instrument, USA) at the oscillatory mode. Experiments were conducted using a parallel plate geometry (4 cm diameter) at 25°C. The

geometry gap of the plate was set at 0.5 mm. The gel was applied on to the lower plate, ensuring that formulation shearing was minimized and allowed to equilibrate for at least 1 min before the analysis. In oscillatory measurements, linear viscoelastic regions (LVR), where the stress was directly proportional to strain and modulus remained constant, was determined first by amplitude sweep from 0.01 to 100 Pa at frequencies of 0.1 and 1.0 Hz. Accordingly, stress or strain values were selected within the defined LVR. Oscillatory frequency sweep analysis was performed over the frequency range of 0.1–10 Hz employing a constant displacement of 0.1% strain. The elasticity modulus G (storage modulus) and the viscosity modulus G (loss modulus) were obtained under dynamic conditions. Each point represented the mean of at least triplicate analysis. Error bars have been omitted to retain clarity. The coefficient of variation of replicate analyses was less than 5% in all cases.

### *2.3.10 In vitro release test (IVRT)*

The *in vitro* release of Crinone® was conducted using an Agilent DS-708 Dissolution system combined with dialysis bag. This method was developed based on the recommended approach for progesterone gel listed in the FDA Dissolution Database, with certain adjustments made according to our laboratory conditions. The Float-A-Lyzers® G2 dialysis bag was pretreated with 10% ethanol to remove the glycerin following the manufacturer's instruction. These resulting bags were rinsed with deionized water overnight to achieve maximum membrane permeability. Crinone® gel (100 mg) was added to the dialysis bag, followed by 2 mL of release medium (water: methanol, 80:20, v/v). Then the top of the dialysis bag was attached to the lower end of the dissolution shaft with tape. The release vessel was filled with 900 mL of release medium, the temperature was set to 37°C, and the stirring speed was adjusted to 100 rpm. After initiating the test, 1 mL release samples were collected at specific time intervals (1, 2, 4, 8, 10, 24 and 48 hours) and an equal volume of fresh release medium was replaced. For each batch, all experiments were repeated three times.

The concentration of progesterone in release sample was quantified by Waters ACQUITY UPLC H-class system with a C18 column (ACQUITY® BEH, 100 mm × 2.1 mm, 1.7 µm). The mobile phase was a mixture of acetonitrile and water (70:30, V/V), using a flow rate at 0.3 ml/min and an isocratic gradient. All solvents used for mobile phase preparation were HPLC grade. Detection wavelength was 254 nm and injection volume was 10 µL. The release samples

were filtered using a 0.22 µm syringe filter before UPLC analysis. The calibration curves exhibited good linearity within the range of 0.1–10 µg/mL, with a correlation coefficient of 0.9997.

An similar factor (f2) comparison test was conducted to identify any significant difference in the release among different batches of Crinone®, employing the following formula [78]:

$$f2 = 50 \log \left[ \frac{100}{\sqrt{1 + \frac{\sum_{i=1}^{n} (R_t - T_t)^2}{n}}} \right]$$

Where n represents the number of time points, Rt and Tt denote the cumulative release value of the reference and test products at time point t, respectively. An f2 $\geqslant$ 50 indicates a comparable release behavior between the reference and test formulation.

### *2.3.11 Statistical analysis*

The data are presented as mean ± standard deviation (SD). Statistical analysis was conducted by ordinary one-way ANOVA multiple comparisons using GraphPad Prism software. Differences were considered statistically significant at a 95% confidence level ($\alpha = 0.05$).

## 2.4 Results

### *2.4.1 Appearance and pH measurement*

Crinone® is a soft, white to off-white gel that contains progesterone across all three tested batches and the pH of those Crinone® is around 3.3 (Table S2). Given that Crinone® is a viscous oil-in-water gel that adheres strongly to surfaces, extra cleaning of pH electrodes should be applied between two measurements. We also employed pH test strips (Fisherbrand™ pH Test Strips, 2-9) as an alternative. All Crinone® lots gave us a reading of 3.5, which shows a deviation from the pH meter readings. pH strips may have some advantage for fast screening where efficiency outweighs the need for minor precision gains. But for applications requiring precise pH determination, pH meter measurements remain the preferred and more reliable method.

### *2.4.2 Globule size distribution*

The results in Table 2.4-1 summarize the globule size distribution of Crinone®. The D10, D50, and D90 values of the three different batches of Crinone® fall within a similar range, indicating consistent size distribution across batches. Figure S2 presents histograms of the globule size distribution for each batch, showing that the distribution ranges are also uniform.

Table 2-1 Globule size distribution of Crinone® determined by Mastersizer. (n = 3, mean ± SD)

| Lot number | D10/μm | D50/μm | D90/μm | Span |
|---|---|---|---|---|
| 100046739 | 9.06±0.52 | 19.85±1.27 | 37.92±2.98 | 1.45±0.03 |
| 100048963 | 7.84±0.63 | 18.18±1.53 | 35.79±3.58 | 1.54±0.03 |
| 100049672 | 9.37±0.37 | 18.33±3.35 | 36.99±5.20 | 1.59±0.09 |

### *2.4.3 Crystal particle morphology of Crinone® under polarized microscopy and SEM*

The optical microscopy image shows the crystal particles of all three batches of Crinone® gel. Under bright field, progesterone, the active pharmaceutical ingredient (API) in Crinone®, is observed as micron-sized suspensions dispersed within the gel matrix (Figure 1, upper panel). This matrix is formed by cross-linked acrylic acid polymers, including carbomer and polycarbophil. Under polarized light, progesterone crystals exhibit anisotropy and produce

birefringence (Figure 2.4-1, lower panel). This birefringence demonstrates that, progesterone retains its crystalline characteristics in the gel and has not undergone polymorphic transformation during the manufacturing process, nor have the matrix materials masked its crystalline properties [79]. If the drug were in an amorphous state, this phenomenon would not occur [79]. The morphology of all three batches of Crinone® under the microscope is very similar, and their crystal habits under polarized light are also consistent.

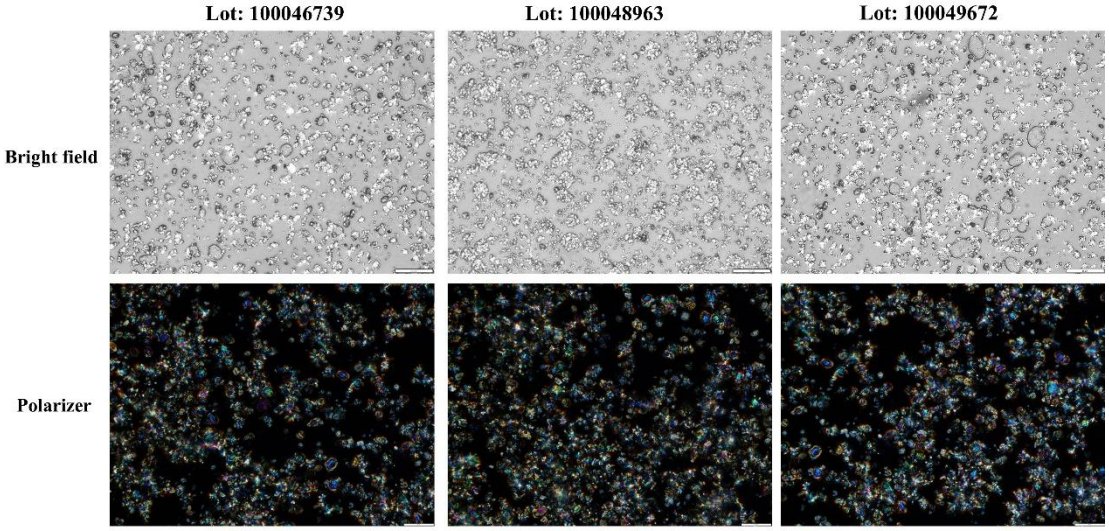


Figure 2-1 Microscopic images of three batches of Crinone® under bright field (upper panel) and polarized light (lower panel). The scale bar represents 20 μm.

We further observed crystal particle using SEM at higher magnification. As shown in Figure 2.4-2, progesterone crystals in all three different batches of Crinone® are encapsulated within the gel matrix in the form of micron-sized suspensions. The crystalline particles of the API are clearly visible and demonstrate good integration with the polymer matrix. The morphological results of the three batches are highly consistent, further demonstrating the stability and uniformity of the product quality.

In preparing the SEM samples, fresh gel was applied directly onto a metal stub and air-dried for 24 hours prior to imaging. Freeze-drying was initially explored but resulted in large sheet-like structures that distorted the native microstructure, and gold coating was also tested but showed no noticeable improvement. Therefore, air-drying without coating was employed to preserve the natural morphology of the gel and crystalline particles. This careful preparation allowed us to reliably visualize the surface features and crystalline distribution within the gel matrix.

These observations not only confirm the uniform dispersion of progesterone crystals but also provide insight into the microstructural interactions between the API and polymer network. Such information is valuable for understanding the product's physical stability and may guide the design and quality control of similar semisolid vaginal formulations.

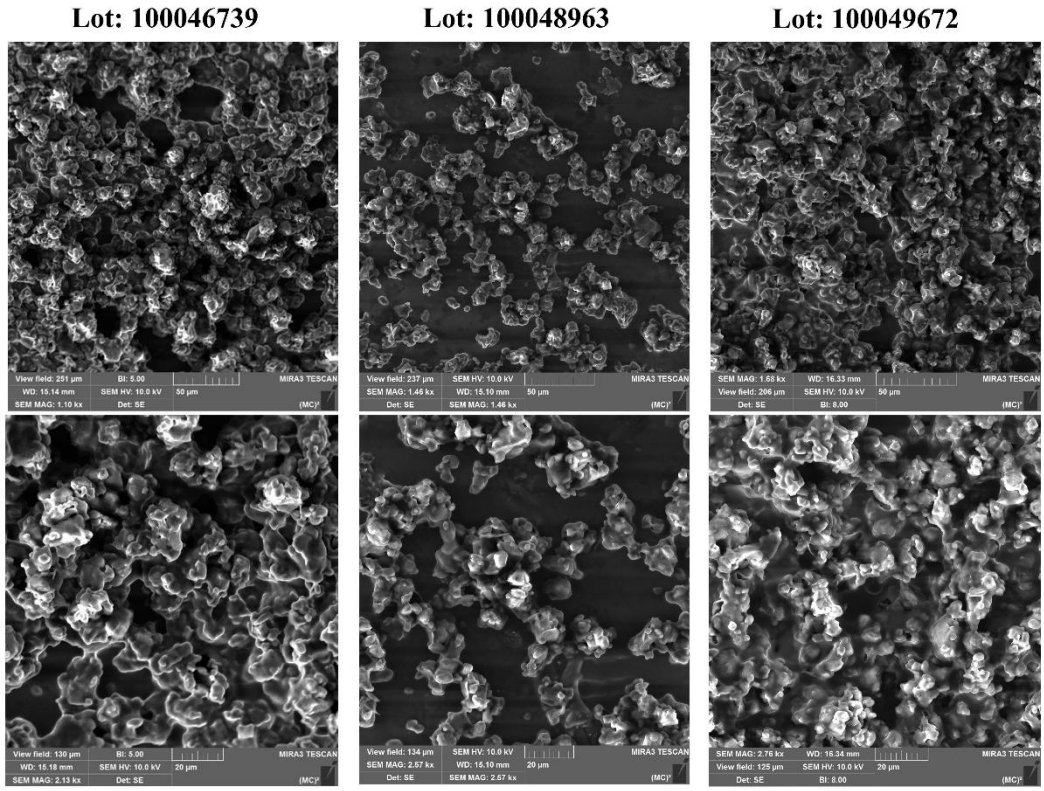


Figure 2-2 SEM images of three batches of Crinone®. The scale bar in the upper panel represents 50 μm and lower panel represents 20 μm.

### *2.4.4 Solid X-ray diffraction (XRD)*

Using polarized light microscopy and scanning electron microscopy, we observed that progesterone remains dispersed in the gel matrix in its crystalline form. To further verify the crystalline state of the API in the gel formulation, solid X-ray diffraction (XRD) of three different batches of Crinone® were studied. The characteristic peaks of progesterone were identified at 10.55°, 12.70°, 14.55°, 15.35°, and 16.95° [80,81]. These diffraction peaks correspond to crystal form I of progesterone. In Figure 2.4-3, these characteristic peaks are consistently present in the three different batches of Crinone®, confirming that progesterone is present in a crystalline form in the gel. The manufacturing process and storage conditions did not alter the crystalline state of the API in Crinone®.

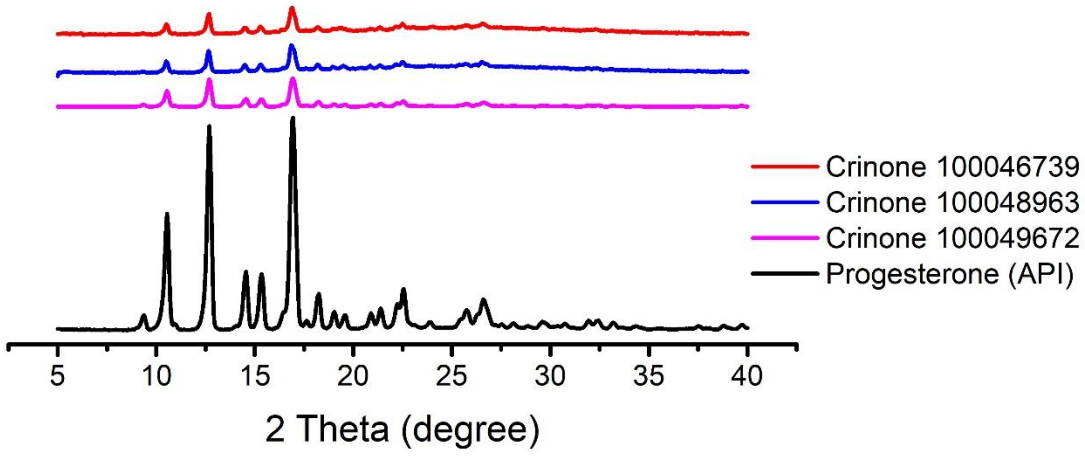


Figure 2-3 X-rays diffraction patterns of progesterone (API) and three different batches of Crinone®. The characteristic peaks of progesterone were identified at 10.55°, 12.70°, 14.55°, 15.35°, and 16.95°.

### *2.4.5 Differential Scanning Calorimetry (DSC)*

As shown in the Figure 2.4-4, the melting point of progesterone is around 128 ℃, demonstrating API is in crystal form I, which is the most common and stable progesterone crystal type [80]. The carbomer 934P and polycarbophil, which are the gel former, do not show obvious endothermic peaks in dry powder state under the current magnification. Physical mixture of API with polymers powder (carbomer 934P and polycarbophil) do not affect API melting point, still around 128 ℃. In contrast, the Crinone® exhibits markedly different calorimetry compared to the API. The gel showed a broad peak in the range of 100–150 °C, rather than the sharp endothermic peak at 128 °C observed for progesterone powder. The primary aim of this study was to compare the *in vitro* characteristics across different batches of Crinone®. All three batches analyzed displayed similar DSC profiles, indicating highly consistent thermodynamic properties and suggesting good batch-to-batch reproducibility of the formulation.

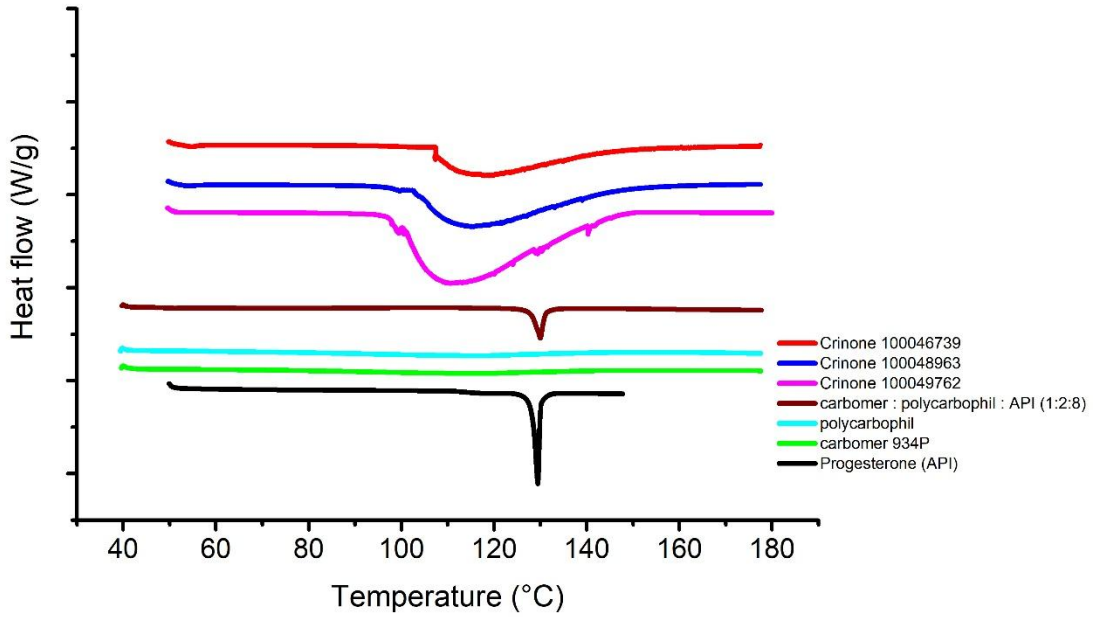


Figure 2-4 Differential scanning calorimetry curves of different ingredients in Crinone® and formulations.

### *2.4.6 Texture analysis*

#### *2.4.6.1 Mechanical properties of Crinone®*

Vaginal gel formulations require optimal mechanical properties to ensure patient acceptability and clinical efficacy. These properties include ease of application, high adhesiveness and recovery, low hardness, and longer retention time at the application site, all of which contribute to the maximum benefit of the formulation [76,82]. TPA is a rapid and straightforward analytical technique widely used for the mechanical characterization of pharmaceutical gels and semi-solid systems. This method involves twice compressing a solid analytical probe into the sample at a defined depth and rate, with a delay period between compressions [76]. The resultant force-time plot provides valuable mechanical parameters that reflect the physical gel structure [83]. In this study, the mechanical properties of the formulations were evaluated using TPA, and the corresponding mechanical properties are summarized in Table 2.4-2.

The hardness and compressibility values of the formulations represent the ease of taking the formulation from the container and applying it to the mucosal area [83]. From the experimental results, we can see that the hardness and compressibility of the three different batches of

Crinone® are very similar. Adhesiveness reflects the strength of the bond between the gel and the application site [77]. The three batches of Crinone® gel exhibit very similar adhesiveness values. Cohesiveness, on the other hand, describes the formulation's structural response to repeated shearing stresses [76]. Similarly, the three batches of Crinone® also demonstrate comparable cohesiveness values. This TPA approach allows for the systematic assessment of textural properties, offering critical insights into the mechanical behavior of semi-solid formulations during development.

Table 2-2 Mechanical properties of Crinone®. (n = 5, mean ± SD)

| Lot number | Hardness (N)[a] | Compressibility (mJ)[b] | Adhesiveness (mJ)[c] | Cohesiveness[d] |
|---|---|---|---|---|
| 100046739 | 0.260 ± 0.006 | 1.92 ± 0.09 | 1.21 ± 0.03 | 0.95 ± 0.03 |
| 100048963 | 0.255 ± 0.002 | 1.93 ± 0.12 | 1.24 ± 0.02 | 0.94 ± 0.03 |
| 100049672 | 0.260 ± 0.011 | 1.94 ± 0.01 | 1.23 ± 0.01 | 0.99 ± 0.01 |

Hardness [a]: the force required to attain a given deformation;

Compressibility[b]: the work required to deform the product during the first compression of the probe;

Adhesiveness[c]: the work necessary to overcome attractive forces between the surface of the sample and the surface of the probe;

Cohesiveness[d]: the strength of the internal bond within product

#### *2.4.6.2 Muco-adhesion test*

Muco-adhesiveness is a critical property of vaginal gels, as it determines the formulation's ability to remain at the application site and provide sustained therapeutic effects [76]. Texture analysis is commonly used to evaluate muco-adhesiveness by measuring the force required (maximum detachment force) or the work needed (area under the force-time curve) to remove a dosage form from a substrate. These measurements provide insights into the force and work of adhesion, respectively. As shown in Table 2.4-3, there is no significant difference in the adhesive force and work among the three batches of Crinone®, demonstrating that all three batches exhibit similar adhesiveness. The consistent adhesive properties across different batches ensure that,

after application, the products provide similar adhesion to the vaginal surface, guaranteeing comparable residence times.

Table 2-3 Muco-adhesiveness and syringeability of Crinone®. (n = 5, mean ± SD)

| Lot number | Adhesive force (N) [a] | Adhesiveness (mJ)[b] | Work of expulsion (mJ)[c] |
|---|---|---|---|
| 100046739 | 0.348 ± 0.017 | 0.20 ± 0.02 | 78.59 ± 7.95 |
| 100048963 | 0.344 ± 0.019 | 0.20 ± 0.02 | 74.40 ± 3.55 |
| 100049672 | 0.340 ± 0.011 | 0.21 ± 0.04 | 75.04 ± 5.53 |

Adhesive force [a]: the force required to remove gel from mucin disc;
Adhesiveness[b]: the work required to remove gel from mucin disc;
Work of expulsion[c]: the work necessary to dispense gel out of syringe;

#### *2.4.6.3 Syringeability*

Syringeability is a critical parameter for the practical administration of gels using a syringe or applicator [76]. It is evaluated based on the force needed to dispense the formulations during application [84]. As shown in Table 2.4-3, the work of expulsion values of the three batches of Crinone® are very similar, indicating that during practical use, a similar amount of gel can be dispensed into the vagina with the same applied force, ensuring consistent drug performance.

### *2.4.7 Rheological characterization*

#### *2.4.7.1 Steady shear behavior*

To determine the rheological characteristics of Crinone®, the shear stress and viscosity changes upon shear rates was evaluated. The flow curves of three different batches of Crinone® are presented in Figure 2.4-5. The relationship between the shear stress and shear rate of Crinone is not linear, and the viscosity is not constant, indicating that this colloid is a non-Newtonian fluid. The viscosity decreases with the increase in shear rate, which is a typical shear-thinning phenomenon [85]. The three different batches of Crinone® all exhibited similar shear-thinning properties, demonstrating their convenience and usability during application.

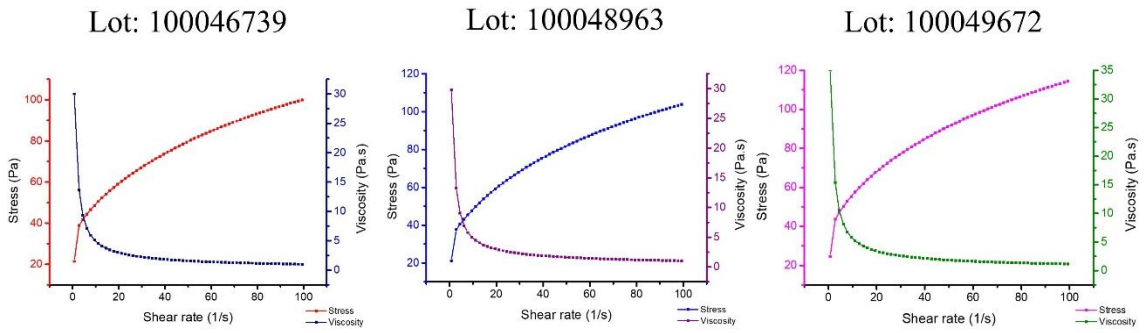


Figure 2-5 Flow curves of different batches of Crinone®: shear stress and viscosity as a function of shear rate.

### *2.4.7.2 Oscillatory rheometry*

The elasticity modulus (G', storage modulus) represents the energy stored and recovered per cycle of deformation, reflecting the solid-like elastic behavior of a material [86]. In contrast, the viscosity modulus (G", loss modulus) measures the material's viscous response under oscillatory deformation, indicating its ability to dissipate energy and its liquid-like behavior. As shown in Figure 2.4-6, oscillatory frequency sweep tests revealed that the elasticity modulus (G') of the gel was consistently higher than the viscosity modulus (G") across all frequency points, demonstrating a predominantly solid-like behavior of Crinone®. This elastic behavior is critical for influencing the spreading, extensibility, and retention of the formulation after *in vivo* administration, particularly during the squeezing and spreading process [87]. These three different batches of Crinone® exhibited similar oscillatory rheometry results, demonstrating the consistency in product quality.

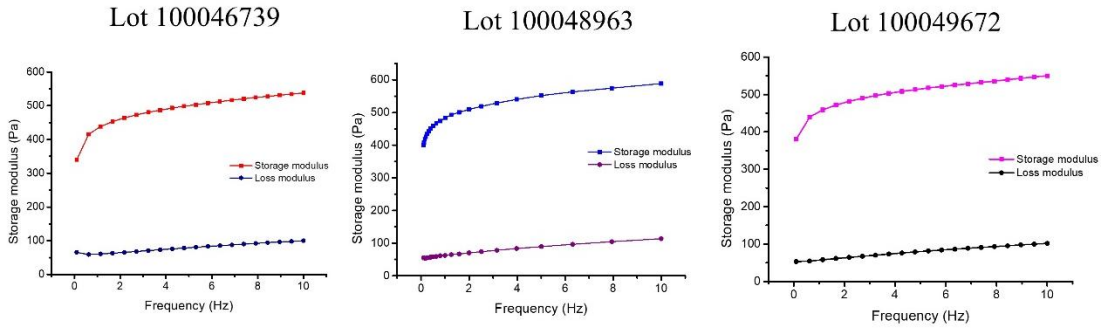


Figure 2-6 Oscillatory rheometry of Crinone®: effect of increasing oscillatory frequency on the elasticity modulus (G', storage modulus) and viscosity modulus (G", loss modulus).

### *2.4.8 In vitro release studies*

The *in vitro* release profiles of Crinone® through a dialysis bag are presented in Figure 2.4-7. As shown, Crinone® achieved a gradual drug release over 48 hours, ultimately exceeding 80%

release. Three different batches of Crinone® exhibited comparable release kinetics, which was further quantified using the f2 similarity factor analysis (Table S3). All f2 values exceeded the 50-threshold, statistically confirming equivalent release patterns. These drug release experiments further confirm the consistency in the quality of different Crinone® batches and the stability of the manufacturing process. In this study, methanol/water (20:80, v/v) was chosen as release medium based on FDA dissolution database recommendation for progesterone gels.

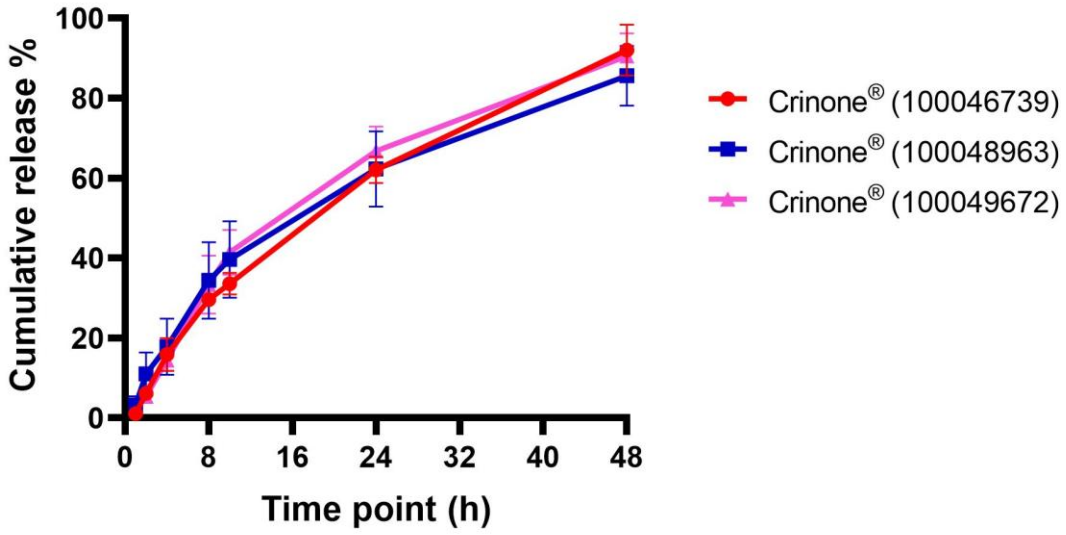


Figure 2-7 The release profiles of different batches of Crinone®. (n = 3, mean ± SD)

## 2.5 Discussion

The development of a generic version of Crinone® requires a comprehensive understanding of the physicochemical and structural attributes that affects its *in vivo* performance. The FDA Draft Guidance for Progesterone Vaginal Gel emphasizes that, in addition to qualitative (Q1) and quantitative (Q2) sameness, generic products should demonstrate equivalence in relevant physicochemical and structural (Q3) properties[73]. These attributes are particularly important for semisolid vaginal formulations because they directly influence product retention, drug release, and ultimately local and systemic exposure. Therefore, this chapter sought to identify and evaluate the key physicochemical attributes of Crinone®, including pH, globule size distribution, morphology, crystalline and thermal properties, mechanical behavior, mucoadhesion, rheological properties, and *in vitro* release. The combined interpretation of these results provides insight into the mechanisms underlying the performance of Crinone® and may

help define the critical attributes that should be matched during development of a therapeutically equivalent generic product.

The physiological pH of the female vagina is acidic, typically around 3.5 to 4.5, primarily due to the lactic acid secreted by healthy vaginal microbiome, predominantly Lactobacillus species, which helps to establish a defense against the invading pathogens [88]. Therefore, maintaining an appropriately low pH is crucial for most vaginal delivery products. The pH of Crinone® gel falls well within the normal fluctuation range, which not only ensures excellent biocompatibility and minimizes irritation, but also supports the stability of the native microbiome.

PLM, SEM, XRD, and DSC together provide important insight into the physical state of P4 within Crinone®. Microscopy demonstrated that progesterone remained dispersed throughout the gel as micro-sized crystalline particles. XRD further confirmed that the characteristic diffraction peaks of progesterone crystal form I were retained in all three batches, indicating that the manufacturing process did not induce polymorphic transformation or amorphization of the drug. Preservation of progesterone in its stable crystalline form is likely important for both the long-term physical stability and sustained-release behavior of the formulation, since crystalline progesterone generally dissolves more slowly than an amorphous or fully solubilized drug.

Interestingly, although the crystalline form of progesterone remained unchanged, DSC revealed that its thermal behavior was substantially modified after incorporation into the gel matrix. Pure progesterone showed a sharp melting endotherm at approximately 128 °C, whereas Crinone® exhibited a broad transition between 100 and 150 °C. A physical mixture of progesterone with carbomer and polycarbophil still retained the sharp melting peak, suggesting that simple mixing of the dry components was not sufficient to alter the thermal behavior of the drug. Instead, the broadened endotherm likely reflects the microenvironment within the complete formulation. Progesterone crystals in Crinone® are dispersed as micron-sized particles within oil droplets and a crosslinked polymeric network, and this reduced particle size may broaden the melting process. In addition, interactions with mineral oil, glycerin, water, carbomer, and polycarbophil may partially wet or plasticize the crystal surface, while the structured gel network may physically constrain the crystals and create a heterogeneous environment with a range of local melting temperatures. Thus, although progesterone retains its crystal structure, its thermodynamic behavior is clearly influenced by the surrounding gel matrix.

The adhesion of semi-solid formulations to biological surfaces is a complex phenomenon influenced by multiple interactions, including polymer-solvent interactions, cohesive forces within the dosage form, and polymer-substrate interactions [77]. Stronger mucoadhesive forces result in better retention of the formulation within the vaginal cavity. For polymers like polycarbophil and carbomer, muco-adhesion is often attributed to the formation of hydrogen bonds between the polymers and the secretory mucins on the tissue surface [77]. Additionally, complementary chemical interactions, such as van der Waals forces and hydrophobic effects, may further enhance muco-adhesion. These interactions collectively contribute to the formulation's ability to adhere effectively to mucosal tissues, ensuring optimal performance.

The rheological properties of Crinone® are also closely related to its expected in vivo performance. Following administration, the vaginal gel spreads over the mucosal surface, coats the epithelium, and remains in place for sufficient time to release the drug or provide adequate protection. This behavior is highly dependent on the rheological properties of the system, which influence its spreading, extensibility, and residence time in the vaginal area [87]. Crinone® exhibited a typical non-Newtonian, shear-thinning behavior, in which viscosity decreased as shear rate increased. Such behavior is advantageous during application because the gel becomes easier to spread under the high shear conditions generated during squeezing and administration. After application, when the shear force is removed, the viscosity recovers to its original high value, helping the formulation remain localized within the vaginal cavity and prolonging its residence time. In addition, the oscillatory rheology results, where G' remained higher than G'' across the tested frequency range, indicate that Crinone® behaves as a predominantly elastic, solid-like material. This elastic network likely contributes to its ability to resist clearance by vaginal fluids and maintain prolonged contact with the mucosal surface.

The *in vitro* release of topical gel formulations is a crucial aspect of drug development. For pharmaceutical companies, *in vitro* release studies can be used to screen lead formulations during the development stage. Through the manufacturing cycle, these studies serve as a quality control tool to ensure batch-to-batch consistency and compliance with pharmaceutical specifications. For regulatory agencies, appropriate *in vitro* release studies can facilitate the comparison between generic and innovator drugs, aiding the drug approval process [75]. Although the experiment we establish in this chapter does not involve physiologically relevant conditions, it can serve as a

powerful reference for discriminative assessment to support future generic bioequivalence assessment and quality control of the final product.

## 2.6 Conclusion

This study presents a comprehensive characterization of Crinone®, elucidating its structural and functional attributes. PLM, SEM, and XRD results confirmed progesterone's crystalline dispersion within the gel matrix, while DSC revealed drug-polymer interactions evidenced by the shift in thermal profile. All batches of Crinone® exhibited consistent properties in terms of globule size distribution, mechanical characteristics, muco-adhesiveness, syringeability, and shear-thinning rheological behavior that facilitates application. Furthermore, the *in vitro* release profiles of Crinone® across batches were highly similar, achieving gradual drug release within 48 hours. This detailed psychochemical profile establishes a scientific foundation for bioequivalent generic development while advancing our understanding of complex vaginal drug delivery systems, ultimately contributing to improved therapeutic outcomes.

# Chapter 3 Development of P4-Cyclodextrin Complex Based Gel for Vaginal Delivery

## 3.1 Abstract

Progesterone (P4) is widely used for vaginal delivery in luteal phase support and prevention of preterm birth; however, its poor aqueous solubility limits drug release and absorption. In this chapter, a novel vaginal hydrogel based on a P4-Cyclodextrin inclusion complex was developed to improve the performance of vaginal progesterone delivery. Phase-solubility screening demonstrated that all tested cyclodextrins produced AL-type profiles with P4, while random methylated β-cyclodextrin (RAME-β-CD) showed the highest solubilization efficiency and the lowest cyclodextrin-to-drug weight ratio. A P4-RAME-β-CD inclusion complex was prepared by microwave irradiation method and characterized by FTIR, DSC, and XRD, which confirmed the formation of P4-CD inclusion complex. The optimized complex was incorporated into a carbomer/polycarbophil hydrogel and compared with Crinone®. The P4-CD gel exhibited significantly greater mucoadhesion and improved syringeability. Rheological evaluation showed that the formulation possessed desirable shear-thinning and predominantly elastic behavior suitable for vaginal application. In Franz cell release testing, the P4-CD gel released P4 more rapidly than Crinone®, while dialysis bag testing showed similar release under sink conditions. In excised sheep vaginal tissue, the P4-CD gel achieved more than three-fold higher P4 permeation than Crinone®. A preliminary *in vivo* pharmacokinetic study in mice further demonstrated significantly increased systemic exposure, with a 2.5-fold higher $AUC_{0–8}$ compared with Crinone®. These findings indicate that cyclodextrin complexation is an effective strategy to enhance the vaginal delivery of progesterone and that the developed P4-CD hydrogel represents a promising alternative to current commercial formulations.

## 3.2 Introduction

In recent decades, infertility has become a significant global public health issue, affecting approximately 8% to 12% of reproductive-aged couples worldwide [89]. Given declining fertility rates and the increasing average age of childbearing, the demand for Assisted Reproductive Technology (ART) has increased. Central to the success of ART and the maintenance of a healthy pregnancy is the steroid hormone progesterone (P4). Known as the "hormone of pregnancy," P4 is indispensable for establishing a receptive uterine environment. It transforms the endometrium from the proliferative into the secretory phase, facilitates embryo implantation, and subsequently promotes maternal immune tolerance while suppressing myometrial contractility to prevent miscarriage and preterm labor. Nowadays, P4 supplementation has become the clinical standard for luteal phase support and the management of high-risk pregnancies [2].

In current clinical practice, P4 is commonly administered via oral, intramuscular, and vaginal routes, each presenting distinct advantages and limitations. Although effective, daily intramuscular injections (IM) often cause patient discomfort and injection site pain, leading to low compliance [32]. Oral delivery can avoid pain caused by IM injection but it is limited by extensive hepatic first-pass metabolism, resulting in a systemic bioavailability of less than 10% and central nervous system side effects related to the system exposure of P4 [19]. Vaginal drug delivery is an effective alternative. It avoids hepatic metabolism and utilizes the ‘uterine first-pass effect’ to direct transport the drug to uterine tissues via local circulatory pathways—to achieve high local concentrations with fewer systemic side effects [22]. Current commercial products, such as Crinone®, use micronized P4 in an oil-in-water emulsion gel. These suspension-based systems often exhibit slow drug release and erratic absorption profiles. Furthermore, Crinone® is often associated with a requirement for twice-daily dosing, messy leakage, and objectionable vaginal discharge from accumulated insoluble carrier residues, all of which significantly reduce patient compliance. There is a clear clinical need for formulations that deliver P4 in a molecularly dispersed state to improve mucosal permeation.

As a BCS Class II compound, P4 has very low aqueous solubility, which limits its dissolution and absorption from aqueous gels. To overcome this solubility limitation, cyclodextrin complexation provides an effective formulation strategy. Cyclodextrins (CDs) are

cyclic oligosaccharides produced from natural starch. As natural sugar-based molecules, usually they are considered safe, non-toxic, and highly biocompatible. The structure of CDs features a hydrophobic inner cavity and a hydrophilic outer surface. This unique geometry allows them to encapsulate various hydrophobic drug molecules through non-covalent interactions, forming stable inclusion complexes. This process significantly increases the water solubility, stability, and bioavailability of poorly soluble drugs. Due to these properties, cyclodextrins are widely used in pharmaceutical development as a standard technology to address drug solubilization challenges [90].

Here, we introduce our novel P4 vaginal hydrogel, based on P4-cyclodextrin inclusion complex. Following a systematic screening of commonly used cyclodextrins, randomly methylated β-cyclodextrin (RAME-β-CD) was identified as the optimal candidate for enhancing P4 solubility. The P4-CD complex was successfully prepared using a microwave-assisted method and subsequently characterized by differential scanning calorimetry (DSC), X-ray diffraction (XRD), and Fourier-transform infrared spectroscopy (FTIR). After incorporating P4-CD complex into a hydrogel, this formulation was evaluated through comprehensive *in vitro* characterization, including mucoadhesion, syringability, rheology, *in vitro* release and permeation with comparison made against Crinone®. This formulation demonstrated improved *in vitro* performance across multiple parameters. Finally, a preliminary pharmacokinetic study in mice was conducted to assess systemic exposure, where the developed formulation exhibited enhanced bioavailability compared to Crinone®, supporting its potential for further investigation.

## 3.3 Materials and Methods

### *3.3.1 Materials*

Progesterone (micronized powder, USP grade) was purchased from Spectrum® Chemical Manufacture Corporation (New Brunswick, NJ, USA). (2-Hydroxypropyl)-α-cyclodextrin, (2-hydroxypropyl)-β-cyclodextrin and mucin from porcine stomach were purchased from Millipore Sigma(St. Louis, MO, USA). (2-hydroxypropyl)-γ-cyclodextrin (CAVASOL W8 HP PHARMA) and randomly methylated-β-cyclodextrin (CAVASOL W7 M PHARMA) were kindly provided by Wacker Chemical (Ann Arbor, MI, USA). Sulfobutylether-β-CD (Captisol®) was kindly provided by Ligand Pharmaceuticals (Jupiter, FL, USA). Carbomer 934P (Carbopol® 934) and polycarbophil (Noveon® AA-1) were kindly provided by Lubrizol (Wickliffe, OH, USA). NaCl,

KOH, $Ca(OH)_2$, bovine serum albumin, lactic acid, acetic acid, glycerol, urea, glucose, sorbic acid, HCl, NaOH, Span 20/80/85 and Tween 20/60/80 were kindly provided by Croda (Plainsboro, NJ, USA). Ethanol (200 proof, USP, Decon™ Labs) was purchased from Fisher Scientific (NH, USA). High-Performance Liquid Chromatography (UHPLC) grade methanol, acetonitrile and water were purchased from Fisher Chemical (Waltham, MA, USA). Progesterone-$d_9$ was purchased from Cayman Chemical (Ann Arbor, MI, USA).

### *3.3.2 Preparation of simulated vaginal fluid (SVF)*

Although there is no standard receipt for simulated vaginal fluid, Owen and Katz's receipt was widely used for vaginal environment involved experiments. formulation: NaCl (3.51 g), KOH (1.40 g), $Ca(OH)_2$ (0.222 g), bovine serum albumin (0.018 g), lactic acid (2 g), acetic acid (1 g), glycerol (0.16 g), urea (0.4 g), and glucose (5 g), equivalent to 1 L. The pH will be adjusted to 4.5 using HCL reflecting the normal pH for a healthy woman in fertile years is between 4.0 and 5.0. This formulation can simulate the of interaction of vaginal fluid with vaginal topical products and proven useful for *in vitro* research of vaginal delivery drugs[91]

### *3.3.3 Solubility test of P4 in common buffer and surfactants solution*

The solubility of progesterone in various buffer and surfactant systems was determined using a shake-flask method. Briefly, excipients were dissolved in 1 mL water to prepare aqueous solutions at the desired concentrations (w/v) in a 2.0mL Eppendorf™ Protein LoBind™ Tubes. An excess amount of progesterone was then added to each solution and vortexed thoroughly for 30 secs. All samples were subsequently incubated at 37 °C in a shaking incubator at 80 rpm for 24 h to reach equilibrium. After incubation, samples were filtered with 0.22 um Millex™ PVDF syringe filter and then analyzed for progesterone concentration using UPLC with UV detection (UPLC-TUV). 1% Span 20, 1% Span 80, 1% Span 85%, 1% Tween 20, 1% Tween 60, 1% Tween 80, 5% HP-β-CD, 5% HP-γ-CD, PBS, acetate buffer and simulated vaginal fluid were prepared and tested for P4 solubility. All experiments were performed in triplicate, and results were reported as mean ± standard deviation.

### *3.3.4 Cyclodextrin screening by phase solubility study*

Phase-solubility analysis was performed to evaluate the solubilizing effect of different cyclodextrins on P4. Aqueous solutions of randomly methylated β-cyclodextrin (RAME-β-CD), hydroxypropyl-γ-cyclodextrin (HP-γ-CD), sulfobutylether-β-cyclodextrin (SBE-β-CD),

hydroxypropyl-β-cyclodextrin (HP-β-CD), and hydroxypropyl-α-cyclodextrin (HP-α-CD) were prepared at concentrations of 0, 5, 10, 20, and 50 mM individually. Excess amount of P4 was added to each solution and vortexed then incubated at 37 °C under 80 rpm for 72 hours. Excess P4 was removed through centrifuging at 13500 rpm for 10 min and filtered through 0.22 um Millex™ PVDF syringe filter. The concentration of dissolved P4 was quantified using the previously described UPLC method (section 2.3.10). Phase-solubility diagrams were constructed by plotting the equilibrium concentration of P4 against cyclodextrin concentration. The apparent stability constant ($K_{1:1}$) was calculated from the slope of the linear portion of the phase-solubility diagram according to the Higuchi–Connors equation [92]:

$$K_{1:1} = \frac{\text{slope}}{D_o(1 - \text{slope})}$$

Where $D_0$ represents the equilibrium solubility of P4 in the absence of the CD.

### *3.3.5 Cyclodextrin progesterone complex preparation*

Cyclodextrin inclusion complex can be obtained through various methods, like co-precipitation, kneading, simple aqueous solution approach, microwave-assisted method. Among these, we chose microwave irradiation to prepare P4-CD inclusion complex due to its advantage of high yields, cost and time saving[93–95]. Progesterone (1 g) and RAME-β-CD (8 g) were accurately weighed and placed into a conical flask. A volume of 5 mL of 50% (v/v) ethanol solution was added to the solid mixture. The flask was immediately vortexed for 30 seconds to ensure complete wetting of all powders. The mixture was then heated in a microwave oven at 900 W for 30 seconds and a transparent solution was obtained. After allowing the sample to cool to room temperature, it was rapidly frozen using liquid nitrogen and subsequently lyophilized overnight to remove all volatile solvents and moisture, yielding a white dry powder. The resulting solid was reconstituted in 10 mL of ultrapure water and placed in an incubator shaker maintained at 37°C with continuous agitation at 80 rpm for 3 hour to facilitate complete dissolution and complex formation. The final solution was filtered through a 0.22 µm filter. This procedure yielded a clear aqueous solution containing approximately 5% (w/w) progesterone encapsulated in the RAME-β-CD complex, ready for subsequent analysis or use.

### *3.3.6 Cyclodextrin progesterone complex characterization*

#### *3.3.6.1 Fourier transform infrared spectroscopy (FTIR)*

To confirm the complex formation, Fourier transform infrared (FTIR) spectra of progesterone (P4), RAME-β-CD, their physical mixture, and the P4–CD complex were recorded using an FTIR spectrophotometer (IRTracer-100, Shimadzu, Japan) equipped with an attenuated total reflectance (ATR) accessory. To enable direct comparison, a physical mixture of progesterone (P4) and cyclodextrin (CD) was prepared at the same weight ratio as in the P4–CD complex (P4:CD = 1:8). All physical mixtures used for subsequent characterization were prepared using this ratio. Spectra were collected over the range of 4000–650 $cm^{-1}$ in transmission mode, with a resolution of 4 $cm^{-1}$ and 40 scans per sample. A background spectrum was acquired prior to measurement.

#### *3.3.6.2 Differential scanning calorimetry (DSC)*

To evaluate the thermal behavior of the drug inclusion complex, a differential scanning calorimetry (DSC) study of P4, RAME-β-CD, their physical mixture and freeze dry P4-CD complex was carried out. The thermograms were recorded on a DSC system (Discovery DSC, TA Instruments, Waters, USA) at a scanning rate of 10 °C/min in an atmosphere of nitrogen using the range of 20–200 °C. The temperature calibration was performed periodically using indium as a standard.

#### *3.3.6.3 Solid X-ray diffraction (XRD)*

The crystalline property of P4-CD complex was analyzed by MINIFLEX 600 XRD (Rigaku, Osaka, Japan) coupled with a Cu Kα radiation. The sample of P4, RAME-β-CD, their physical mixture and freeze dry P4-CD complex were spread evenly into a thin layer with the spatula, and then gently compressed with a clean microscope slide to ensure a smooth and uniform surface suitable for diffraction analysis. The measurements were conducted at 40 kV and 15 mA. Diffraction patterns were collected over a 2θ range of 5°- 40°, with a step size of 0.05° and a scanning rate of 2°/min.

### *3.3.7 Preparation of P4-CD hydrogel formation*

The optimized P4–CD inclusion complex was incorporated into a mucoadhesive gel matrix comprising 4% P4 (as complex), 1% (w/w) carbomer 934P, 2%(w/w) polycarbophil, and 0.08% (w/w) sorbic acid in purified water. Accurately weighed amounts of carbomer 934P and polycarbophil were premixed and then slowly added to the P4–CD aqueous solution under

continuous stirring at 800 rpm using a homogenizer (IKA® EuroStar 20 Digital). After addition of the polymers, the homogenizer speed was reduced to 200 rpm, and the mixture was allowed to stir for 3 hours to ensure full hydration and swelling of the polymers. The sample will be centrifuged at 3000 rpm for 10 mins to remove the bubble and form a semitransparent homogenized hydrogel. Three different batches were prepared and stored in 5 ml tubes for further characterization.

### *3.3.8 Muco-adhesion test*

The muco-adhesion of the P4-CD gel and Crinone® gel was compared using the modified method we set up for reverse engineering of Crinone® (refer to section 2.3.8.2). In short, we prepared the 8% porcine stomach mucin solution by mixing 0.1M acetic acid buffer and porcine stomach mucin. Filter paper was cut into small discs with a diameter of 3.18 cm and sink in the 8% porcine stomach mucin solution for 10 secs and attached to the probe bottom (TA10) using a double side tape. The force and work required to detach the gel from the mucin disc under a 1.5 kg load cell in compression mode was measured. The P4-CD gel and Crinone® gel (100 uL) were transferred to fixture. The probe holding the mucin disc was lowered to the surface of the gel with a target force of 1 N and kept in contact for 60 s, and then the probe was moved upward with a constant speed (1 mm/s). Maximum detachment force was obtained from the force-distance graph as adhesive force (N). The area under the curve (AUC) was calculated from force-distance plot as adhesiveness (mJ). The tests were conducted at ambient temperature, and each experiment was carried out at least three times.

### *3.3.9 Syringeability test*

The syringeability of the P4-CD gel was determined following method previously described (Section 2.3.8.3.) using the texture analyzer in compression mode. In short, 1 mL syringe (Air-Tite™ Bulk Unsterile Syringe) was filled with 1 mL of the P4-CD gel and held in place with a clamp. The upper probe of the texture analyzer moved downwards until it contacted the syringe barrel base. The work required to expel the contents for a distance of 20 mm was measured. The area under the resulting curve was used to determine the work of expulsion (mJ). The tests were conducted at room temperature and each experiment was repeated three times.

### *3.3.10 Steady shear viscosity*

The rheological properties of the P4-CD gel were evaluated using the same procedures described in Sections 2.3.9.1. Briefly, measurements were performed using a Discovery HR-3 hybrid rheometer (TA Instruments, USA) with a parallel plate geometry (40 mm diameter, 0.5 mm gap) at 25°C. 700 µL of gel sample was accurately transfer to the center of lower plate using positive displacement pipette (Gilson® Microman® E, 100-1000 µL) and was allowed to equilibrate for at least 1 min before analysis. The flow curves were obtained over a shear rate range of 0.1–100 $s^{-1}$ within 60 seconds in flow ramp mode. Three different batches of P4-CD gel were each tested in triplicate.

### *3.3.11 Oscillation measurement*

Oscillation test was performed for P4-CD gel based on method described in Section 2.3.9.2. A parallel plate geometry (40 mm diameter, 0.5 mm gap) and 700 µL of P4-CD sample were used for this assay. In oscillatory measurements, linear viscoelastic regions (LVR), where the stress was directly proportional to strain and modulus remained constant, was determined first in oscillation amplitude sweep mode from 0.01 to 100% strain at frequencies at 1.0 Hz. Accordingly, 0.5% strain value was selected within the defined LVR. Oscillatory frequency sweep analysis was performed over the frequency range of 0.1–10 Hz employing a constant displacement of 0.5% strain. The elasticity modulus G' (storage modulus) and the viscosity modulus G'' (loss modulus) were obtained under dynamic conditions. Three different batches of P4-CD gel were each tested in triplicate.

### *3.3.12 In vitro release study*

Two in vitro release methods were established for preliminary performance assay. Based on FDA guidance for progesterone gel, Franz cell system is recommended for in vitro release test. Vertical Franz diffusion cells from PermeGear (Allentown, PA) with 1 $cm^2$ application area and 8 mL receptor volume were used for first method. An artificial MCE membrane (MF-Millipore™, 0.8 µm Pore Size, filter diam. 25 mm, hydrophilic) was mounted between the donor cell and receptor cell. Approximately 50 uL of gels were applied using the plunger rod of 3 mL syringes. The gel covered plunger was then gently pressed onto the MCE membrane to ensure uniform contact and full coverage of the predefined 1 $cm^2$ area. The exact loading weight of gels was calculated by the weight difference of the plunger rod before and after gel applying. The top of donor cell was sealed with a parafilm and the whole experiment was performed under 37 °C,

800 rpm stirring for each Franz cell. At predetermined time points (0.5, 1, 2, 4, 6, 8, 12, and 24 h), approximately 400 μL of the release medium was withdrawn from the sampling port and replaced with an equal volume of release medium. Collected samples were stored at 4°C until analysis. Progesterone concentrations were quantified using the previously described UPLC method. Each formulation (P4-CD gel or Crinone 4%) was tested in triplicate.

Besides, a simplified dialysis-based release method was evaluated using Spectrum™ Spectra/Por™ Float-A-Lyzer™ G2 dialysis devices (50 kDa MWCO). Before use, the dialysis bags were preconditioned overnight according to the manufacturer's instructions by sequential treatment with ethanol and water. Approximately 100 mg of P4-CD gel or Crinone 4% was loaded into each dialysis device using 100/200 μL Wiretrol micropipets (Drummond Scientific) and the exact loading amount was recorded by weight. Then 1.9 mL of release medium consisting of 5% (w/v) HP-β-CD in simulated vaginal fluid (SVF) was added into the dialysis bag. Then dialysis bags were then closed and immersed in 48 mL of the same release medium in capped glass bottles. The bottles were placed in an orbital shaking incubator maintained at 37°C and 80 rpm. At predetermined time points (0.5, 1, 2, 4, 6, 8, 12, and 24 h), 400 μL of the external release medium was withdrawn and immediately replaced with an equal volume of fresh medium maintained under the same conditions. Collected samples were stored at 4°C until analysis. Progesterone concentrations were quantified using the previously described UPLC method. Each formulation (P4-CD gel or Crinone 4%) was tested in triplicate.

### *3.3.13 In vitro permeation test*

*In vitro* permeability of P4 formulation was evaluated using vertical Franz diffusion cells from PermeGear (Allentown, PA). Sheep vaginal tissue was obtained from adult ewe, University of Michigan. The whole vaginal tract was fresh excised postmortem and sink in PBS in ice bath. Before mounted on the receptor cell, excess tissue was removed and cut into suitable size. Average thickness for all tissue samples was 700-800 um. Approximately 50 uL of vaginal gel formulation was pre-loaded onto the plunger rod of a 3-mL syringe barrel after removing the needle hub. The gel covered plunger was then gently pressed onto the excised tissue surface to ensure uniform contact and full coverage of the predefined 1 $cm^2$ application area of Franz Cell (diameter 11.28 mm, flat ground joint, 8ml receptor volume). Then 50 ul of SVF was added to each donor cell and the top of donor cell was sealed with a parafilm. After application, both the plunger and syringe barrel were weighed before and after gel deposition using an analytical

balance to determine the exact amount of formulation transferred to the tissue. The receptor chamber was filled with simulated vaginal fluid (SVF) containing 5% (w/v) hydroxypropyl-β-cyclodextrin (HP-β-CD) as the release medium. Franz cells were maintained at 37 °C using a circulating water bath to preserve physiologically relevant conditions. Following sample application, 50 µL of SVF was added to each donor chamber, which was then sealed with Parafilm. At predetermined time points (0.5, 1, 2, 4, 6, and 8 h), 500 µL of receptor medium was withdrawn from sampling port and immediately replaced with an equal volume of release medium. The experiments were performed in triplicates. All samples were kept in 4℃ and analyzed using UPLC-TUV method described above.

### *3.3.14 Pharmacokinetic study*

A total of 24 female rats were randomly assigned to six groups to receive a single intravaginal dose of either Crinone® or P4-CD gel (n = 4 groups per treatment). Mice were divided into two groups and received a single vaginal dose 50 µL of either 4% P4–CD gel or 4% Crinone® using 50/100µL Wiretrol micropipets (Drummond Scientific). Blood samples were collected from the submandibular vein at specific intervals (0.5,1,2, 3, 4, 8 h), and approximately 100 µL of whole blood was collected from cheek vein at each designated time point. The blood samples were immediately transferred into pre-chilled EDTA tubes and centrifuged at 4°C for 10 minutes at 13500 rpm to separate plasma. Following centrifugation, 40 µL of plasma was carefully aspirated and transferred into clean 1 ml tubes and stored at −80°C until further analysis by LC-MS.

### *3.3.15 Plasma sample pretreatment and LC/MS condition*

Mice plasma P4 concentrations were quantified using LC-MS(QDA) method adapted from a previously published method[96]. Liquid–liquid extraction (LLE) was performed to pretreat plasma samples for analysis. Briefly, 200 µL of methanol, 100 µL of progesterone-$d_9$ internal standard (ISTD, 50 ng/mL in acetonitrile), and 40 µL of sample or P4 standards were combined in 1.0 mL microcentrifuge tubes. Samples were vortex-mixed twice for 5 s and allowed to stand for 5 min to facilitate protein precipitation. The mixtures were then centrifuged at 13500 rpm for 10 min, and the supernatant was transferred to clean 2.0 mL glass vials (Millipore sigma, 29000-U). Subsequently, 400 µL of water and 1 mL of methyl tert-butyl ether (MTBE) were added to each vial. Samples were vortexed twice for 10 s and allowed to stand for 5 min to enable phase

separation. 600 ul of the upper organic phase was carefully collected and transferred to new high-recovery vials (Phenomenex, ARO-9981-13), avoiding disturbance of the aqueous phase. The collected organic extracts were dried under nitrogen evaporator under 50℃ with gentle nitrogen flow for approximately 1hr. Dried residues were reconstituted in 150 μL of methanol/water (50:50, v/v) containing 0.1% formic acid. Samples were briefly vortexed, capped, and placed in autosampler rack prior to analysis.

Quantitative analysis was performed using a Waters ACQUITY UPLC H-class system with an ACQUITY UPLC BEH C18 column (100 × 2.1 mm, 1.7 μm). The mobile phase consisted of (A) water containing 0.1% formic acid and (B) acetonitrile containing 0.1% formic acid. Isocratic elution was carried out with 70% mobile phase B at a flow rate of 0.3 mL/min. The injection volume was 5 μL. Mass detection was performed using a Waters ACQUITY QDa Mass Detector operated in positive ion mode. Two channels were monitored for quantification: progesterone (m/z 315.13) and the internal standard (m/z 324.20). The cone voltage was set at 15 V. Data acquisition and processing were conducted using Empower 3 software. A calibration curve for progesterone was prepared over a concentration range of 0.1–2000 ng/mL (0.1, 0.5, 1, 5, 10, 25, 50, 100, 200, 500, 1000, and 2000 ng/mL).

## 3.4 Results

### *3.4.1 Solubility of P4 in common buffer and surfactants solution*

P4 solubility in common buffers and surfactants were measured. As shown in Table 3.4-1, P4 showed very low solubility in buffer systems (<14 μg/mL) across test buffers (PBS, acetate

buffer, and SVF), confirming its highly hydrophobic nature. Conventional pharmaceutical surfactants, like Span and Tween, provided limited enhancement in solubility, typically in the range of 10–30-fold. However, the addition of cyclodextrins significantly enhanced solubility over 500-1000-fold.

Table 3-1 P4 solubility in different buffer/surfactant solution (n=3, mean ± SD)

| Buffer/Surfactant solution | P4 Solubility (μg/mL) |
|---|---|
| Phosphate buffer (pH=7.4) | 3.74±0.53 |
| Acetate buffer (pH=4.5) | 6.06±0.54 |
| Simulated vaginal fluid (pH=4.5) | 13.12±2.94 |
| 1% Span20 | 94.24 ± 0.38 |
| 1% Span80 | 51.12 ± 0.46 |
| 1% Span85 | 57.09 ± 9.74 |
| 1% Tween20 | 32.34 ± 1.03 |
| 1% Tween60 | 94.30 ± 11.15 |
| 1% Tween80 | 105.71 ± 8.78 |
| 5% HP-β-CD | 1520 ± 100 |
| 5% HP-γ-CD | 4770 ± 190 |

### *3.4.2 Phase solubility of different CDs*

Phase solubility studies were conducted to evaluate the solubilization efficiency of common cyclodextrins (CD) derivatives for P4. As shown in Figure 3.4-1, all tested CDs exhibited a linear increase in P4 solubility over the tested concentration range, corresponding to an AL-type phase solubility profile defined by the Higuchi–Connors theory. Among the tested CDs, RAME-β-CD demonstrated the highest solubilization ability, increasing P4 solubility to 9.82 ± 0.56 mg/mL with 50 mM RAME-β-CD, corresponding to approximately a 2600-fold enhancement compared to aqueous buffer. Based on the phase solubility diagrams, the stability constant ($K_{1:1}$) (Eqn. 1), complexation efficiency (CE) (Eqn. 2), and CD-to-drug molar ratio (CD:D) were

calculated for each CD using the established equations. Furthermore, the corresponding theoretical CD:D weight ratios were derived by incorporating the molecular weights of each CD (Table 3.4-2) (Eqn. 3). Among the tested CDs, RAME-β-CD exhibited the lowest CD:D weight ratio, indicating the most efficient drug solubilization with minimal excipient requirement. Therefore, RAME-β-CD was selected for further formulation development and subsequent studies.

$$K_{1:1} = \frac{\text{Slope}}{S_0(1-Slope)} \quad \text{(Eqn. 1)} \qquad CE = S_0 \times K_{1:1} = \frac{\text{Slope}}{S_0(1-Slope)} \quad \text{(Eqn. 2)}$$

$$D{:}\,CD\ molar\ ratio = 1{:}\frac{(CE+1)}{CE} \quad \text{(Eqn. 3)}$$

| CD type | MW(Da) | Slope | $K_{1:1}$ ($mM^{-1}$) | CE | CD:D molar ratio | CD:D weight ratio |
|---|---|---|---|---|---|---|
| RAME-β-CD | 1311 | 0.63 | 86.57 | 1.73 | 1.58:1 | 6.58:1 |
| HP-γ-CD | 1540 | 0.50 | 49.56 | 0.99 | 2.01:1 | 10.88:1 |
| SBE-β-CD | 2163 | 0.38 | 30.36 | 0.61 | 2.65:1 | 18.23:1 |
| HP-β-CD | 1400 | 0.29 | 20.84 | 0.42 | 3.40:1 | 14.94:1 |
| HP-α-CD | 1180 | 0.11 | 6.34 | 0.13 | 8.89:1 | 27.46:1 |

Table 3-2 Phase-solubility analysis and calculated CD:P4 ratios of different cyclodextrins

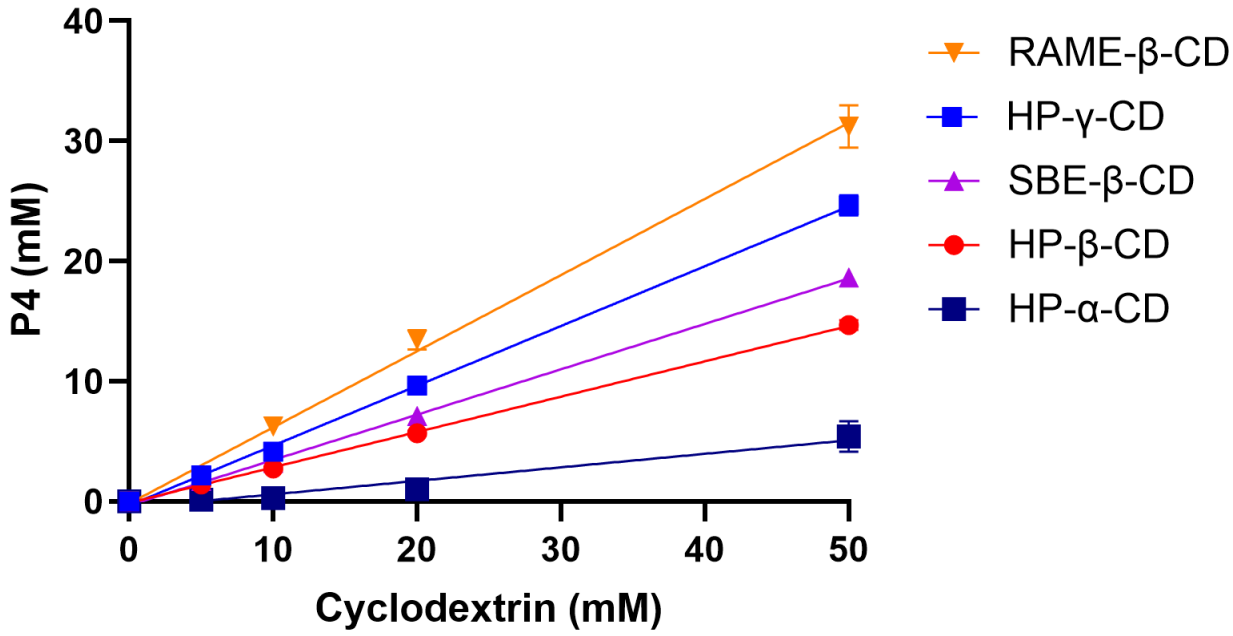


Figure 3-1 Phase solubility diagram of different CDs

### *3.4.3 Characterization for P4-CD complex*

#### *3.4.3.1 P4 quantification in P4-CD complex and final gel formulation*

The amount of P4 incorporated into the P4-CD complex following microwave irradiation was quantified at different P4:CD weight ratios. At a P4:CD ratio of 1:6, the resulting solution contained 42.77 mg/mL P4, corresponding to a yield of 70.74%. Increasing the ratio to 1:7 increased the P4 concentration to 48.46 mg/mL and the yield to 80.11%. The highest P4 loading was obtained at a ratio of 1:8, which produced a final P4 concentration of 54.21 mg/mL with a yield of 89.72%. These results indicate that increasing the amount of CD facilitated more efficient incorporation of P4 into the inclusion complex during microwave irradiation. Therefore, the 1:8 P4:CD ratio was selected for subsequent gel preparation.

To evaluate the reproducibility of the selected formulation, three independent batches of the 1:8 P4-CD complex were prepared and incorporated into the final gel formulation. The resulting complex solution showed a P4 concentration of 54.22 ± 1.05 mg/mL and a density of 1.112 ± 0.003 g/cm³. After incorporation into the gel, the final P4 concentration was 41.80 ± 0.63 mg/mL, demonstrating good reproducibility of both the complex preparation and the final gel manufacturing process.

### *3.4.3.2 FTIR*

FTIR spectroscopy was used to investigate the interaction between P4 (Figure 3.4-3) and RAME-β-CD (3.4-2) in the inclusion complex. As shown in Figure 3.4-4, pure RAME-β-CD exhibited a broad O–H stretching band around 3400 $cm^{-1}$ and strong bands between 850–1250 $cm^{-1}$, corresponding to C–O–C stretching and glycosidic bond vibrations. Pure P4 showed characteristic absorption bands at 1660 and 1699 $cm^{-1}$, assigned to the conjugated carbonyl stretching vibrations of the C3 and C20 ketone groups, as well as a band at 1620 $cm^{-1}$ corresponding to C=C stretching. The physical mixture retained the characteristic carbonyl bands of P4, indicating that no significant interaction occurred upon simple mixing. In contrast, in the P4-CD complex these characteristic carbonyl peaks became markedly weaker and broadened,

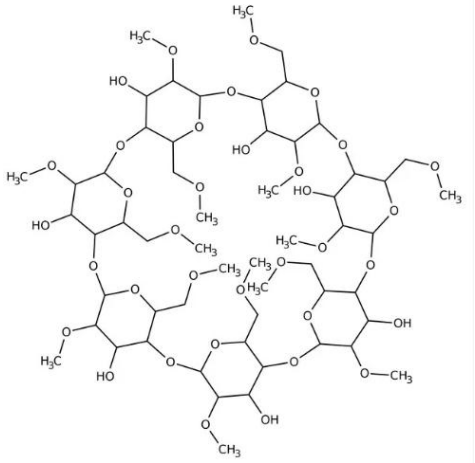

Figure 3-3 Structure of RAME-β-CD

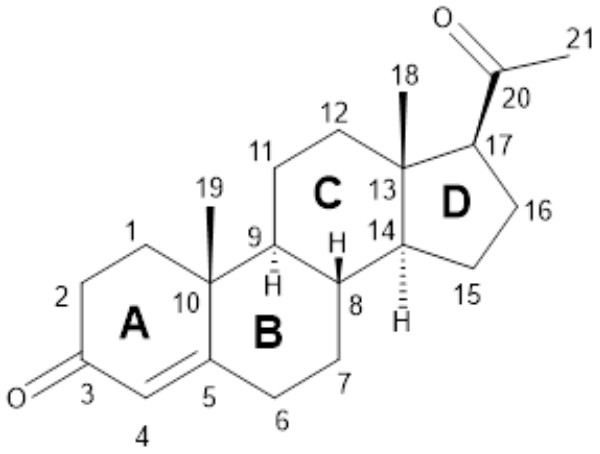


Figure 3-2 Structure of progesterone

particularly the band near 1660 $cm^{-1}$. The change in the ketone stretching region suggests an interaction between the carbonyl groups of P4 and the hydroxyl groups of RAME-β-CD, likely through hydrogen bonding during inclusion. These spectrum changes support the successful formation of the P4-CD inclusion complex.

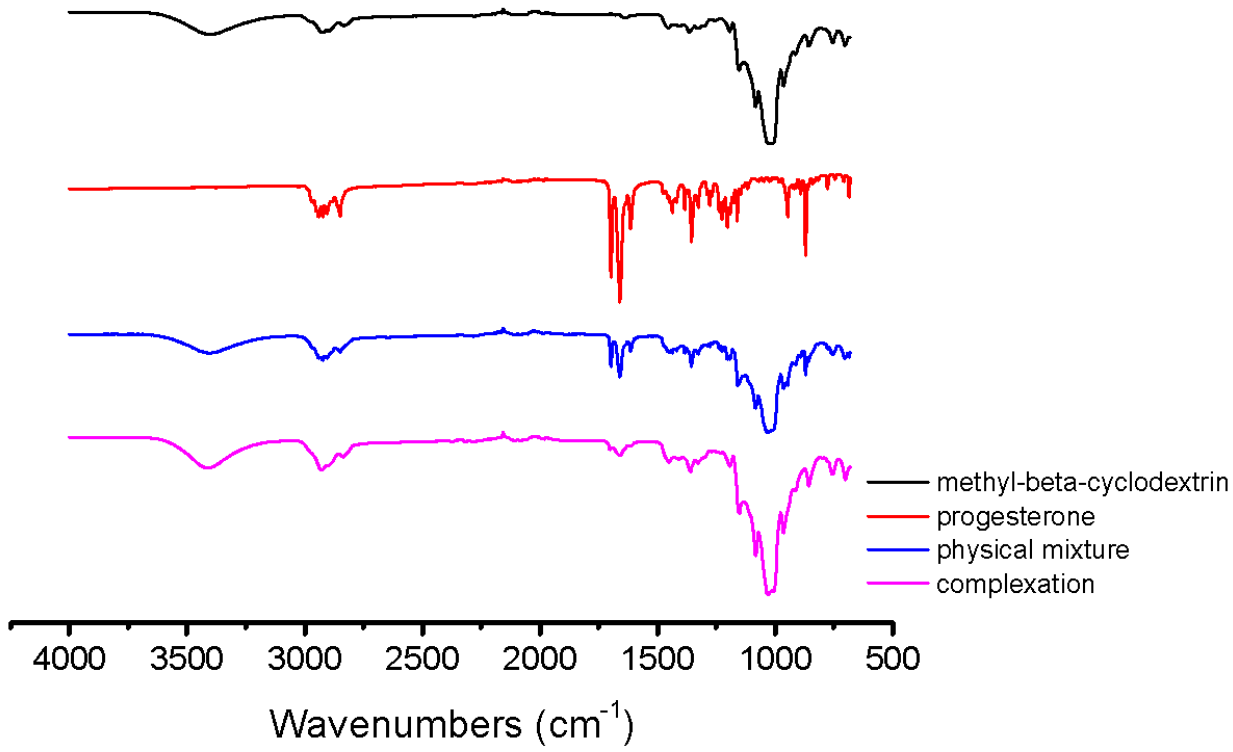


Figure 3-4 FTIR spectra of progesterone, RAME-β-CD, their physical mixture, and the resulting P4–RAME-β-CD inclusion complex

### *3.4.3.3 Differential scanning calorimeter (DSC)*

Differential Scanning Calorimeter (DSC) was used to evaluate the crystalline nature of P4, RAME-β-CD, physical mixture (CD: P4=8:1) and their complex. As shown in the Figure 3.4-5, the melting point of pure progesterone is around 128 ℃, corresponding to progesterone crystal form I. In contrast, RAME-β-CD showed only a broad baseline without a distinct thermal event, consistent with its amorphous nature. The physical mixture of P4 and RAME-β-CD still retained the characteristic melting peak of progesterone near 128 °C, indicating that P4 remained crystalline. In the thermogram of the complexation sample, the characteristic melting endotherm of progesterone completely disappeared. This suggests the loss of P4 crystallinity and its molecular dispersion within the RAME-β-CD cavity, confirming successful inclusion complex formation.

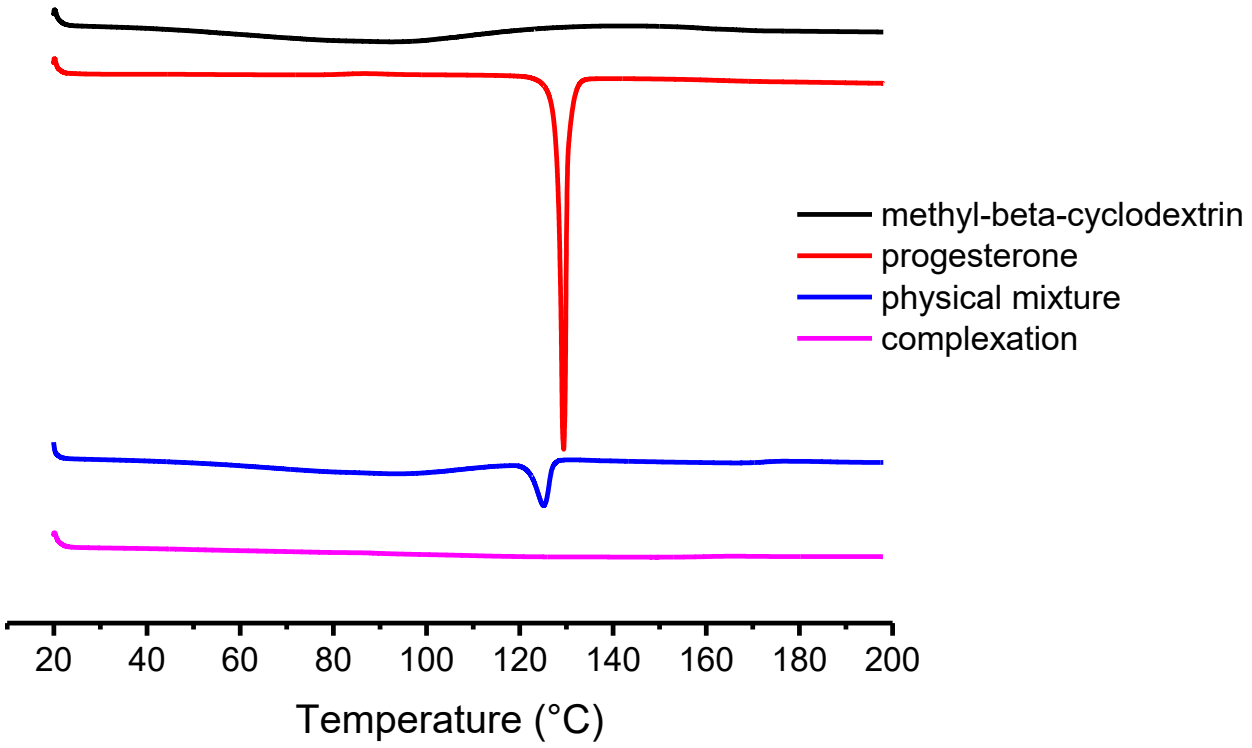


Figure 3-5 DSC thermograms of progesterone, RAME-β-CD, their physical mixture, and the P4–RAME-β-CD inclusion complex

#### *3.4.3.4 Solid X-ray diffraction (XRD)*

To further verify the formation of P4-CD complex, solid X-ray diffraction (XRD) of pure P4, RAME-β-CD, physical mixture (CD: P4=8:1) and P4-CD complexation powder were obtained. In Figure X, the characteristic peaks of progesterone were identified at 10.55°, 12.70°, 14.55°, 15.35°, and 16.95°. These diffraction peaks correspond to crystal form I of P4. RAME-β-CD displayed only two broad diffuse halos, consistent with its amorphous nature. The physical mixture retained several characteristic diffraction peaks of P4 at 12.70° and 16.95°, which appeared on top of the broad halo of RAME-β-CD, indicating that P4 remained crystalline after simple mixture. In contrast, these characteristic peaks disappeared completely in the complexation sample, which showed only a broad amorphous halo similar to that of RAME-β-CD. This suggests that P4 was converted from a crystalline to an amorphous or molecularly dispersed state after complexation, supporting the successful formation of the P4-CD inclusion complex using microwave irradiation.

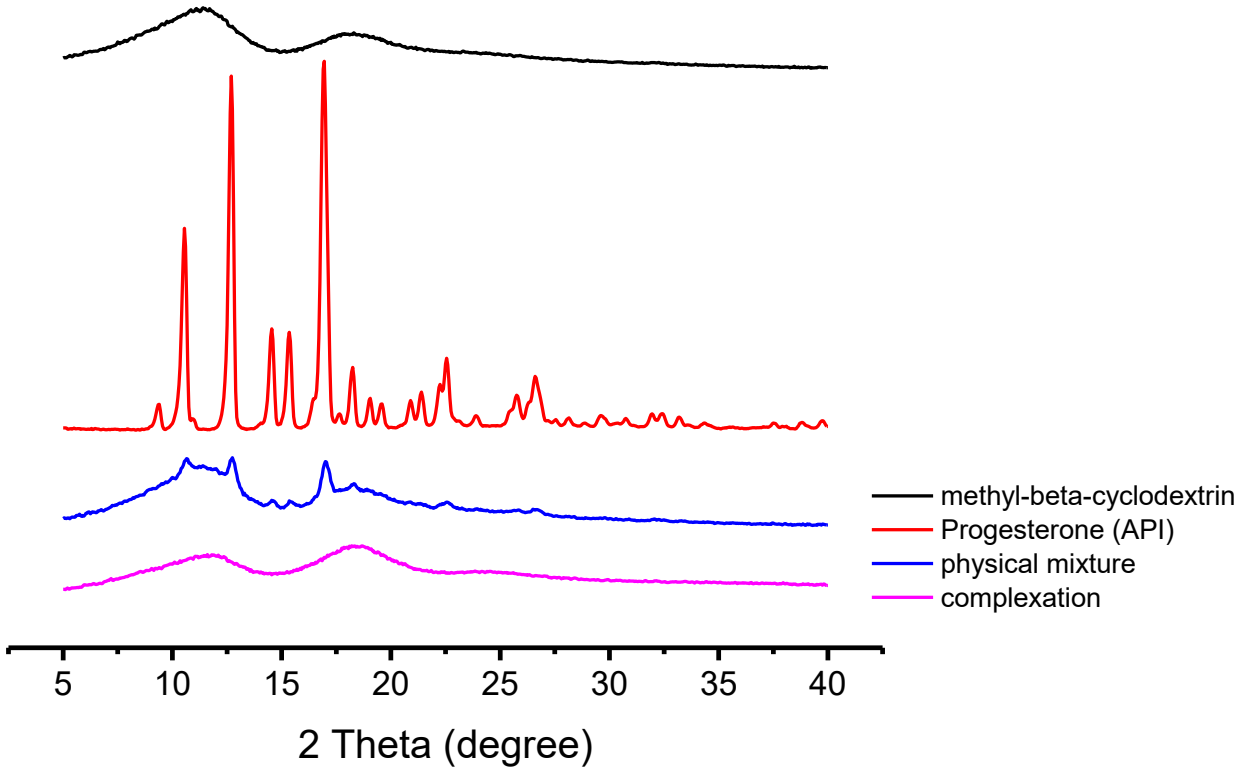


Figure 3-6 X-ray diffraction patterns of progesterone, RAME-β-CD, their physical mixture, and the P4–RAME-β-CD inclusion complex

### *3.4.4 P4-CD hydrogel characterization*

#### *3.4.4.1 Muco-adhesion and syringeability test*

Mucoadhesion of the P4-CD gel was evaluated using a mucin disc model and compared with Crinone. As shown in Table 3.4-3, the P4-CD gel exhibited significantly greater mucoadhesive strength than Crinone. Both formulations contain poly(acrylic acid)-based mucoadhesive polymers, including carbomer 934 and polycarbophil, which can interact with the mucin layer through hydrogen bonding between their carboxyl groups and the hydroxyl and amine groups of mucin glycoproteins. In addition, after hydration these polymers swell and their flexible polymer chains interpenetrate with the mucin network, further strengthening adhesion. The higher mucoadhesion of the P4-CD gel may also be attributed to the high content of cyclodextrin. The high CD content can enhance mucoadhesion because its multiple hydroxyl groups can increase its internal viscosity and provide additional hydrogen-bonding interactions with mucin.

Syringeability testing showed that the P4-CD gel required a substantially lower force for extrusion than Crinone, indicating that it was easier to administer through the applicator. Despite its strong mucoadhesion after administration, the P4-CD gel maintained good flowability during extrusion, suggesting a favorable balance between ease of administration and vaginal retention.

Table 3-3 Comparison of mucoadhesion and syringeability between the P4–CD gel and Crinone®

| Sample | P4-CD gel | Crinone | P-value |
|---|---|---|---|
| Adhesive force (N) | 1.10 ± 0.05 | 0.84 ± 0.14 | <0.001** |
| Adhesiveness (mJ) | 0.30 ± 0.05 | 0.18 ± 0.03 | 0.0045** |
| Syringeability (mJ) | 29.02 ± 4.20 | 78.59 ± 7.95 | <0.001** |

#### *3.4.4.2 Steady shear viscosity*

The steady shear behavior of the P4-CD gel was evaluated by measuring the changes in shear stress and viscosity with increasing shear rate (Figure 3.4-7). The relationship between the shear stress and shear rate of the P4-CD gel is not linear, and the viscosity is not constant, indicating that this gel is a non-Newtonian fluid. The viscosity decreases with the increase in shear rate, which is a typical shear-thinning phenomenon like Crinone [85]. Under low shear conditions, the gel maintained a relatively high viscosity, which is favorable for retention at the administration site. In contrast, under high shear conditions, such as during extrusion from an applicator or spreading over the vaginal mucosa, the reduced viscosity would facilitate administration and improve spreadability. The three different in house batches of P4-CD all exhibited similar shear-thinning properties with minimal deviation, indicating the consistence and reproducibility of our preparation.

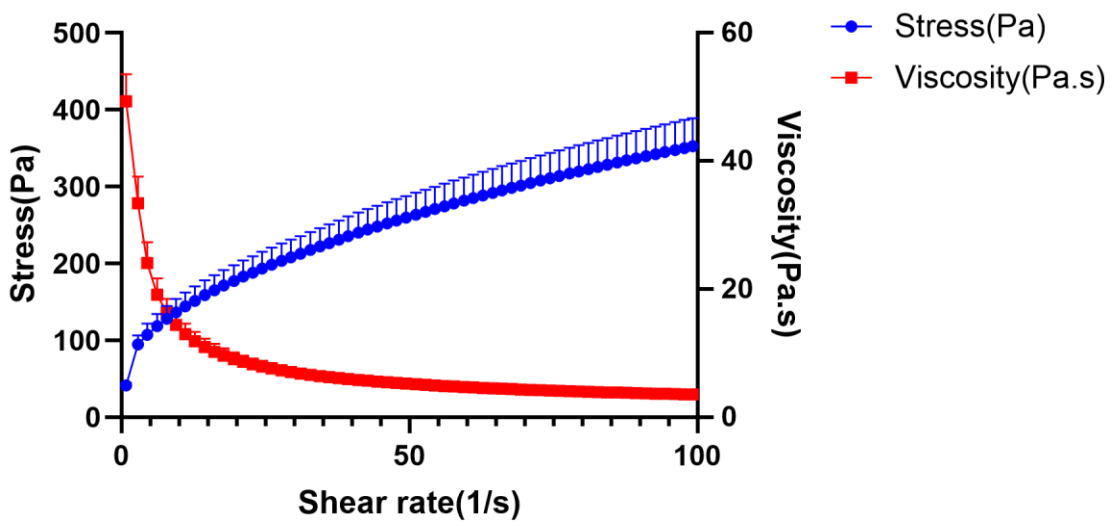


Figure 3-7 Steady shear rheological behavior of the P4–CD gel: shear stress and viscosity as a function of shear rate

### *3.4.4.3 Oscillatory rheometry*

Oscillatory frequency sweep testing showed that the storage modulus (G′) of the P4-CD gel was consistently higher than the loss modulus (G″) over the entire tested frequency range, indicating that the formulation exhibited predominantly elastic, solid-like behavior (Figure 3.4-8). The absence of a crossover between G′ and G″ suggests that the gel network remained stable and was not disrupted under the applied oscillatory stress. Compared with Crinone, the P4-CD gel showed lower values of both G′ and G″ throughout the frequency range. Crinone exhibited a storage modulus of approximately 400–550 Pa and a loss modulus of approximately 50–100 Pa, indicating a stronger and more rigid internal structure. This stronger elastic network is likely related to the suspended P4 crystals and oil droplets in the emulsion gel. In contrast, the P4-CD gel showed a weaker but still predominantly elastic network, consistent with a more homogeneous system in which P4 was fully dissolved and dispersed within the gel matrix. The three independently prepared batches of the P4–CD gel exhibited highly similar oscillatory rheological profiles with minimal variation, demonstrating good formulation reproducibility and batch-to-batch consistency.

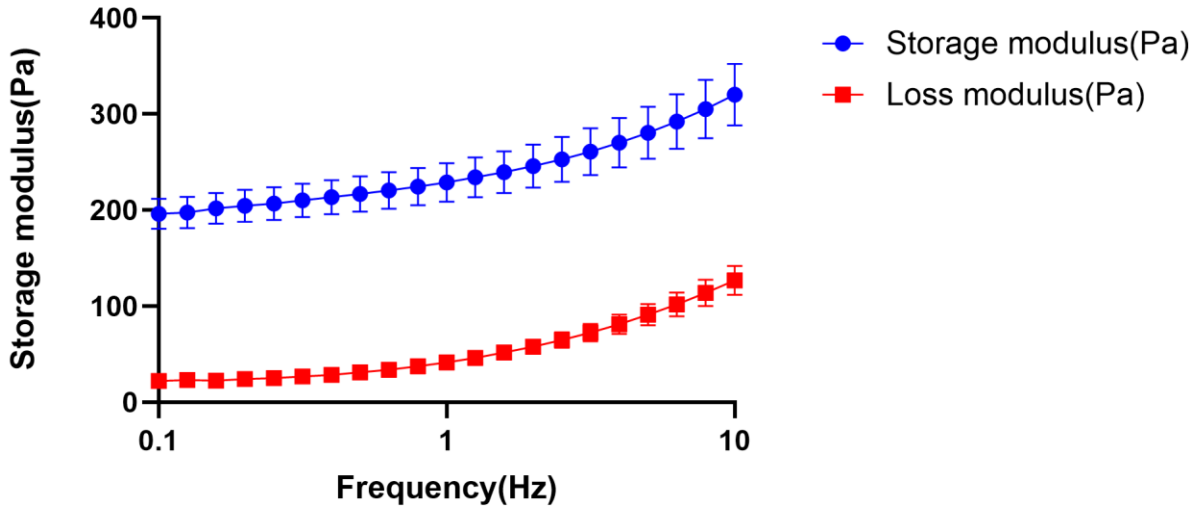


Figure 3-8 Oscillatory frequency sweep rheology of the P4–CD gel: storage modulus (G′) and loss modulus (G″) as a function of frequency

### *3.4.4.4 In vitro release (IVRT) study*

Figure 3.4-9-a shows the results of dialysis bag based single-cell IVRT method for the two formulations. Both formulations show similar sustained release patterns and can achieve nearly complete release within 24 hours. This indicates that when both formulations are fully exposed to the release medium under sink condition, both gel matrix disintegrated at a similar rate and P4 dissolution was not the rate limiting step for release.

However, a clear difference between the two formulations was observed in the Franz cell IVRT using a 0.8 µm MCE membrane (Figure 3.4-9-b). The P4–CD gel showed significantly faster release than Crinone, reaching approximately 70% release within 4 h and maintaining this level thereafter, while Crinone can reach only about 50% release after 24 h. These results suggest that P4 in the P4-CD gel was readily released from the cyclodextrin complex and diffused through the membrane. This slower release from Crinone may be attributed to its unique structure, in which P4 crystal is distributed within both the oil and aqueous phases of the emulsion gel. Under this condition, P4 release is likely limited by dissolution of the suspended drug particles and diffusion from the emulsion droplets, making the release rate dependent on P4 crystal size and distribution within the formulation.

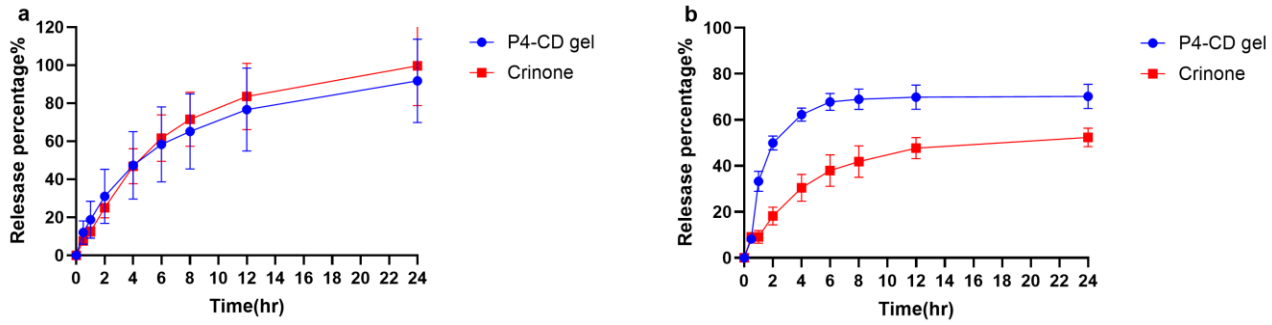


Figure 3-9 Result of two different IVRT methods

### *3.4.4.5 In vitro permeation test (IVPT)*

The permeation behavior of progesterone from Crinone® and the P4-CD gel across excised sheep vaginal tissue was evaluated using Franz diffusion cells under sink conditions. As shown in Figure 3.4-11, both formulations exhibited a time-dependent increase in progesterone concentration in the receptor chamber; however, the P4-CD gel produced substantially greater permeation throughout the experiment. Only minimal amounts of P4 were detected in the receptor chamber during the first 1-2 h for either formulation, indicating an initial lag period associated with diffusion across the vaginal tissue. Beginning at 4 h, the permeation profiles of the two formulations diverged markedly. The enhanced permeation of the P4–CD gel was further confirmed by calculation of the steady state flux ($J_{ss}$) and cumulative permeation at 8 h ($Q_{8h}$) (Table 3.4-4). The P4–CD gel exhibited a $J_{ss}$ of 1.91 ± 0.66 μg/cm²/h, which was approximately 3.5-fold higher than that of Crinone® (0.55 ± 0.34 μg/cm²/h, p = 0.034). Similarly, the cumulative amount permeated at 8 h reached 11.02 ± 4.23 μg/cm² for the P4–CD gel, compared with only 3.01 ± 1.70 μg/cm² for Crinone® (p = 0.038).

This increased the apparent solubility of P4 and generated a larger concentration gradient across the vaginal tissue, thereby promoting transvaginal diffusion. In contrast, progesterone in Crinone is present primarily as suspended crystalline particles within the emulsion gel, requiring dissolution before permeation can occur, which likely limited its transport through the sheep

vaginal tissue.

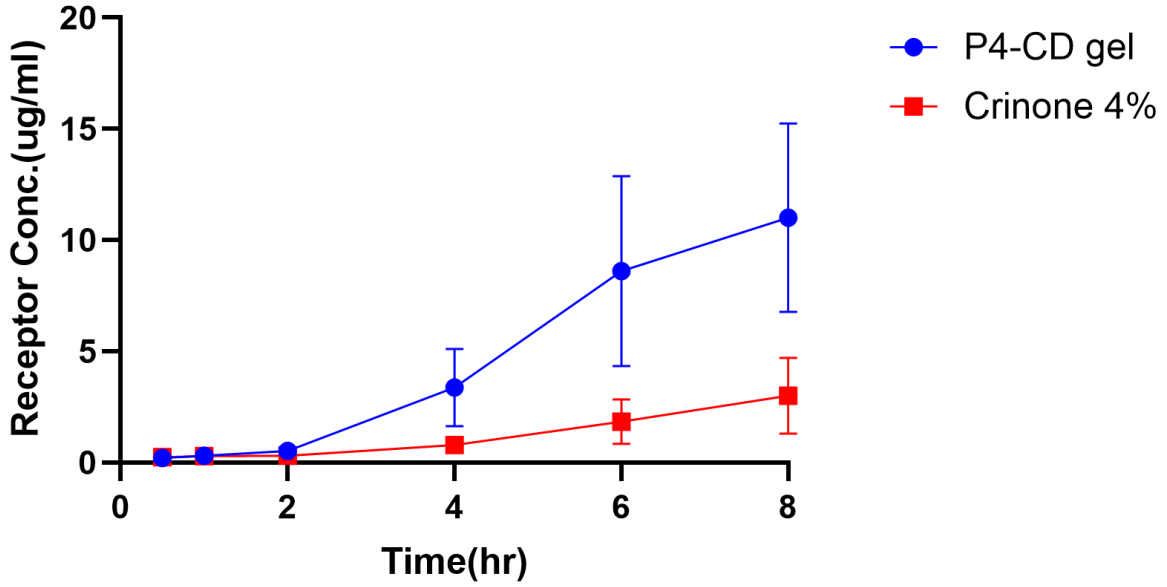


Figure 3-10 IVPT comparison of P4 permeation across sheep vaginal tissue between Crinone® and P4-CD gel

| Group | Crinone | P4-CD gel | P value |
|---|---|---|---|
| $J_{ss}$ (ug/cm$^2$/h) | 0.55 ± 0.34 | 1.91 ± 0.66 | 0.034* |
| $Q_{8h}$(ug/cm$^2$) | 3.01 ± 1.70 | 11.02 ± 4.23 | 0.038* |

Table 3-4 Comparison of steady-state flux ($J_{ss}$) and cumulative permeation at 8 h ($Q_{8h}$) of P4 across sheep vaginal tissue between Crinone® and P4-CD gel

### *3.4.5 Pharmacokinetics of intravaginal single dose in healthy mice*

The preliminary pharmacokinetic study in CD-1 mice confirmed improved systemic absorption. Plasma P4 concentrations after administration of the P4-CD gel were consistently higher than those of Crinone during the first 4 h, with an earlier and greater peak concentration observed for the P4-CD gel. The basic pharmacokinetic parameters are calculated and listed in Table 3.4-1. Although the difference in $C_{max}$ did not reach statistical significance, the P4-CD gel showed a trend toward a higher $C_{max}$ compared with Crinone (759.9 ± 232.6 vs. 419.6 ± 323.7 ng/mL, p = 0.139). More importantly, the overall exposure of P4 from the P4-CD gel was significantly increased. The $AUC_{0-8}$ of the P4-CD gel was approximately 2.5-fold higher than

that of Crinone (2464.5 ± 1057.9 vs. 1001.6 ± 105.7 ng·h/mL, p = 0.032). In addition, the apparent clearance (CL/F) of P4 was significantly lower for the P4-CD gel than for Crinone (0.83 ± 0.19 vs. 1.75 ± 0.44 L/h, p = 0.014), indicating improved bioavailability (F). These results are consistent with the result of IVPT and suggest that P4-CD complex can enhance mucosal permeation and systemic absorption compared with the P4 crystal in Crinone formulation.

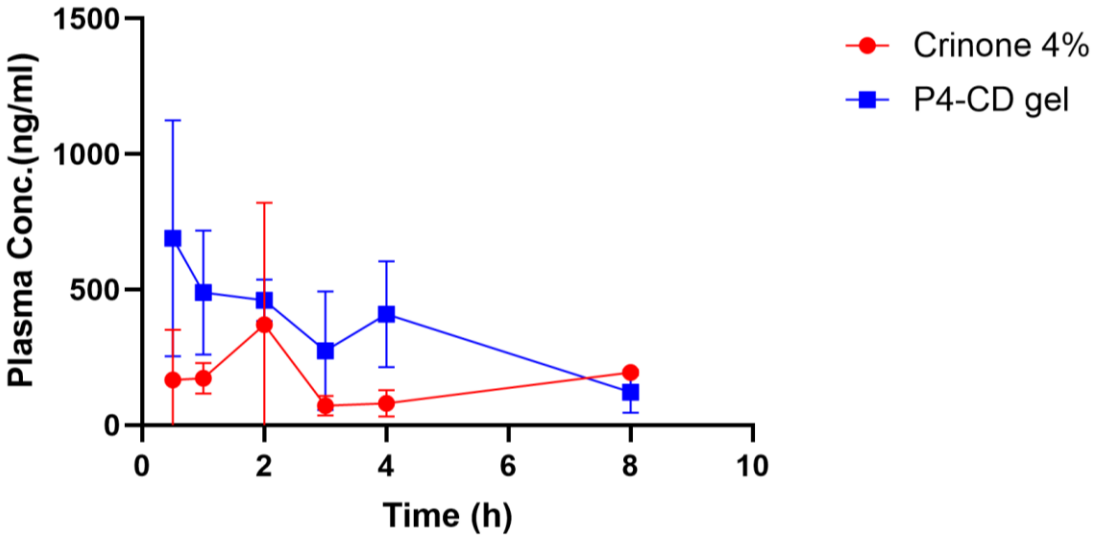


Figure 3-11 *In vivo* plasma P4 concentration–time profiles following single vaginal administration of Crinone® and P4-CD gel in mice

| Group | Crinone 4% | P4-CD gel | P value |
|---|---|---|---|
| $AUC_{0-8}$ (ng·h/mL) | 1001.6 ± 105.7 | 2464.5 ± 1057.9 | 0.032* |
| $C_{max}$ (ng/mL) | 419.6 ± 323.7 | 759.9 ± 232.6 | 0.139 |
| CL/F (L/h) | 1.75 ± 0.44 | 0.83 ± 0.19 | 0.014* |

Table 3-5 Pharmacokinetic parameter of Crinone and P4-CD gel group

### 3.5 Discussion

Cyclodextrin complexation represents one of the most widely used strategies to overcome the intrinsically poor aqueous solubility of drug candidates. In the present study, all tested cyclodextrins increased the apparent solubility of progesterone in a concentration-dependent manner, and the phase-solubility diagrams exhibited a typical AL-type profile according to the Higuchi-Connors classification, indicating the formation of soluble drug-CD inclusion complexes[92]. The enhanced apparent solubility observed here cannot be attributed simply to co-

solubilization. Rather, FTIR, DSC, and XRD analysis in this chapter confirmed the loss of the crystalline state of P4 and the formation of a true inclusion complex.

Our phase solubility screening indicates that RAME-β-CD has better complexation efficiency than hydoxypropyl-β-CD (HP-β-CD) and sulfobutylether-β-CD (SBE-β-CD) and other CD with different ring size. This phenomenon can be explained by the structural constraints of the host-guest interaction. Specifically, the hydroxypropyl groups in HP-β-CD, primarily located at the secondary rim, exert substantial steric hindrance that obstructs the deep insertion of the bulky, rigid four-ring steroid scaffold of P4 into the hydrophobic cavity. Similarly, the anionic sulfobutyl ether chains and the associated high charge density of SBE-β-CD are suboptimal for the electrically neutral progesterone, as the large substituent groups further increase the entry barrier for the guest[97]. Compared with native β-CD and hydroxypropyl-substituted derivatives, methyl substitution substantially increases the hydrophobicity of the CD cavity[98]. Besides, the methyl substation can reduce the intermolecular hydrogen bonds, which typically rigidifies the native β-cyclodextrin macrocycle[99]. This disruption enhances the conformational flexibility of the RAME-β-CD framework, enabling an "induced-fit" for rigid P4 molecule. Furthermore, the higher aqueous solubility of RAME-β-CD makes the preparation of highly concentrated P4 aqueous solutions (>4% w/w) feasible.

In the sheep vaginal tissue *in vitro* permeation testing (IVPT), the novel gel formulation containing the P4-CD inclusion complex demonstrated a significantly superior permeation profile compared to Crinone®. This enhancement in transmucosal delivery can be attributed to a dual-mechanism permeation enhancement mediated by the RAME-β-CD. First mechanism relies on the "carrier-shuttle" model proposed by Loftsson *et al* [100]. The vaginal mucosal barrier comprises an external, high-water-content mucous layer that serves as an unstirred water layer, and an underlying lipophilic epithelial membrane. For hydrophobic drugs like P4, diffusion through this hydrophilic mucous layer is the primary rate-limiting step for absorption [101]. Crinone® is a conventional bioadhesive gel that contains micronized P4 suspension with a particle diameter about 10 um; these particles exhibit extremely low thermodynamic activity in the aqueous phase and struggle to diffuse through the vaginal mucus. On the contrast, cyclodextrin acts as a dynamic, water-soluble shuttle. By encapsulating the lipophilic P4, cyclodextrin transforms the drug into a highly water-soluble complex capable of rapidly diffusing across the aqueous layer. Upon reaching the immediate surface of the lipophilic

epithelium, the dynamic equilibrium shifts, allowing the complex to spontaneously dissociate. The released free progesterone readily partitions into and permeates the lipid membrane, while the hydrophilic cyclodextrin molecules remain in the aqueous exterior. Second, as reported in epithelial models (e.g., Caco-2 monolayers), methylated cyclodextrins possess a high affinity for membrane lipids. Upon contact with the vaginal epithelium, RAME-β-CD acts as a permeation enhancer by transiently extracting cholesterol from the epithelial cell membranes and intercellular lipid domains. This localized cholesterol depletion transiently disrupt intercellular junctions and increases membrane fluidity, thereby widening the paracellular spaces for drug partition [102]. Nevertheless, because only free P4 can permeate across the membrane, the inclusion complex should be regarded as a dynamic reservoir rather than the actual permeating species. The improved tissue permeation observed in this study therefore likely results from a rapid equilibrium between free and complex progesterone rather than direct transport of the intact cyclodextrin complex.

The rheological results suggest that cyclodextrin incorporation does not simply function as a solubilizer, but instead significantly influences the gel microstructure. In Crinone®, P4 is present as suspended crystalline particles and oil droplets that may act as rigid fillers within the polymer matrix, thereby reinforcing the gel structure. Compared with Crinone®, the P4-CD gel exhibited a lower elastic modulus and weaker overall network strength despite maintaining a predominantly solid-like behavior[65]. Several mechanisms may account for this effect. First, the structural integrity of polyacrylic acid based hydrogels, like carbomer and polycarbophil, heavily relies on the dense network of intermolecular polymer-polymer and polymer-water hydrogen bonds. The high concentration of RAME-β-CD in the formulation, with numerous peripheral hydroxyl groups on its ring, may compete with carbomer and polycarbophil for hydrogen-bonding interactions, thereby partially disrupting the strength of gel network. In addition, cyclodextrin molecules may interact directly with or partially thread onto segments of the polymer chains, interfering with chain entanglement and reducing the overall strength of the gel network. Second, a significant "solvent displacement" effect occurs due to the high loading of the cyclodextrin complex in our gel. As a substantial portion of the formulation volume is occupied by the P4-CD complex, the absolute weight fraction of the aqueous solvent is inherently reduced. Consequently, the carbomer and polycarbophil chains are unable to access sufficient free water for full hydrating and swelling, affecting its rheology behavior [103,104].

Although incorporation of CD weakened the elastic strength of the polymer network, the overall adhesiveness of the final gel increased. This effect is likely related to the very high concentration of CD incorporated in the final formulation (approximate 30% w/w). As a highly water-soluble oligosaccharide derivative, cyclodextrin can substantially increase the viscosity of the aqueous phase, like the thickening effect observed in concentrated sugar solutions or syrups. At high concentrations, the large number of hydroxyl groups on CD molecules forms extensive hydrogen bonding with surrounding water molecules, creating a more structured and less mobile aqueous phase. In addition, these hydroxyl groups can form additional hydrogen bonds with mucin glycoproteins present on the vaginal surface, leading to an increase in mucoadhesion.

Clinical practice routinely monitors plasma P4 concentrations as a critical indicator during pregnancy, systemic exposure alone is not the most definitive endpoint for evaluating a vaginal formulation [8]. For potential indications like luteal phase support and the prevention of preterm birth, therapeutic efficacy is related to the local drug concentrations within the uterus and surrounding reproductive tissues. Vaginal administration has its uniquely feature called "uterine first-pass effect," a mechanism that will preferentially deliver drug to the uterus before entering the systemic blood circulation [22]. Consequently, the increased systemic plasma exposure demonstrated by the P4-CD gel in our pharmacokinetic study could be interpreted as a strong indirect indicator of higher uterine P4 concentration. Nevertheless, to definitively validate this localized therapeutic advantage, future *in vivo* studies directly quantifying tissue drug concentrations in the uterus and endometrium remain warranted.

Besides, it is crucial to acknowledge the intrinsic physiological discrepancies between the murine model used in this study and the human vaginal environment. The vaginal pH of mice is generally close to neutral (pH 6.0–7.0), whereas the healthy human vagina is strictly acidic (pH 3.5–4.5) due to the colonization of lactic acid-producing *Lactobacillus* species [34,105]. This pH difference is particularly critical for polyacrylic acid-based vehicles, such as carbomer and polycarbophil, whose ionization state, hydration kinetics, swelling capacity, and ultimate mucoadhesive behavior are highly pH-dependent. Furthermore, notable cross-species variations in mucus composition, epithelial thickness, basal vaginal fluid volume, and the rapid physiological shifts during the short murine estrous cycle can profoundly alter local drug retention and subsequent transmucosal absorption [106]. Consequently, while our mice model

successfully demonstrated enhanced systemic exposure, these pharmacokinetic outcomes must be interpreted with caution and may not seamlessly translate to human clinical performance.

Unlike Crinone®, which relies on a complex oil-in-water emulsion matrix to suspend micronized P4 crystals, our formulation retained the same carbomer/polycarbophil-based mucoadhesive gel matrix while replacing the P4 suspension with a fully solubilized P4-CD inclusion complex. Because P4 was molecularly dispersed within the CD complex, the oil phase required in Crinone® was no longer necessary and was intentionally removed, resulting in a simplified single-phase system. By maintaining the same FDA-approved gel-forming excipients, uncertainties associated with introducing new materials were minimized. This formulation strategy also enabled a more direct comparison between two fundamentally different forms of P4 within a highly similar gel environment. Nevertheless, the field of biomaterials for gel delivery is evolving rapidly. In recent years, numerous novel gel systems have emerged, including thiolated polymers, self-healing hydrogels, stimuli-responsive materials, mucus-penetrating nanoparticles, and multifunctional bioadhesive networks. These materials may offer advantages such as improved retention, better mucus penetration, enhanced control of drug release, or greater patient acceptability [34,39,48,107]. Therefore, although the present study intentionally focused on clinically established excipients, future work may further improve vaginal progesterone delivery by integrating cyclodextrin complexation with more advanced biomaterial platforms.

Finally, and most importantly, we would like to emphasize a broader issue: women's health. Vaginal drug delivery and the treatment of diseases of the female reproductive tract have long remained underappreciated areas of research, despite their substantial clinical importance [68,107]. Historically, many vaginal formulations have been adapted directly from topical skin products with only minimal modification. As a result, they often fail to address challenges unique to vaginal administration, such as ease of application, leakage, discharge, and the persistent problem of messiness [108,109]. This is not simply a scientific question of drug delivery. It is also a matter of gender equity [68]. Through studies such as this, we hope to increase awareness and understanding of vaginal drug delivery and to encourage the development of formulations that are better suited to the unique physiology and diseases of the female reproductive tract. Ultimately, our goal is to facilitate the development of more effective novel products or high-quality generic alternatives, thereby making safe, affordable, accessible, and effective medications available to more women and girls around the world.

## 3.6 Conclusion

A novel progesterone vaginal hydrogel based on a microwave-prepared P4-CD inclusion complex was successfully developed. RAME-β-CD was identified as the most efficient cyclodextrin for progesterone solubilization and enabled the conversion of crystalline progesterone into a molecularly dispersed state. Incorporation of the complex into a carbomer/polycarbophil gel produced a formulation with favorable mucoadhesion, syringeability, and rheological behavior. Compared with Crinone®, the P4–CD gel exhibited faster release, greater vaginal tissue permeation, and significantly improved systemic exposure after vaginal administration. These findings suggest that cyclodextrin complexation can overcome the dissolution-limited behavior of conventional crystalline progesterone formulations and may provide a promising strategy for next-generation vaginal progesterone products.

# Chapter 4 Reverse Engineering of Complex Liposomal Injections

## 4.1 Abstract

Doxil®, a PEGylated liposomal doxorubicin (DOX) hydrochloride suspension, was the first liposome drug product approved by the U.S. Food and Drug Administration (FDA). Although off-patent, limited generic products have been approved due to challenges in achieving bioequivalence compounded by manufacturing complexity. Regulatory agencies require generic drug products to be bioequivalent to the reference listed drug. In this regard, we developed various analytical methods to analyze Doxil® and its generic drug products for multiple attributes, including liposome size distribution, zeta potential, DOX content, lipid content, purity, non-encapsulated doxorubicin, morphology, nanostructure similarity, and quantified in vitro release.

Batch-to-batch variation exists across attributes for different formulations. Minor differences in particle size and zeta potential were observed. Cryo-TEM imaging reveals the distinct coffee bean shape and morphology of the Doxil® liposome. SAXS similarity analysis shows a distinct difference in nanostructure for Dr. Reddy's formulation compared to the innovator formulation. Still, it is revealed to be a consequence of liposome uniformity and homogeneity as depicted in cryoTEM images. Several methods developed in this work can be complementary to provide a more thorough physicochemical analysis for generic evaluation. Size, morphology, and nanostructure evaluated by DLS, cryo-TEM, and SAXS should be readily employed to assess physicochemical similarity. Content, impurity identification, and amount of free non-encapsulated DOX are used to evaluate formulation sameness. The methods developed in this work provide a physicochemical framework for analytical comparison of complex

liposomal generics and may support subsequent development efforts to improve generic drug availability for patient populations in need.

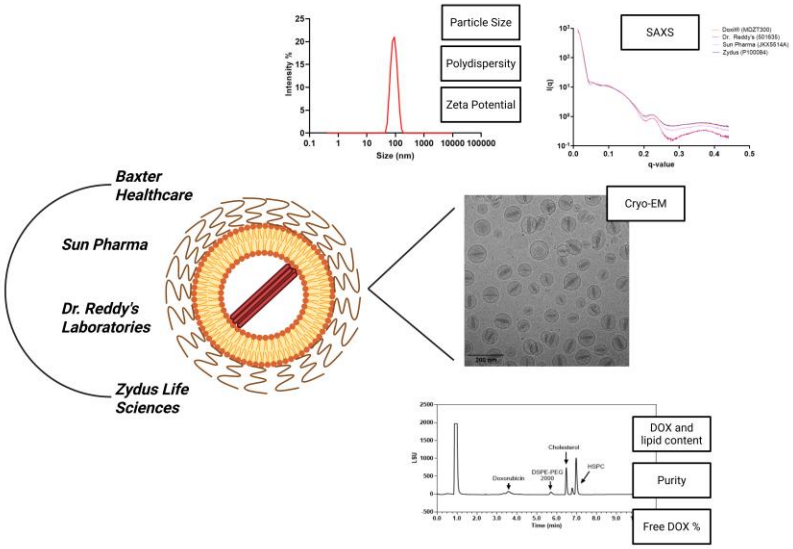


Figure 4-1. Chapter 4 Graphical Abstract

## 4.2 Introduction

Doxil® is a liposomal doxorubicin (DOX) hydrochloride suspension intended for intravenous infusion approved in 1995 by the United States (U.S.) FDA [110]. As the premier liposomal drug product, Doxil® became a highly sought-after product for generic development upon patent expiration in 2010. The global market for liposomal DOX has grown exponentially over the last decade. In 2020, the market was estimated at US $992.8 million and projected to reach US $1.3 billion in 2026, but the projection was actualized earlier as of 2024 [110]. The global market for liposomal DOX is currently estimated at US $1.28 billion and is expected to increase at a compound annual growth rate of 6.3% over the next decade [111]. In 2034, the projected market value is expected to nearly double to an estimated $2.37 billion [111]. An increase in the generic availability of liposomal DOX has been noted as a significant agent influencing the sales

of liposomal DOX formulations, in addition to several advancements in developing and optimizing nanodrugs as chemotherapeutic medications.

However, developing generic drug products for Doxil® is challenging due to its manufacturing complexity and its direct correlation to in vitro in vivo bioequivalence. Minor variations in processing are known to significantly affect the physiochemical properties of liposomal drug products, and subsequently, drug performance [112]. Parameters such as liposome size, zeta potential, drug and lipid composition, the quantity of degradation products, and in vitro leakage are among some of the essential attributes for liposomal generic development as detailed in the FDA draft guidance for liposomal doxorubicin hydrochloride formulations [56]. Additional considerations for manufacturing should include in vitro measures to prove bioequivalence of the generic formulation to the reference listed drug (RLD) and be included in the submission of abbreviated new drug applications (ANDA). According to the FDA, a generic formulation is considered bioequivalent if it is qualitatively (Q1) and quantitatively (Q2) the same in comparison with the RLD and possesses physicochemical similarity (Q3). Q3 should demonstrate that the physical arrangement of matter in the formulation, characterized by nanostructure, is similar to the RLD. Q1/Q2(Q3)-compliant generics require extensive in vitro and in vivo evaluation, however, the FDA describes in the Code of Federal Regulations (21 CFR 320.22, 21 CFR 320.24) that different types of evidence may be used to establish bioequivalence between a generic and reference product. A waiver of evidence for in vivo bioequivalence for generic drug products that meet specific criteria can be obtained using sufficient in vitro data [113,114].

In this work, we developed a series of methods using techniques commonly employed for standard characterization of liposomal formulations to evaluate the similarities and differences of several approved generic, liposomal DOX products with the RLD. Comparative analysis of the measured in vitro physicochemical properties for different approved liposomal DOX formulations can inform formulators of the specification ranges deemed acceptable for the assessment of critical quality attributes (CQA) in subsequent development efforts [115,116].

Few liposomal DOX generics have been successfully developed and approved by the U.S. FDA. Approved generic formulations include those from Sun Pharmaceuticals (Goregaon, Mumbai, India), Dr. Reddy's Laboratories (Hyderabad, Telangana, India), Zydus LifeSciences Global FZE (Ahmedabad, Gujarat, India), and Ayana Pharmaceuticals (Jerusalem, Israel) [117].

The work described in this manuscript details the physicochemical characterization and analytical comparison of the innovator (Baxter Healthcare) and generic liposomal DOX formulations developed by Sun Pharmaceuticals, Dr. Reddy's Laboratories, and Zydus LifeSciences.

Table I lists the drug vendor/manufacturer, batch number, and expiration date for each formulation tested. Few reports in literature detail a comparative physicochemical analysis for each generic, liposomal DOX formulation in reference to the RLD. Approval of generic, liposomal doxorubicin hydrochloride injection developed by Ayana Pharmaceuticals was approved in 2021 and was not available for purchase from our university pharmacy for testing during our study period. Therefore, our work describes quantitative information about the physicochemical nature of each generic formulation, excluding Ayana Pharmaceuticals, and highlights the stability of formulations during their shelf-life that may impact in vitro drug performance.

Table 4-1. Sample Inventory

| Vendor | Batch No. | Expiry Date |
|---|---|---|
| Doxil® (Baxter Healthcare) | KGZTG01 | Feb 2022 |
| | KIZTI00 | Apr 2022 |
| | KJZU901 | May 2022 |
| | LJZTS00 | May 2023 |
| | MDZT300 | Nov 2023 |
| Dr. Reddy's Laboratories | 501451 | Feb 2022 |
| | 501630 | May 2022 |
| | 501635 | Aug 2023 |
| | 501693 | Aug 2023 |
| Sun Pharmaceuticals | JKX5514A | May 2022 |
| | HAC1612A | Sep 2022 |
| Zydus Pharmaceuticals | P100084 | Feb 2022 |

We developed several physicochemical assays using dynamic light scattering (DLS) and ultra performance liquid chromatography (UPLC) methods for accelerated evaluation and

characterization of the following attributes of Doxil®: drug and lipid content, size distribution, zeta potential, free non-encapsulated doxorubicin present in each liposomal formulation, degradation products, and drug and lipid impurity profiles. We expanded our characterization to include properties and analyses relevant to determining the microstructure of liposomal formulations, such as morphology via cryogenic transmission electron microscopy (cryo-TEM) and structural similarity using small angle X-ray scattering (SAXS). Finally, we assess in vitro drug performance using an in vitro dissolution method to characterize release rates across manufacturers compared to the reference product. Using this framework, we can assess the in vitro physicochemical similarity of generic, liposomal formulations with the same composition developed by different manufacturers in reference to the RLD.

Thus, the objective of the present research was to compare the physicochemical similarity of Doxil® with each FDA-approved generic, liposomal DOX formulation available on the market during the time of study. Existing literature only compares one generic formulation with the RLD, and we seek to evaluate the similarities and differences of several approved generic, liposomal DOX products with the RLD. This research provides measured specification ranges to evaluate the in vitro physicochemical sameness of the CQAs measured in formulations of the same composition, which were developed by different manufacturers. From this work, the current knowledge of the CQAs associated with developing Q1/Q2(Q3) compliant generic formulations can be expanded to encourage subsequent development and approvals of generic products.

### 4.3 Materials and Methods

Doxil® was manufactured by Baxter Healthcare (Deerfield, IL, USA) and Doxorubicin Hydrochloride Liposome Injection formulations (2 mg/mL) manufactured by Sun Pharmaceuticals (Goregaon, Mumbai, India), Dr. Reddy's Laboratories (Hyderabad, Telangana, India) and Zydus LifeSciences Global FZE (Ahmedabad, Gujarat, India) were purchased from the University of Michigan Hospital Pharmacy. Daunorubicin hydrochloride was purchased from Sigma Aldrich (St. Louis, MO, USA). Doxorubicinone and daunorubicinone were purchased from Cayman Chemical (Ann Arbor, MI, USA). Hydrogenated soy phosphatidylcholide (HSPC) and 1,2-distearoyl-sn-glycero-3-phosphoethanolamine-N-[amino (polyethylene glycol)-2000] (ammonium salt) (DSPE-PEG 2000) were purchased from Lipoid GmbH (Ludwigshafen, Germany). Lyso-PC (16:0) and Lyso-PC (18:0) were purchased from Avanti Polar Lipids

(Birmingham, AL, USA). Cholesterol and ammonium acetate were purchased from Sigma Aldrich (St. Louis, MO, USA). Poly-Prep chromatography columns (Cat No. 731-1550 and 731-1553) were purchased from Bio-Rad Laboratories (Hercules, CA, USA). TOYOPEARL HW-55F resin in ethanol was purchased from Tosoh Bioscience (Grove City, OH, USA). Holey carbon grids (R 1.2/1.3, 300 Mesh, Copper) were obtained from Quantifoil (Großlöbichau, Germany). Round cryo grid boxes with lids were obtained from MiTeGen (Ithaca, NY, USA). C-clips and c-clip rings were purchased from Thermo Fisher (Waltham, MA, USA). Liquid nitrogen and dewars were provided by the University of Michigan Life Sciences Institute Cryo-EM Core Facility (Ann Arbor, MI, USA). Axygen 96-well full-skirt clear PCR microplate and nonsterile, 96 Round Well Sealing Mat for PCR microplates were purchased from Corning (Corning, NY, USA). All other solvents and reagents were of analytical grade and were purchased from Fisher (Waltham, MA, USA).

### *4.3.1 Particle Size*

Particle size was measured using the Malvern ZetaSizer Nano ZSP (Worcestershire, England, UK). Liposomal doxorubicin samples were diluted 10-fold in deionized water and transferred to Plastibrand® semi-micro disposable cuvettes (BRAND GMBH, Wertheim, Germany) for analysis. Water and liposome were selected as the dispersant and material, respectively, and the measurement temperature was 25°C. The refractive index for water and liposome were set to 1.33 and 1.45. The viscosity was 0.8872 cp for water at 25°C and sample equilibrium time was set to 120 seconds. All samples were measured in triplicates, and the particle size data obtained was zeta average, an intensity-based harmonic mean, plotted as a function of intensity (%) versus particle size (nm). Particle size data was directly obtained from the built-in software.

### *4.3.2 Zeta Potential*

Zeta potential measurements were performed using the samples prepared for particle size analysis. A 1 mL syringe was used to handle and transfer the sample solution from semi-micro disposable cuvettes to DTS1070 folded capillary cells (Malvern Panalytical Ltd, England). Sufficient volume of solution covered the electrodes on both sides of the capillary cell. Zeta potential was measured using the Malvern ZetaSizer Nano ZSP under the same system

parameters for the particle size method and the dielectric constant was set to 78.5. Data was reported in millivolts.

### *4.3.3 Doxorubicin Content*

DOX content was quantified using ultra performance liquid chromatography (UPLC). An Acquity UPLC-TUV detector system with Empower 3 software was used with a BEH C18 column (100 × 2.1 mm, 1.7 µm) (Waters Corporation, Milford, MA, USA) under isocratic conditions consisting of deionized water with 0.1% formic acid as aqueous solvent (A), and methanol with 0.1% formic acid as organic solvent (B). Liposomal DOX samples were diluted 100-fold in methanol. A 45% to 55% ratio of mobile phase for solvent A to B was employed. Flow rate was set to 0.3 mL/min, injection volume was 10 µL, detection wavelength was 254 nm, and the run time lasted 15 minutes. A method description for standard curve generation is provided in Supplementary Materials.

### *4.3.4 Lipid Content*

Lipid concentration was quantified using an Acquity UPLC with an evaporative light scattering detector (ELSD) system with Empower 3 software (Waters Corporation, Milford, MA, USA). A gradient mobile phase was used to separate HSPC, DSPE-PEG (Mw 2000) and cholesterol, and consisted of two solvent systems: A) a mixture of 40% v/v deionized water and 60% v/v methanol with 10 mM ammonium acetate buffer pH 6.4, and B) a mixture of 90% v/v isopropanol and 10% v/v methanol with 10 mM ammonium acetate buffer pH 6.4. The 10 mM ammonium acetate buffer was prepared by adding 77 mg of ammonium acetate to 100 mL of deionized water, and the pH of the solution was adjusted to 6.4.

Liposomal DOX samples were diluted 40-fold in methanol and vortexed to mix. An Xbridge C18 column (4.6 x 150 mm, 3.5 µm) (Waters Corporation, Milford, MA, USA) was used to separate the lipids. The flow rate and column temperature were set to 1 mL/min and 45 °C. Injection volume was 10 µL and the run time was 15 min. ELSD gas pressure was set to 40 psi, data rate was set to 10 points per second and the temperature of the drift tube was set to 55 °C. Gain was set to 150 and the nebulizer was set to heating at 45%. Compressed gas was used for ELSD operation. A method description for the gradient and standard curve generation is provided in Supplementary Materials.

### *4.3.5 Doxorubicin Purity*

Another UPLC-TUV method was developed to identify DOX impurities. The mobile phase consisted of two solvents: A) deionized water with 0.1% formic acid, and B) a mixture of 80% v/v acetonitrile and 20% v/v methanol with 0.1% formic acid. Daunorubicin hydrochloride, doxorubicinone, and daunorubicinone are designated as doxorubicin process and product-related impurities by the United States Pharmacopeia (USP). Liposomal DOX samples were prepared by diluting the samples 10-fold in methanol. A UPLC BEH C18 column (100 × 2.1 mm, 1.7 μm) was used to separate impurities from doxorubicin. Column temperature and flow rate were set to 35 °C and 0.5 mL/min. An injection volume of 10 μL, run time of 10 minutes, and dual detection wavelengths (220 and 254 nm) were used to identify doxorubicin and impurity peaks. The relative retention time (RRT) for each impurity standard in reference to the doxorubicin standard was calculated and impurities were identified by assigning corresponding peaks in each sample based on standard RRT ± 5%. Doxorubicin and impurity concentration were calculated using the linear regression equation from the standard curve (Supplemental Materials).

#### *4.3.6 Lipid Purity*

Lipid purity was determined using a UPLC assay with an evaporative light scattering detector (ELSD) under the same conditions detailed in section 2.2.4. Lysophosphatidylcholine (Lyso-PC) 16:0 and 18:0 are two common lipid degradants from hydrolysis that often occurs in dissolution. Impurity stock solutions (1 mg/mL) were prepared in methanol and diluted to 0.05 mg/mL. Liposomal DOX samples were diluted 40-fold in methanol. The UPLC-ELSD method for lipid purity was performed and a doxorubicin standard was spiked with Lyso-PC (16:0) and Lyso-PC (18:0) to identify the retention time of each impurity peaks in our sample. The concentration of each lipid impurity was quantified by calculating the percentage ratio of peak area for the lipid impurity to the cumulative lipid peak area.

#### *4.3.7 Free, Non-Encapsulated Doxorubicin in Liposomal Formulations*

Separation of free, non-encapsulated DOX from liposomal DOX was achieved using size exclusion chromatography. Poly-Prep columns were washed with methanol and water. 600 μL of TOYOPEARL HW-55F resin (in ethanol) was added to the column and installed on a vacuum manifold processing station. Excess water was drained from the columns before loading the sample and the resin surface was kept flat. Liposomal DOX (10 μL) was carefully added to the resin surface. A free DOX solution (20 μL) prepared at a concentration of 1 mg/ml in methanol was loaded onto an equivalent resin bed volume (600 ul) for equivalent measurement of free

doxorubicin recovery. Deionized water (400 µL) was slowly added to the column and the wash solution was collected under vacuum into a microtube. The water wash was repeated three times and 1.2 mL of water wash solution was collected. Next, 400 µL of a 50:50 acetonitrile/methanol solution was slowly added to the column. The same wash procedure was performed using the organic solution and 1.2 mL of organic wash solution was collected. The wash solution tubes were transferred to a nitrogen evaporator set to 50 °C to dry the samples. Dry sample residues were reconstituted with 250 µL of methanol. A reference sample was prepared by adding 240 µL of methanol to 10 µL of liposomal DOX. Samples were transferred to UPLC vials and free, non-encapsulated doxorubicin content was quantified using the previously developed UPLC-TUV method described in section 2.2.5. Free doxorubicin content was calculated using the following equation:

$$\%\ Free\ Doxorubicin = \frac{Peak\ Area\ of\ DOX\ in\ test\ sample}{Peak\ Area\ of\ DOX\ in\ reference\ sample} \times 100 \qquad \text{(Eqn. 1)}$$

***4.3.8 Cryogenic Transmission Electron Microscopy (Cryo-TEM)***

Doxorubicin liposome morphology was determined utilizing the cryo-TEM technique in collaboration with the University of Michigan (U-M) Life Sciences Institute (LSI) CryoEM Core Facility. Liposomal DOX formulations at a doxorubicin concentration of 2 mg/mL were plunged frozen in liquid ethane cooled to freezing point in liquid nitrogen using a Vitrobot plunge freezer (ThermoFisher Scientific, Waltham, MA, USA). 3 µL of liposomal DOX samples were deposited onto glow-discharged (PelcoEasiGlow discharger) Cu 300 R 1.2/1.3 holey carbon grids (Quantifoil, Großlöbichau, Germany) and samples were frozen on the grids using the following Vitrobot parameters (10 second wait time, 5 second blot time, 100% humidity, 4°C). Samples were visualized under cryogenic conditions on a Talos Arctica (ThermoFisher Scientific, Waltham, MA, USA) operated at 200 kV. Images were recorded using a Gatan K2 Summit direct electron detector (Gatan, Pleasanton, CA, 94588) in counting mode at 17.5 kx magnification, corresponding to a pixel size of 2.48 Å/pixel. SerialEM v4.1 was used to control microscope and camera functionality [118,119]. The exposure time was set to deliver 20 electrons/Å2 cumulative dose to the area of interest. Representative images of each sample were recorded from the center of the holes. FIJI/ImageJ was used to manually measure particle dimensions of length, width, and membrane thickness using a minimum sample size of 500 liposomes [120].

***4.3.9 Small Angle X-Ray Scattering (SAXS)***

The SAXS technique was used to characterize the microstructure similarity of DOX liposomes present in liposomal DOX formulations developed by different manufacturers. Microstructure was analyzed using the high-throughput SAXS technique (HT-SAXS) and similarity between batches was compared using the SAXS Similarity tool developed and conducted by the SIBYLS Beamline (12.3.1) of the Advanced Light Source at the Lawrence Berkeley National Laboratory (Berkeley, CA, USA), supported by the US Department of Energy and National Institutes of Health [121]. Liposomal DOX samples were added to an AXYGEN 96-well full-skirt clear PCR microplate with a consistent volume of 30 µL of buffer and sample at three concentrations between 1-10 mg/mL. Labeled concentration for liposomal doxorubicin hydrochloride formulations is 2 mg/mL. Therefore, the following concentrations were prepared for SAXS analysis: 1 mg/mL (low concentration), 1.5 mg/mL (medium concentration) and 2 mg/mL (high concentration).

Buffer preparation is critical for SAXS analysis as it can impact the scattering profile of the sample. The prepared formulation buffer should be as closely resemblant of the buffer present in the original sample. Therefore, the prepared formulation buffer was comprised of a 9.4% sucrose solution with 1.55 mg/mL histidine at pH 6.5 similar to the buffer used in the manufacturing of the commercial formulation. 100 mL of buffer was prepared by adding 9.4 g of sucrose and 155 mg of L-histidine to deionized water. The pH of the solution was adjusted to 6.5 with 1 N of sodium hydroxide and/or hydrochloric acid. Prepared buffer and sample solutions were transferred to two 96-well PCR microplates, sealed, and kept under cold conditions prior to analysis by the SIBYLS Beamline at the Lawrence Berkeley Laboratory.

#### *4.3.10 In Vitro Dissolution*

In vitro dissolution testing provides critical information to characterize the rate and extent of drug release from a finished dosage form, which can be correlative of *in vivo* drug performance. From a regulatory perspective, dissolution testing is used in formulation evaluation during product development for batch-to-batch quality control and assurance [122]. A dissolution method with discriminative capability, capable of characterizing release profiles of formulations of the same composition but from different manufacturers when compared to the reference product, is crucial to assess a product's performance and efficacy. Yuan et al developed a conventional release method using dialysis membranes and the referenced method was employed in the present work to evaluate dissolution profiles for one batch per manufacturer [123].

Briefly, 0.8 mL of each liposomal DOX formulation ($C_{DOX}$ = 2 mg/mL) was added to 300 kDa Float-a-lyzer dialysis tubes which were inserted into 50-mL centrifuge tubes containing 39.2 mL release media containing 100 mM ammonium bicarbonate, 75 mM MES buffer, 5% w/v hydroxypropyl-β-cyclodextrin, 5% w/v sucrose, 0.02% sodium azide at pH 6. The centrifuge tubes were placed on an orbital shaker (ThermoFisher MaxQ 6000) operating at 320 rpm speed and incubated at 45°C. A free DOX solution was prepared with doxorubicin hydrochloride in the same release media at an equivalent concentration ($C_{DOX}$ = 2 mg/mL) as the liposomal formulation. 0.8 mL of the free DOX solution was added directly to a 50-mL centrifuge tube containing 39.2 mL of release media and was used as a positive control. At 0, 1, 2, 4, 8, 12, and 24 hours, 150 µL of release media was sampled for UV detection at 480 nm on a plate reader (Synergy NEO HTS Multi-Mode Microplate Reader (Bio-Tek) and replaced with an equal amount of fresh release media. Samples were prepared and analyzed in triplicate. The cumulative percent DOX release was calculated using the following equation:

$$Cumulative\ DOX\ release\ (\%) = \frac{C_{DOX\ of\ liposome\ formulations}}{C_{DOX\ of\ free\ DOX\ control}} \times 100\% \qquad \text{(Eqn. 2)}$$

## 4.4 Result

### *4.4.1 Size Characterization*

We used dynamic light scattering (DLS) to determine the liposome size, size distribution and polydispersity index (PDI) for each batch formulation. All liposomal formulations were similar in liposome size on average around 90 nm using water as the diluent (Fig. 1a, Appendix Table A.7). Particle size across all batches of the innovator formulation ranged between 86 – 95 nm, whereas the particle size across generic formulations was slightly smaller ranging from 84 – 90 nm (Appendix Table A.7). Minor variations in PDI between innovator and generic formulations existed with PDI ranging from 0.045 ± 0.007 to 0.082 ± 0.035 (Fig. 1b, Appendix Table A.7). The median PDI value was approximately 0.050 while batch no. MDZT300 from Baxter Healthcare (0.082 ± 0.035) and batch no. HAC1612A from Sun Pharmaceuticals (0.082 ± 0.015) showed the highest index value.

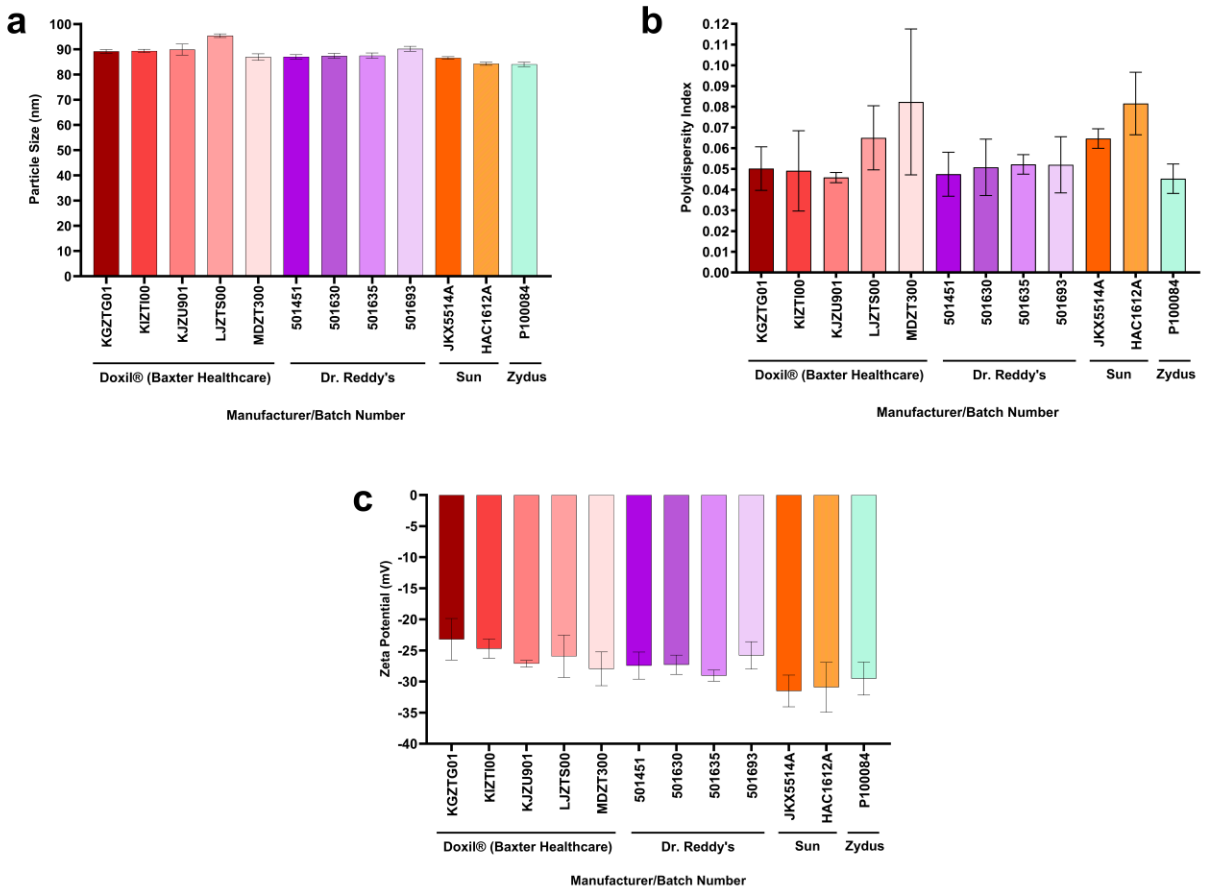


Figure 4-2. Size characterization of doxorubicin liposomes in formulation developed by innovator and different generic manufacturers: Baxter Healthcare, Dr. Reddy's Laboratories, Sun Pharmaceuticals and Zydus. a) Particle size, b) polydispersity index, and c) zeta potential was measured using the Malvern Zetasizer (mean ± SD, $n \geq 3$)

### *4.4.2 Zeta Potential*

DLS was also used to determine the zeta potential of each formulation. The doxorubicin liposome possesses a negative surface charge that falls within –20 to –32 mV when diluted in water (Fig. 1c, Appendix Table A.7). The most negatively charged formulation was developed by Sun Pharma (batch no. JKX5514A) with a zeta potential of –31.5 ± 2.5 mV. Batch-to-batch variation for innovator formulations ranged from –23.2 ± 3.34 mV to –27.9 ± 2.72 mV, and the least negatively charged liposomal formulation was batch no. KGZTG01. Minimal batch-to-batch variation in zeta potential existed between generic formulations, however, batch formulations developed by Sun and Zydus Pharmaceuticals measured were much more negatively charged than the innovator formulations. Dr. Reddy's batches fell between –25.8 ±

2.20 mV and –29.0 ± 0.90 mV, and Sun Pharma and Zydus batches were comparable, between –29.5 ± 2.65 mV and –31.5 ± 2.55 mV.

### *4.4.3 Doxorubicin & Lipid Content*

Several ultra performance liquid chromatography (UPLC) methods for quantifying DOX and lipid ingredients were established. Label claim states that each vial of Doxil® contains 2 mg/mL of DOX hydrochloride, 9.58 mg/mL HSPC, 3.19 mg/mL of MPEG-DSPE, and 3.19 mg/mL of cholesterol. Quantification was carried out on several batches of each product, and batch-to-batch variation falls within + 5% of the label claim value. Measured DOX concentrations for innovator Doxil® formulations ranged between 1.94 + 0.02 and 2.03 + 0.06 mg/mL. Dr. Reddy formulations ranged between 1.97 + 0.03 and 2.09 + 0.06 mg/mL. Sun Pharma batch formulations #JKX5514A and #HAC1612A had measured DOX concentrations of 1.90 + 0.04 and 1.91 + 0.03 mg/mL, respectively, and Zydus batch formulation #P100084 had a measured DOX concentration of 2.09 + 0.06 mg/mL (Fig. 2a, Appendix Table A.8).

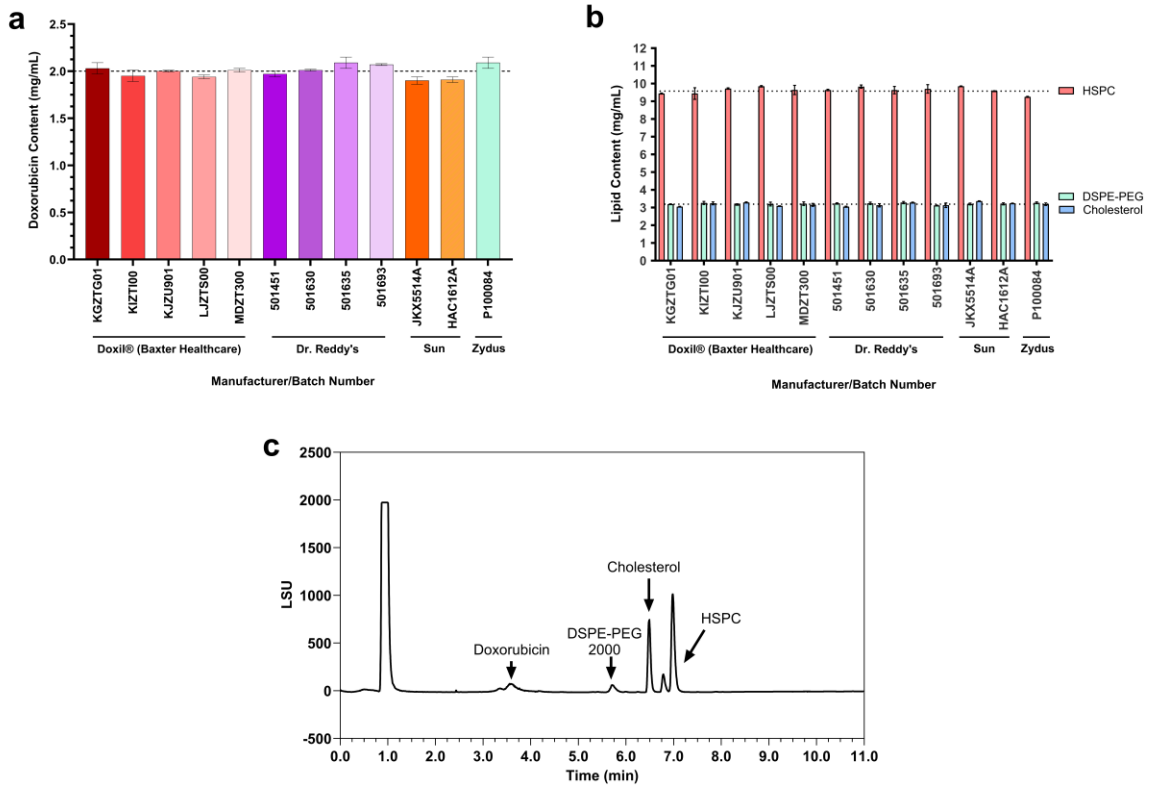


Figure 4-3. Measured doxorubicin and lipid content present in different liposomal preparations of doxorubicin hydrochloride produced by different manufacturers (mean ± SD, n = 3). a) Doxorubicin content, b) Lipid content for HSPC, DSPE-PEG (MW 2000) and cholesterol. **c**)

Chromatographic separation of doxorubicin from lipid components using an UPLC-ELSD assay under a gradient mobile phase

HSPC concentrations for innovator Doxil® formulations ranged from 9.44 + 0.03 to 9.85 + 0.04 mg/mL which fell within + 5% of the label claim value (Fig. 2b, Appendix Table A.8). Dr. Reddy's batch formulations ranged from 9.63 + 0.21 to 9.83 + 0.09 mg/mL. HSPC content for Sun Pharma batch #JKX5514A and HAC1612A was 9.85 + 0.02 and 9.58 + 0.02 mg/mL, and HSPC content for Zydus batch #P100084 was measured at 9.25 + 0.03 mg/mL (Fig. 2b, Appendix Table A.8).

Cholesterol levels for innovator Doxil® formulations ranged between 3.05 + 0.02 and 3.29 + 0.03 mg/mL, which also fell within + 5% of label claim concentration (Fig. 2b, Appendix Table A.8). Cholesterol concentration for Dr. Reddy batch formulations fell within the same range from 3.05 + 0.03 and 3.28 + 0.03 mg/mL. Sun Pharma batch formulation #JKX5514A and #HAC1612A had measured cholesterol levels of 3.36 + 0.02 and 3.24 + 0.01 mg/mL, respectively, and Zydus batch formulation #P100084 had a measured cholesterol concentration of 3.19 + 0.07 mg/mL (Fig. 2b, Appendix Table A.8).

Measured DSPE-PEG (Mw 2000) concentration was comparable with label claim concentration (3.19 mg/mL), fell within acceptable limits of variation across all batch manufacturers and within a narrow range of measurement from 3.12 + 0.02 and 3.26 + 0.09 mg/mL (Fig. 2b, Appendix Table A.8). Fig. 2c shows chromatographic separation and identification of lipids in reference to the elution profile of doxorubicin using the UPLC-ELSD method described in section 2.2 4. The initial peak in Fig. 2c corresponds to the sucrose/histidine buffer component present in the liposomal formulation.

#### *4.4.4 Doxorubicin Purity*

Greater than 99% DOX purity using the UPLC-TUV method was observed across innovator and generic batch formulations (Fig. 3a, Appendix Table A.9). For innovator Doxil® formulations, impurity levels for doxorubicinone, daunorubicin and daunorubicinone ranged from 0.11 + 0.20% to 0.33 + 0.06%, 0.00 + 0.00% to 0.18 + 0.24%, and 0.00 + 0.00% to 0.50 + 0.07%, respectively (Fig. 3b-d, Appendix Table A.9). The greatest impurity level measured for doxorubicinone is found in Sun Pharma batch #JKX5514A, HAC1612A and Zydus batch #P100084 at 0.67 + 0.43%, 0.40 + 0.35%, and 0.42 + 0.24%, respectively (Fig. 3d, Appendix Table A.9). In consideration of these results, method variability may be a probable cause for

some variation; thus, the data should be interpreted with caution. Fig 3e shows a representative chromatogram of the elution profile for doxorubicin, daunorubicin, doxorubicinone and daunoribicinone at retention times of 5.50, 6.62, 6.83, and 8.37 minutes respectively.

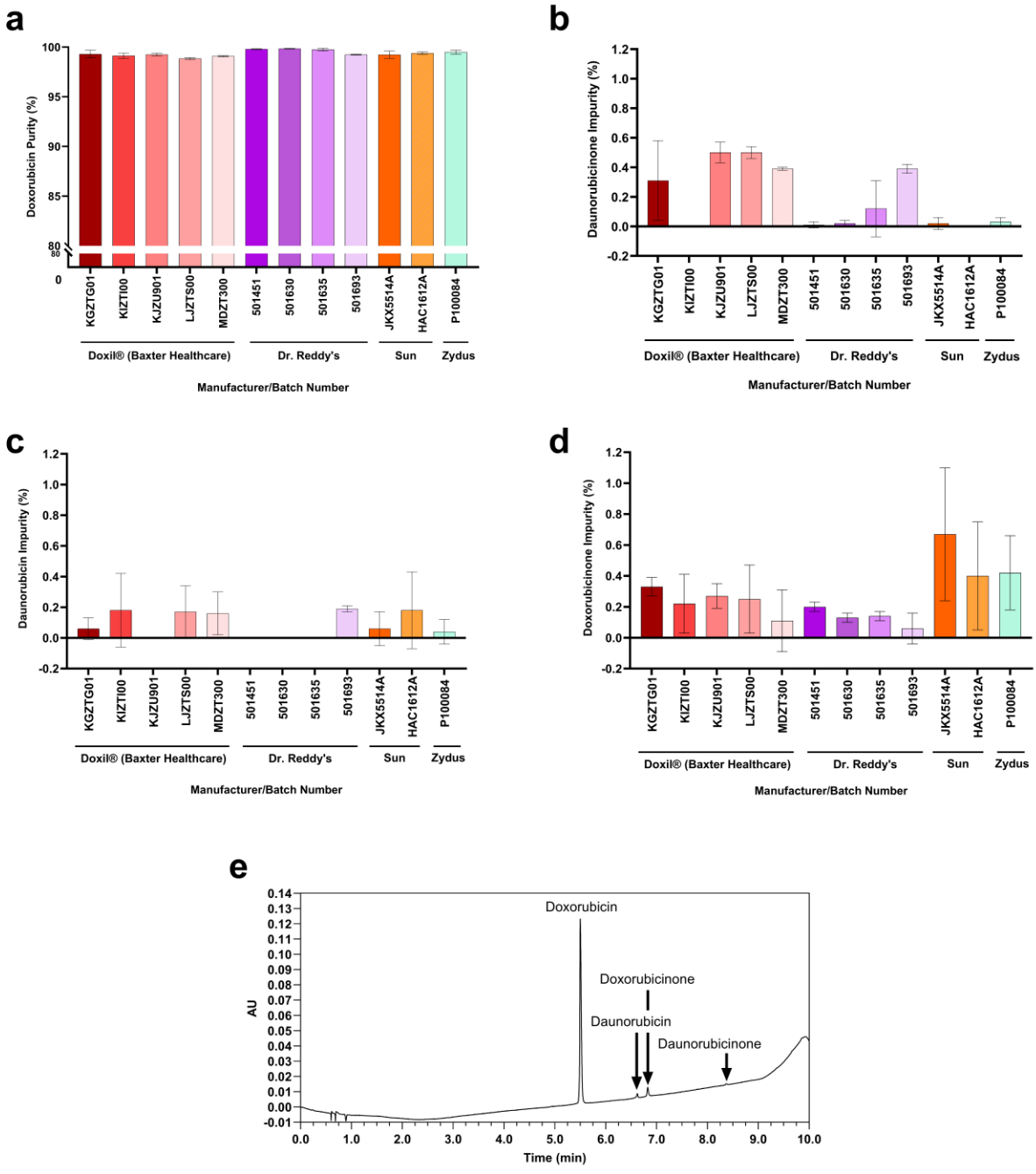


Figure 4-4. Purity of liposomal doxorubicin formulations quantified as a percentage of peak AUC over cumulative peak AUC in each sample using UPLC-TUV analysis. a) Doxorubicin purity (%), b) daunorubicinone impurity levels (%), c) daunorubicin impurity levels (%), d)

doxorubicinone impurity levels (%), e) chromatographic separation of doxorubicin and the respective impurities (mean ± SD, $n = 3$)

### *4.4.5 Lipid Purity*

Quantification of cumulative lipid impurities, lyso-PC 16:0 and 18:0, present in different liposomal DOX formulations ranged from 0.44 ± 0.21 to 2.21 ± 0.03 percent (Fig. 4a). The elution of lyso-PC 16:0 and 18:0 standards compared with the chromatographic profile of Dr. Reddy's formulation in Fig. 4b shows lyso-PC 16:0 and 18:0 peaks that are slightly offset from the standards at low quantities in terms of peak area. We quantified the percentage of cumulative lipid impurity by calculating the ratio of cumulative impurity peak area to the cumulative lipid peak area.

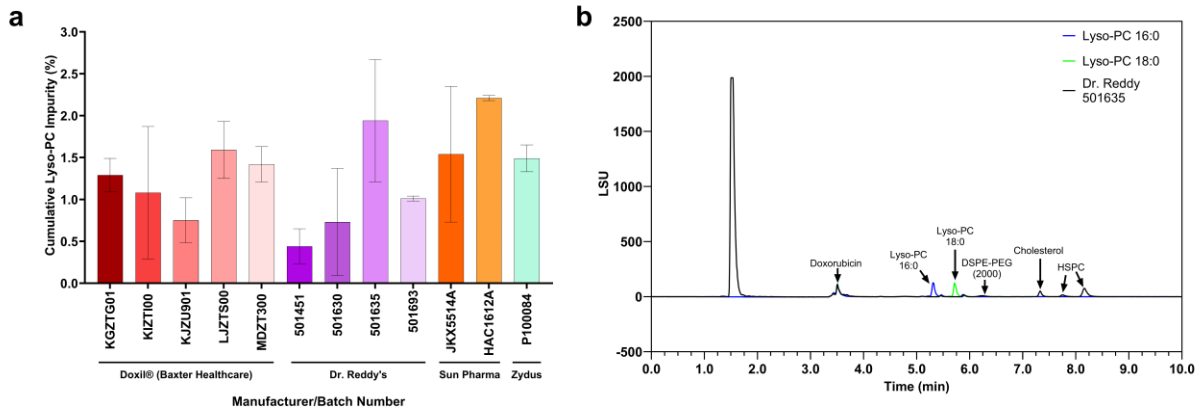


Figure 4-5. Quantification of lipid impurities in liposomal doxorubicin hydrochloride formulations. a) cumulative lyso-PC (16:0) and (18:0) impurities (mean ± SD, n ≥ 2). b) Chromatographic separation of lyso-PC (16:0) and (18:0) impurities in a representative, liposomal DOX sample manufactured by Dr. Reddy's Laboratories

### *4.4.6 Free, Non-Encapsulated Doxorubicin in Liposomal Formulations*

Varying levels of free, non-encapsulated doxorubicin were quantified in different liposomal formulations using the UPLC-TUV method described herein. All batches across manufacturers had non-encapsulated DOX levels less than 2%, ranging from 0.37 ± 0.04% for Sun Pharmaceuticals batch JKX5514A to 1.99 ± 0.03% for Dr. Reddy's batch 501451. The greatest level of non-encapsulated DOX present in Baxter formulations was 1.93 ± 1.01% for batch KIZTI00 whereas the amount of non-encapsulated DOX present in Zydus P100084 was 1.32 ± 0.92 % (Fig. 5, Appendix Table A.10). The recovery of free doxorubicin hydrochloride loaded at an equivalent weight relevant for the test was 90.98 + 0.18%.

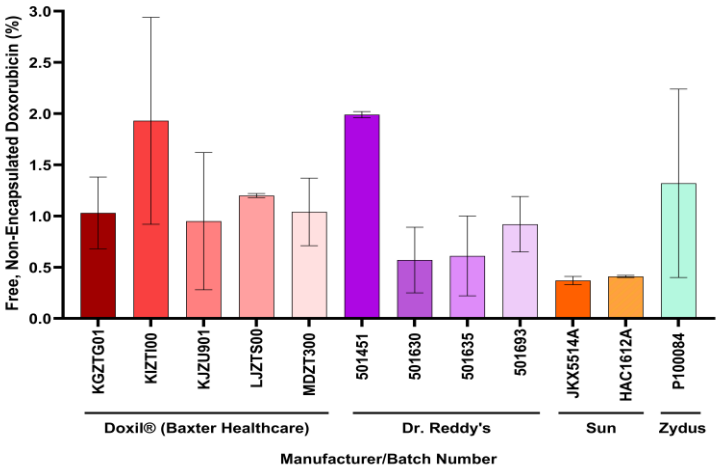


Figure 4-6. Quantification of free, non-encapsulated doxorubicin present in liposomal doxorubicin hydrochloride formulations produced by different manufacturers (mean ± SD, n ≥ 2)

### *4.4.7 Cryo-TEM*

One representative batch of liposomal DOX was analyzed for morphology of the DOX liposome using the cryo-TEM technique, MDZT300 (Baxter Healthcare), 501635 (Dr. Reddy's), JKX5514A (Sun Pharmaceuticals), and P100084 (Zydus). The shape and morphology of the DOX liposome is consistent across formulations developed by each manufacturer. DOX liposomes posess a "coffee bean" like shape and thread-like filaments visible in the aqueous core of the liposome represent the insoluble, doxorubicin-sulfate crystal [124]. Differences in uniformity and homogeneity of particles can be directly observed in Fig. 6. While each formulation appears heterogeneous and less uniform, Dr. Reddy's batch no. 501635 (Fig. 6c) shows good uniformity of liposomes.

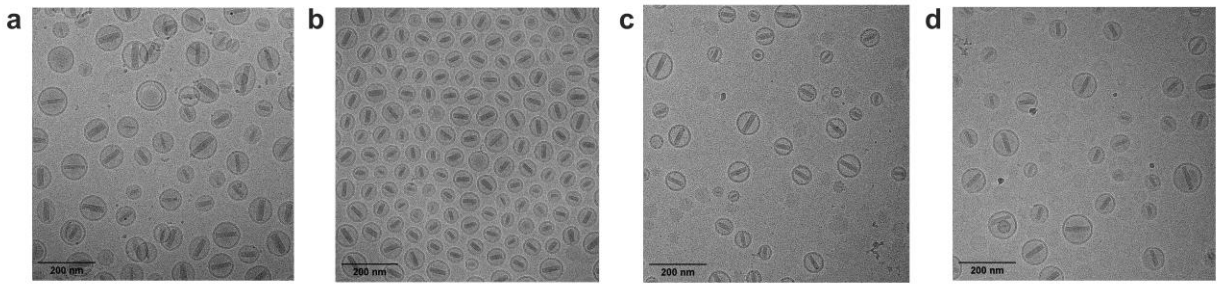


Figure 4-7. Morphology of the doxorubicin liposome from different formulations: a) Doxil.® (batch no. MDZT300); b) Dr. Reddy's (batch no. 501635); c) Sun Pharmaceuticals (batch no. JX5514A); d) Zydus (batch no. P100084)

Appendix Table A.11 describes the size dimensions and membrane thickness of doxorubicin liposomes measured manually via FIJI/Image J processing software (mean ± SD, n ≥ 500). The length of the DOX liposome from each formulation ranged from 60.9 ±5 15.1 nm to 73.3 ± 13.1 nm, whereas the width ranged between 57.6 ± 14.8 nm and 66.0 ± 13.0 nm (Appendix Table A.11). Each generic batch imaged had dimensions that were smaller than those of the reference batch from Baxter. Sun Pharma was the smallest at a length and width of 60.9 ± 15.1 and 57.6 ± 14.8 nm, respectively. Membrane thickness was comparable between formulations between 4.5 ± 0.7 and 5.0 ± 0.4 nm among batches (Appendix Table A.11). Fig. S2 depicts the distribution histograms for the measured length and width of each formulation.

### *4.4.8 SAXS*

For complementary analyses, SAXS scattering profiles were generated for the four liposomal DOX formulations imaged using the cryo-TEM technique (Fig. 7a). The scattering profiles were generated using the SAXS technique performed by the SIBYLS Beamline, Advanced Light Source (12.3.1) at the Lawrence Berkeley Laboratory. The data shown in Fig. 7b is matrix comparison of SAXS scattering profiles with formulations that are highly similar in structure clustered together in the upper left corner, while the most dissimilar formulations are clustered in the lower quadrants of a SAXS similarity map. The center diagonal compares each SAXS curve against itself, which results in perfect similarity agreement and zero radius of gyration, ΔRG [125]. Our results demonstrate that the nanostructure of DOX liposomes developed by Dr. Reddy's is different from the innovator formulation and the generic formulations tested. Formulations developed by Zydus and Sun Pharma are more similar in nanostructure than the innovator formulation developed by Baxter Healthcare.

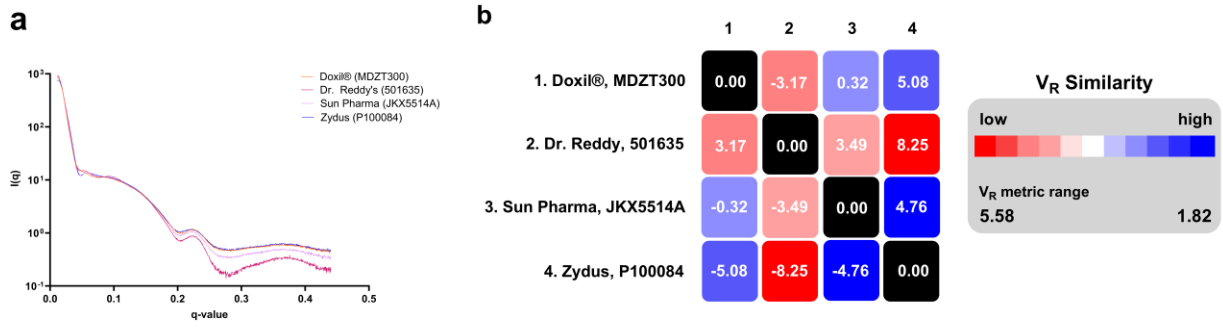


Figure 4-8. SAXS scattering profiles for a) one liposomal DOX formulation representative of each manufacturer (n = 4). b) Structural similarity between generic and reference, liposomal

DOX formulations was compared and depicted using the SAXS similarity map (SSM) developed by SIBYLS at the Advanced Light Source (12.3.1), Lawrence Berkeley Laboratory. The Volatility of Ratio, $V_R$, correlation method was used to define similarity and dissimilarity between samples (mean ± SD, $n \geq 2$)

### *4.4.9 In Vitro Dissolution*

To support the physicochemical evaluation of generic liposomal DOX formulations with the reference Doxil® formulation, we conducted dissolution testing using the conventional dialysis method published by Yuan and colleagues on an individual batch from each manufacturer in our sample inventory (Doxil® #KIZTI00; Dr. Reddy's #501630; Sun Pharma #HAC1612A; Zydus #P100084) (Fig. 8)[123].

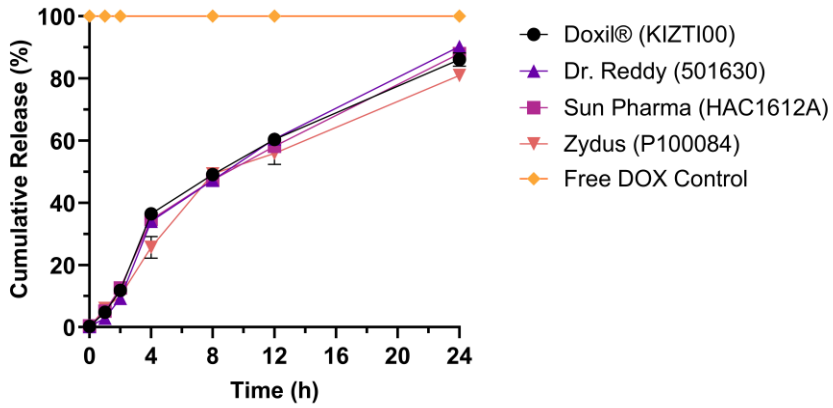


Figure 4-9. Characterization and comparison of in vitro dissolution profiles for individual batches of approved generic liposomal doxorubicin hydrochloride formulations with the reference Doxil® formulation (mean ± SD; n = 3)

Cumulative DOX release was 86.0 + 2.12%, 90.2 + 0.96%, 87.9 + 1.00%, and 81.0 + 1.31% for the batch formulations of Doxil®, Dr. Reddy's, Sun Pharma, and Zydus, respectively. We employed the f2 similarity test to evaluate the similarity of the dissolution profile of each generic formulation with the reference Doxil® formulation. f2 values for Dr. Reddy's (#501630), Sun Pharma (#HAC1612A) and Zydus (#P100084) compared to Doxil® (#KIZTI00) were 91.3, 92.2 and 89.8, respectively.

## 4.5 Discussion

Approval of ANDA submissions for generic, liposomal formulations are dependent upon the success of bioequivalence evaluation of the generic drug candidate. The FDA recommends in vitro and in vivo testing to establish bioequivalence as described in the draft guidance for liposomal doxorubicin hydrochloride [56]. Physicochemical characterization is critical for the evaluation of liposomal dosage forms as these properties dictate in vivo drug product behavior. Previous studies have identified critical quality attributes (CQA) relevant for drug performance in alignment with liposome characteristics detailed in the FDA draft guidance that should be equivalent to the reference listed drug in order for the generic drug candidate to become eligible for bioequivalence studies [56,112,115,126,127]. These characteristics include liposome composition, size distribution, electrical surface potential, state of encapsulated drug, internal environment of the liposome, and in vitro leakage rates comparable to the reference standard [56].

Key attributes of Doxil® evaluated in this work included particle size, polydispersity, zeta potential, DOX and lipid content, DOX and lipid purity, the amount of non-encapsulated DOX present in the formulation, morphology, nanostructure and in vitro release. We identified these attributes as critical for in vitro drug performance for liposomal DOX formulations due to their in vivo implications related to drug safety and efficacy. Changes in size and zeta potential between generic and reference formulations may influence the stability, circulation and absorption of the liposomal nanoparticle [128]. Our results confirmed the similarity of particle size and polydispersity between different products despite dilution in water which would subsequently decrease the 9.4% sucrose content of the liposomal formulations. Given that the formulation was diluted 10-fold by water, the final sucrose concentration was 0.94%. At such low concentration, sucrose has a minimal impact on the viscosity and refractive index of the solution. Thus, we sought to characterize particle size in water using the viscosity (0.8872 cP) and refractive index (1.330) of water at 25°C for size analysis via DLS.

For zeta potential, the pH of the dissolving media plays a crucial role as it influences ionization of the functional groups on the particle surface and ion distribution within the electrical double layer. At acidic conditions, these surface groups may become protonated which could reduce the net negative charge making the zeta potential less negative or even give a positive charge. At basic conditions, surface groups may become deprotonated which would increase the negative charge on the liposome surface [129,130]. Diluting these liposomal samples in

water at neutral pH reflected pH values that were very similar to the original, undiluted suspensions minimizing the impact on zeta potential. Differences in drug and lipid content can affect the drug-to-lipid ratio and consequently, membrane rigidity and liposome stability in plasma. Quantification of non-encapsulated DOX present in liposomal formulations can provide insight into the state of the drug in each formulation. The package insert states that greater than 90% of DOX is encapsulated in liposomes, however, an increase in non-encapsulated drug may present safety and toxicity concerns related to the free drug analog [131].

Morphology and nanostructure assessment utilizing electron microscopy and x-ray light scattering techniques is particularly useful for visualization and comparison of different liposomal formulations of the same composition. Qualitative visualization using cryo-TEM imaging complements quantitative characterization for assessing formulation similarity and in vitro bioequivalence evaluation. We observed the heterogeneous inner structure of the liposome, whose impact on drug performance may warrant further investigation as differences in nanostructure may impact the rate and extent of drug release. The liposomes imaged in Figure B from the Dr. Reddy's batch display a greater degree of liposome uniformity in terms of size, shape, density and morphology when compared to the representative innovator Doxil® batch, as well as Sun Pharma and Zydus batches. Possible explanations for these differences may lie in minor processing differences in during liposome formation lending itself to increased uniformity of the liposome population. In this regard, the application of cryo-TEM can serve as a useful tool to evaluate liposome uniformity during the formulation development stage.

Selective characterization of these properties in vitro can highlight the similarities and differences between approved, generic and innovator formulations for liposomal dosage forms containing DOX and provide the rationale for future work to develop an in vitro in vivo correlation using drug release assays. Subsequent evaluation of in vitro release for individual batches from each manufacturer revealed similar cumulative release rates for Doxil®, Dr. Reddy's, Sun Pharma and Zydus formulations, suggesting a high degree in formulation sameness and physicochemical similarity necessary for bioequivalence evaluation. For liposomal formulations, dissolution testing can provide critical insights into the release kinetics of the active ingredient, and determination of a faster or slower release rate may adversely influence the product's performance and efficacy when considered among other physicochemical properties as a predictive correlation of in vivo performance.

This chapter provides a framework for multiple tests which strengthens the comparative assessment between generics and innovator products. Although, the methods repeated in our labs showed high reliability, additional research at other laboratories to confirm the integrity of the framework is useful. Cost of testing with the SIBYLS Beamline, Advanced Light Source at the Lawrence Berkeley Laboratory is not onerous as it is largely funded by the NIH and the DOE through the ALS-ENABLE and High-End Instrumentation grants. Other costs associated with sample preparation and shipping cold transport are with the originating laboratory which otherwise makes this method to structurally characterize liposomal samples using HT-SAXS highly accessible. However, CryoTEM can be costly, requires extensive training and access to a core facility that offers or specializes in electron microscopy. CryoTEM and SAXS can be used as complimentary methods for structural characterization and comparative analysis of complex liposomal products, however, with subsequent model fitting and simulation, SAXS analysis can also be used to estimate size parameters in lieu of direct measurement from cryoTEM images.

**4.6 Conclusion**

In this work, we devised a series of analytical methods for physicochemical characterization and comparison of DOX liposomes in formulations with the same composition developed by different manufacturers. Size distribution, zeta potential, drug and lipid content, impurity identification, free non-encapsulated DOX in formulation, morphology via cryo-TEM, microstructure via SAXS, and in vitro release were parameters assessed for the Q1/Q2(Q3) evaluation of the selected sample population. Several batches from three FDA-approved, generic products and the reference Doxil® formulation developed by the innovator company, Baxter Healthcare, were compared in each of our characterization studies with representative batches used for TEM/SAXS analysis.

Our results showed formulation similarities and minor variation across different attributes assessed in the Q3 evaluation of generic, liposomal DOX products. DOX purity, lipid purity, and the amount of free non-encapsulated DOX within liposomal formulations are critical to ensure the safety, efficacy, stability, and quality of each liposomal product. Our experimental results show a low prevalence of drug and lipid impurities and acceptable levels of non-encapsulated DOX in each formulation. Complementary methods using DLS, cryo-TEM, and SAXS provide useful information to elucidate the morphology and nanostructure similarity of different liposomal DOX formulations, which are essential to minimize differences that could adversely

impact drug performance. Ultimately, structural characterization techniques can support physicochemical evaluation and uphold commitment to product safety and quality for patients. It is our intent that the comparative analysis and methods outlined in this study may provide a useful framework for subsequent evaluation of complex, liposomal generics and similar follow-on products to increase the generic availability of complex, liposomal products on the market.

# Chapter 5 Conclusions and Future Directions

The overarching goal of this dissertation was to bridge the gap between understanding the microstructural complexity of existing complex drug products and leveraging those insights to develop improved novel therapeutics. By employing rigorous reverse-engineering strategies, we successfully decoded the intricate relationships between physicochemical attributes and drug performance in two complex systems: emulsion-based semi-solid vaginal gels (Crinone®) and PEGylated liposomes (Doxil®). Building upon the mechanistic understanding gained from these commercial benchmarks, we successfully designed a novel progesterone vaginal hydrogel that overcomes the inherent clinical limitations of the reference product. Together, this work not only provides a robust, multi-dimensional analytical framework to accelerate complex generic drug development but also demonstrates the power of rational formulation science in creating next-generation, patient-centric drug delivery systems.

Chapter 2 reviewed the comprehensive physicochemical and functional characterization of Crinone®, with the aim of elucidating the critical attributes governing its performance as a complex vaginal gel product. Structural analyses by polarized light microscopy, scanning electron microscopy, and X-ray diffraction confirmed that P4 remained dispersed within the formulation as crystalline particles, while differential scanning calorimetry suggested interactions between progesterone and the gel matrix through the observed shift in thermal behavior. Across all tested batches, Crinone® demonstrated highly consistent globule size distribution, rheological properties, syringeability, mucoadhesion, and mechanical characteristics. In particular, the formulation exhibited a shear-thinning and predominantly elastic behavior, which facilitates vaginal application while maintaining retention after administration. IVRT further demonstrated highly similar release profiles among batches, with gradual P4 release extending over 48 hours. Together, these findings establish a detailed physicochemical profile of Crinone® and provide a scientific basis for future bioequivalent generic development, while also improving the understanding of structure–performance relationships in complex vaginal drug delivery systems.

Future studies should focus on manufacturing in-house generic versions of the Crinone® formulation. By systematically adjusting manufacturing parameters—such as shear rate, processing temperature, and the size of API—we can evaluate whether the characterization established in this work can successfully discriminate between structurally distinct formulations. This approach will help in the understanding of the process-structure-performance relationships, ultimately defining how specific manufacturing deviations impact the CQAs of emulsion-based gels.

Based on the formulation insights gained from Chapter 2, Chapter 3 investigated the development and performance of a novel P4 vaginal hydrogel based on a microwave-prepared P4-RAME-β-CD inclusion complex. Among the CDs evaluated, RAME-β-CD exhibited the highest capacity to solubilize P4 and enabled the conversion of crystalline P4 into a molecularly dispersed form. Incorporation of the inclusion complex into a carbomer/polycarbophil gel resulted in a formulation with favorable syringeability, mucoadhesion, and rheological properties suitable for vaginal administration. Compared with Crinone®, the P4-CD gel showed a faster IVRT profile, greater permeation across vaginal tissue, and substantially increased systemic exposure following vaginal administration. These results indicate that CD complexation can effectively overcome the dissolution-limited behavior associated with conventional crystalline P4 formulations.

To advance the novel P4-CD hydrogel toward clinical application, extensive *in vivo* studies are required. Future work must include pharmacokinetic evaluations in animal models to quantify P4 distribution within the uterine tissue. Additionally, the actual therapeutic efficacy of the P4-CD gel should be directly compared with Crinone® using a mouse preterm birth model. Future exploration should include screening of alternative mucoadhesive hydrogel matrices. By replacing poorly water-soluble polymers like polycarbophil—which are known for causing vaginal residue and local irritation—with fully soluble, highly biocompatible materials, we can significantly improve patient comfort and clinical compliance.

Chapter 4 examined the establishment and application of analytical methodologies for the characterization of liposomal doxorubicin products, including particle size analysis, zeta potential, quantification of doxorubicin and lipid content and purity, free non-encapsulated doxorubicin content in liposomal formulations, morphology and nanostructure. These methods

were applied to reference Doxil® and all approved generics available at the time of study. A comparative study of the physicochemical profiles of liposomal doxorubicin hydrochloride formulations revealed batch to- batch variation across attributes within and between manufacturers. Morphology and nanostructure analysis utilized cryo-TEM and SAXS techniques to identify direct similarities and differences in shape, lamellarity and size between individual batches from each reference and generic manufacturer. Standard characterization data for particle size, zeta potential, drug and lipid content all agreed with label claim and literature, and a comparison of *in vitro* drug performance between products was conducted using a conventional dialysis-based *in vitro* release test (IVRT). Results of the IVRT demonstrated that despite minor differences in certain physicochemical attributes, a high degree of similarity in *in vitro* release is observed suggesting physicochemical similarity for bioequivalence assessment.

Chapter 4 successfully characterized the *in vitro* behaviors of liposomal doxorubicin. Future studies should focus more on the correlation of these microstructural findings with *in vivo* performance and safety profiles. More importantly, future research should apply these methodologies to other complex liposomal formulations whose patents are expiring or have expired, such as Onivyde® (liposomal irinotecan) and AmBisome® (liposomal amphotericin B). Expanding this regulatory science framework will help demystify the Q3 requirements for these advanced nanocarriers, facilitating the rapid development of generic liposomes and ensuring that more patients have access to affordable, high-quality therapeutics.

# Appendices

## Appendix A: Supplementary Materials for Chapter 2

Table A-0-1 Composition of Crinone® vaginal gel and the functions of its excipients

| Composition | Weight percentage (%) | Functions |
|---|---|---|
| Progesterone | 8 | API |
| Glycerin | 12.9 | Humectant |
| Mineral oil | 4.2 | Lubricating agent |
| Polycarbophil | 2 | Gel former |
| Hydrogenated palm oil glyceride | 1 | Lubricating agent |
| Carbomer 934P | 1 | Carbomer 934P |
| Sorbic acid | 0.08 | Preservative |
| Sodium hydroxide | 0 - 2 | pH adjustment |
| Purified water | remaining | Solvent |

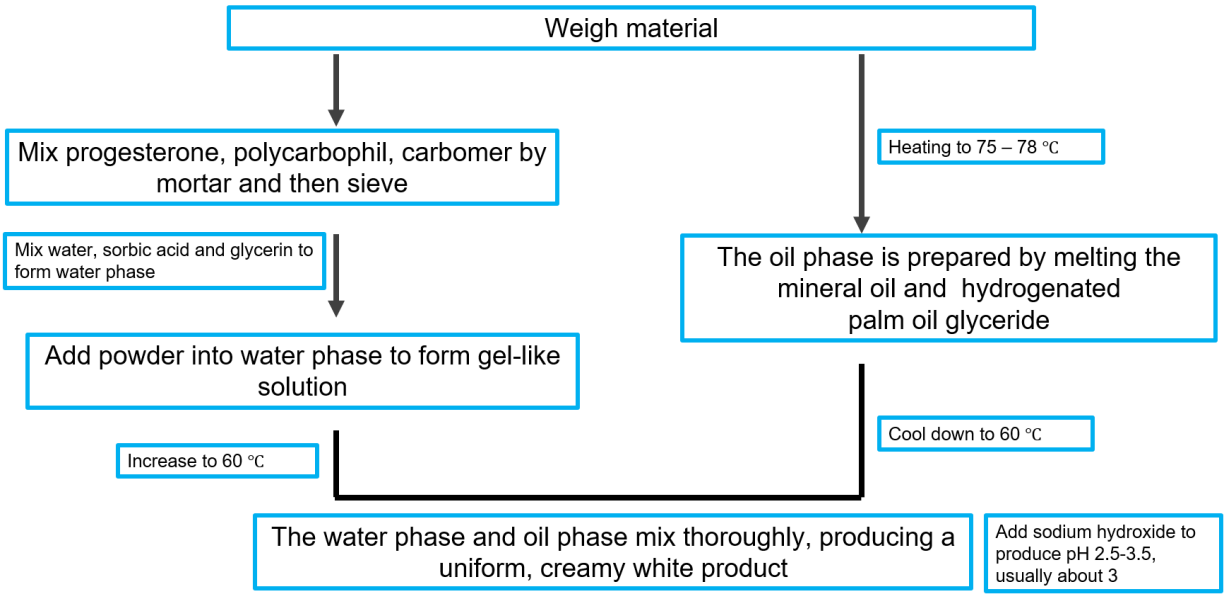


Figure A-0-1 Manufacturing process of Crinone®

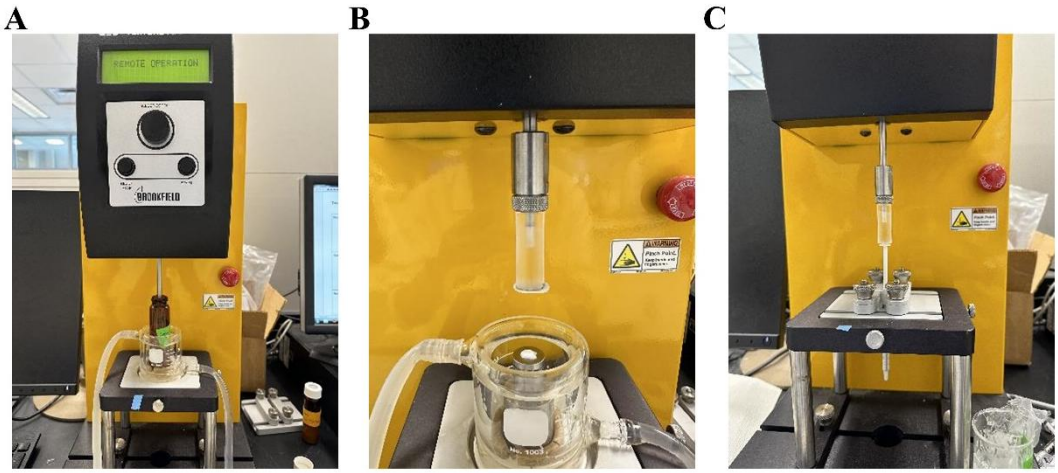


Figure A-0-2 Schematic diagrams of texture analysis: (A) mechanical test; (B) muco-adhesion test; (C) syringeability test.

Table A-0-2 Appearance and pH value of three batches of Crinone®. (n = 3, mean ± SD)

| Lot number | Appearance | pH |
|---|---|---|
| 100046739 | Soft, white to off-white gel | 3.33±0.00 |
| 100048963 | Soft, white to off-white gel | 3.34±0.01 |

| | | |
|---|---|---|
| 100049672 | Soft, white to off-white gel | 3.28±0.01 |

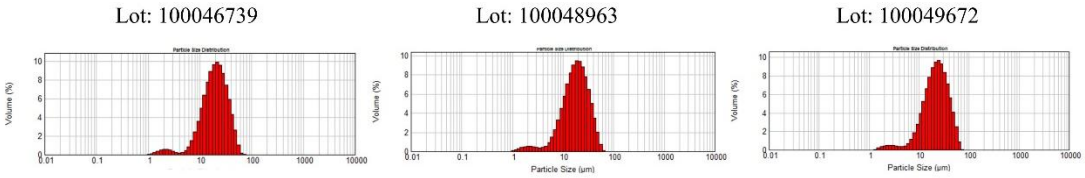


Figure A-0-3 Histograms of globule size distribution of three batches Crinone®.

Table A-0-3 The f2 values of in vitro release profiles comparing different batches of Crinone®

| **Formulations** | **f2 values** |
|---|---|
| 100046739 and 100048963 | 67.47 |
| 100046739 and 100049672 | 69.91 |
| 100048963 and 100049672 | 71.24 |

## Appendix B: Supplementary Materials for Chapter 3

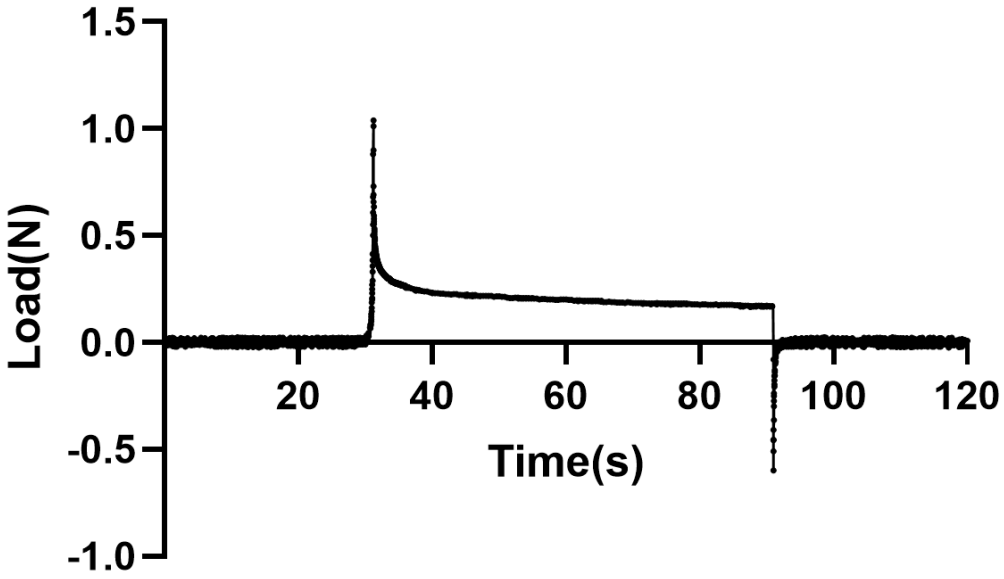


Figure B-0-4 Specificity of mucoadhesion test assay (P4-CD gel)

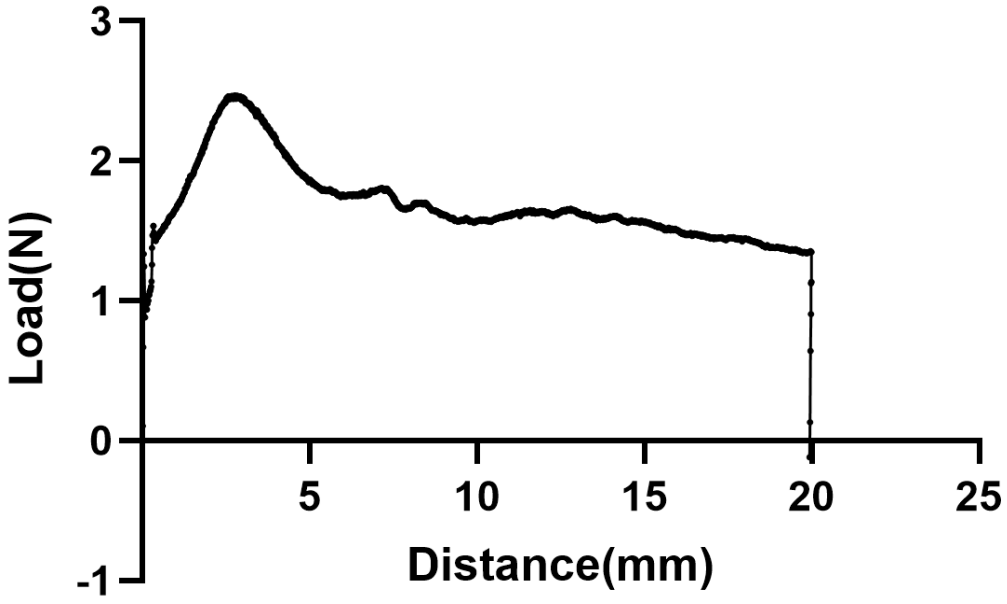


Figure B-0-5 Specificity of syringeablilty test assay (P4-CD gel)

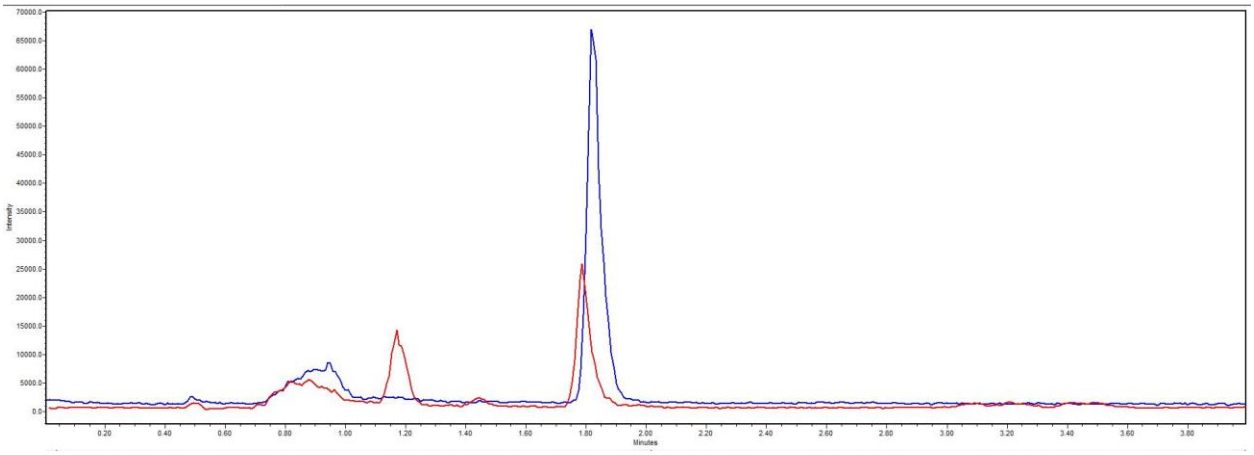

Figure B-0-6 Representative LC/MS chromatography of P4 (red) and P4-d9 internal STD (blue)

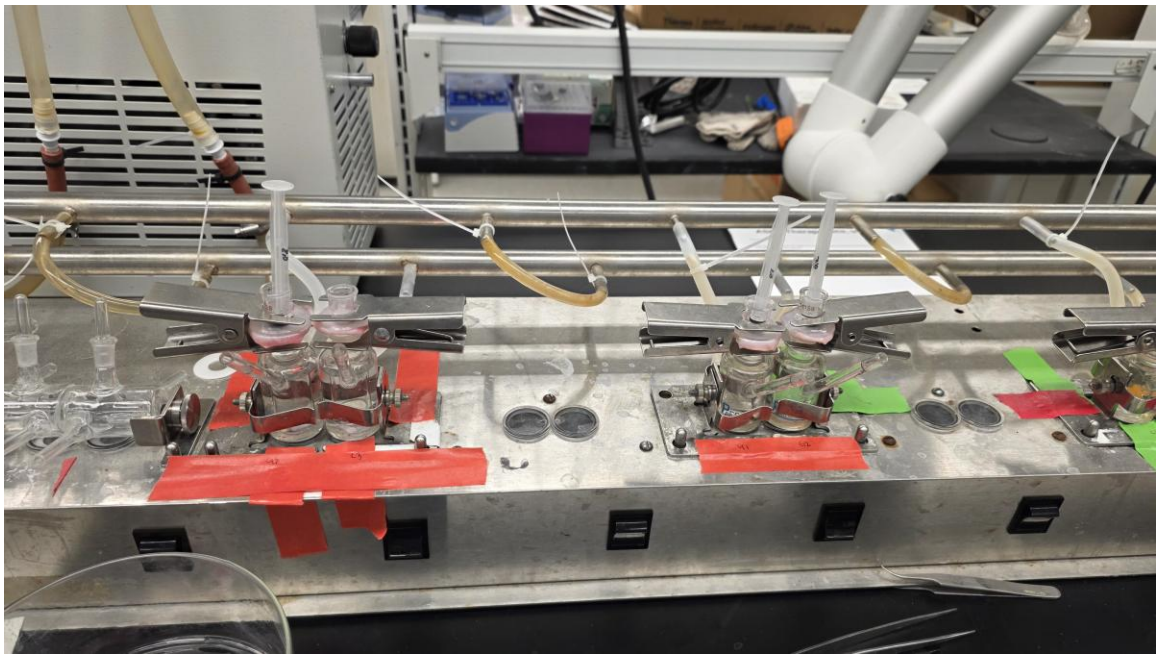

Figure B-0-7 Schematic diagrams of IVPT using sheep vaginal tissue



Figure B-0-8 Visual leakage check after 8hr IVPT

## Appendix C: Supplementary Materials for Chapter 4

Table C-0-4 ICH Q2(R1) validation results for the doxorubicin quantitation method.

| | |
|---|---|
| Sensitivity | LOD = 1.68 µg/mL<br>LOQ = 5.10 µg/mL |
| Linearity | y = 12686x+4306.8<br>0-50 µg/mL<br>$R^2$ = 0.999 |
| Accuracy (n=9) | LQC, % Recovery = 105 ± 4%<br>MQC, % Recovery = 106 ± 3%<br>HQC, % Recovery = 103 ± 2% |
| Precision (n=6) | LQC, RSD = 3.74%<br>MQC, RSD = 2.93%<br>HQC, RSD = 2.09% |

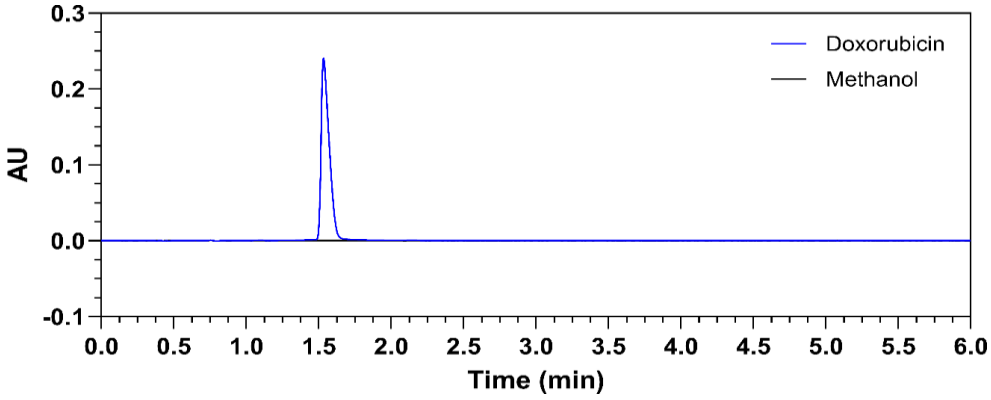


Figure C-0-9 Specificity of doxorubicin quantification assay. Blank is in black, doxorubicin in blue.

Table C-0-5 ICH Q2(R1) validation results for the lipid quantitation method for HSPC.

| | |
|---|---|
| Sensitivity | LOD = 20.52 μg/mL<br>LOQ = 62.17 μg/mL |
| Linearity | y = 53340.4x-1939931.9<br>50-250 μg/mL<br>$R^2$ = 0.994 |
| Accuracy | LQC, % Recovery = 113 $\pm$ 1%<br>MQC, % Recovery = 91 $\pm$ 4%<br>HQC, % Recovery = 104 $\pm$ 3% |
| Precision (n=6) | LQC, RSD = 0.81%<br>MQC, RSD = 4.17%<br>HQC, RSD = 2.88% |

Table C-0-6 ICH Q2(R1) validation results for the lipid quantitation method for cholesterol.

| | |
|---|---|
| Sensitivity | LOD = 10.48 μg/mL<br>LOQ = 31.77 μg/mL |
| Linearity | y = 87285.2x-1823519.3<br>25-125 μg/mL<br>$R^2$ = 0.995 |
| Accuracy | LQC, % Recovery = 112 $\pm$ 2%<br>MQC, % Recovery = 97 $\pm$ 3%<br>HQC, % Recovery = 102 $\pm$ 2% |
| Precision (n=6) | LQC, RSD = 1.93%<br>MQC, RSD = 2.87%<br>HQC, RSD = 2.42% |

Table C-0-7 ICH Q2(R1) validation results for the lipid quantitation method for DSPE-PEG 2000.

| | |
|---|---|
| Sensitivity | LOD = 2.51 μg/mL<br>LOQ = 7.61 μg/mL |
| Linearity | y = 24271x-511889<br>25-125 μg/mL<br>$R^2$ = 0.995 |
| Accuracy (%Recovery) | LQC, % Recovery = 100 ± 1%<br>MQC, % Recovery = 98 ± 3%<br>HQC, % Recovery = 89 ± 3% |
| Precision (n=6) | LQC, RSD = 1.15%<br>MQC, RSD = 3.48%<br>HQC, RSD = 3.48% |

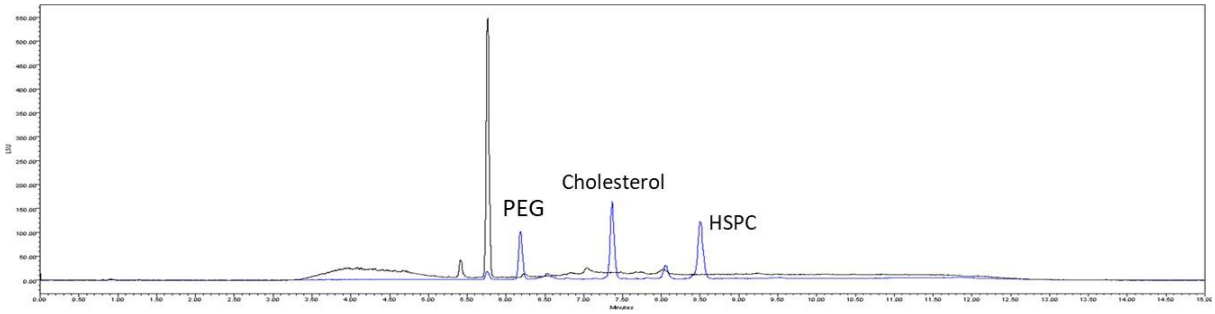


Figure C-0-10 Specificity of the lipid quantification assay. Blank is in black, lipids in blue.

Table C-0-8 Size distribution, polydispersity index and zeta potential measurements of different liposomal doxorubicin formulations analyzed by DLS (n ⩾ 3, mean ± SD).

| | Batch No. | Size (nm) | Polydispersity Index | Zeta Potential (mV) |
|---|---|---|---|---|
| Doxil® | KGZTG01 | 89.1 ± 0.71 | 0.050 ± 0.011 | -23.2 ± 3.34 |
| | KIZTI00 | 89.3 ± 0.64 | 0.049 ± 0.019 | -24.7 ± 1.53 |
| | KJZU901 | 89.9 ± 2.19 | 0.046 ± 0.002 | -27.1 ± 0.53 |
| | LJZTS00 | 95.4 ± 0.73 | 0.065 ± 0.015 | -25.9 ± 3.39 |
| | MDZT300 | 86.9 ± 1.28 | 0.082 ± 0.035 | -27.9 ± 2.72 |
| Dr. Reddy's Laboratories | 501451 | 87.0 ± 0.85 | 0.047 ± 0.011 | -27.4 ± 2.18 |
| | 501630 | 87.4 ± 1.00 | 0.051 ± 0.014 | -27.3 ± 1.54 |
| | 501635 | 87.5 ± 1.04 | 0.052 ± 0.005 | -29.0 ± 0.90 |
| | 501693 | 90.2 ± 0.99 | 0.052 ± 0.014 | -25.8 ± 2.20 |
| Sun Pharmaceuticals | JKX5514A | 86.6 ± 0.51 | 0.065 ± 0.005 | -31.5 ± 2.55 |
| | HAC1612A | 84.3 ± 0.62 | 0.082 ± 0.015 | -30.9 ± 4.02 |
| Zydus Pharmaceuticals | P100084 | 84.0 + 0.85 | 0.045 + 0.007 | -29.5 + 2.65 |

Table C-0-9 Quantification of doxorubicin and lipid content within liposomal doxorubicin formulations by different manufacturers (mean ± SD; n = 3).

| | Batch No. | Doxorubicin (mg/ml) | HSPC (mg/ml) | DSPE-PEG 2000 (mg/ml) | Cholesterol (mg/ml) |
|---|---|---|---|---|---|
| | *Label Claim* | *2.00 ± 0.10* | *9.58 ± 0.48* | *3.19 ± 0.16* | *3.19 ± 0.16* |
| Doxil® | KGZTG01 | 2.03 ± 0.06 | 9.44 ± 0.03 | 3.19 ± 0.02 | 3.05 ± 0.02 |
| | KIZTI00 | 1.95 ± 0.06 | 9.44 ± 0.33 | 3.26 ± 0.09 | 3.24 ± 0.08 |
| | KJZU901 | 2.00 ± 0.01 | 9.72 ± 0.04 | 3.17 ± 0.04 | 3.29 ± 0.03 |
| | LJZTS00 | 1.94 ± 0.02 | 9.85 ± 0.04 | 3.20 ± 0.11 | 3.09 ± 0.01 |
| | MDZT300 | 2.01 ± 0.02 | 9.64 ± 0.26 | 3.22 ± 0.10 | 3.15 ± 0.08 |
| Dr. Reddy's Laboratories | 501451 | 1.97 ± 0.03 | 9.64 ± 0.04 | 3.23 ± 0.04 | 3.05 ± 0.03 |
| | 501630 | 2.01 ± 0.01 | 9.83 ± 0.09 | 3.24 ± 0.07 | 3.13 ± 0.09 |
| | 501635 | 2.09 ± 0.06 | 9.63 ± 0.21 | 3.28 ± 0.06 | 3.28 ± 0.03 |
| | 501693 | 2.07 ± 0.01 | 9.70 ± 0.24 | 3.12 ± 0.02 | 3.13 ± 0.13 |
| Sun Pharmaceuticals | JKX5514A | 1.90 ± 0.04 | 9.85 ± 0.02 | 3.20 ± 0.05 | 3.36 ± 0.02 |
| | HAC1612A | 1.91 ± 0.03 | 9.58 ± 0.02 | 3.21 ± 0.06 | 3.24 ± 0.01 |
| Zydus Pharmaceuticals | P100084 | 2.09 ± 0.06 | 9.25 ± 0.03 | 3.27 ± 0.05 | 3.19 ± 0.07 |

Table C-0-10 Quantification of doxorubicin purity and identification of USP impurities within liposomal doxorubicin formulations by different manufacturers (mean ± SD; n = 3).

| | Batch No. | Doxorubicin (%) | Doxorubicinone (%) | Daunorubicin (%) | Daunorubicinone (%) | Other/Unspecified (%) |
|---|---|---|---|---|---|---|
| Doxil® | KGZTG01 | 99.3 ± 0.38 | 0.33 ± 0.06 | 0.06 ± 0.07 | 0.31 ± 0.27 | 0.00 ± 0.00 |
| | KIZTI00 | 99.1 ± 0.26 | 0.22 ± 0.19 | 0.18 ± 0.24 | 0.00 ± 0.00 | 0.47 ± 0.21 |
| | KJZU901 | 99.2 ± 0.15 | 0.27 ± 0.08 | 0.00 ± 0.00 | 0.50 ± 0.07 | 0.00 ± 0.00 |
| | LJZTS00 | 98.9 ± 0.11 | 0.25 ± 0.22 | 0.17 ± 0.17 | 0.50 ± 0.04 | 0.24 ± 0.11 |
| | MDZT300 | 99.1 ± 0.07 | 0.11 ± 0.20 | 0.16 ± 0.14 | 0.39 ± 0.01 | 0.26 ± 0.10 |
| Dr. Reddy's Laboratories | 501451 | 99.8 ± 0.04 | 0.20 ± 0.03 | 0.00 ± 0.00 | 0.01 ± 0.02 | 0.00 ± 0.00 |
| | 501630 | 99.8 ± 0.04 | 0.13 ± 0.03 | 0.00 ± 0.00 | 0.02 ± 0.02 | 0.00 ± 0.00 |
| | 501635 | 99.7 ± 0.15 | 0.14 ± 0.03 | 0.00 ± 0.00 | 0.12 ± 0.19 | 0.00 ± 0.00 |
| | 501693 | 99.3 ± 0.05 | 0.06 ± 0.10 | 0.19 ± 0.02 | 0.39 ± 0.03 | 0.11 ± 0.10 |
| Sun Pharmaceuticals | JKX5514A | 99.2 ± 0.36 | 0.67 ± 0.43 | 0.06 ± 0.11 | 0.02 ± 0.04 | 0.02 ± 0.03 |
| | HAC1612A | 99.4 ± 0.14 | 0.40 ± 0.35 | 0.18 ± 0.25 | 0.00 ± 0.00 | 0.04 ± 0.04 |
| Zydus Pharmaceuticals | P100084 | 99.5 ± 0.20 | 0.42 ± 0.24 | 0.04 ± 0.08 | 0.03 ± 0.03 | 0.01 ± 0.01 |

Table C-0-11 Quantification of free doxorubicin present in liposomal doxorubicin formulations by different manufacturers (n > 2).

| | Batch No. | Doxorubicin (mg/ml) |
|---|---|---|
| Doxil® | KGZTG01 | 1.03 ± 0.35 |
| | KIZTI00 | 1.93 ± 1.01 |
| | KJZU901 | 0.95 ± 0.67 |
| | LJZTS00 | 1.20 ± 0.02 |
| | MDZT300 | 1.04 ± 0.33 |
| Dr. Reddy's Laboratories | 501451 | 1.99 ± 0.03 |
| | 501630 | 0.57 ± 0.32 |
| | 501635 | 0.61 ± 0.39 |
| | 501693 | 0.92 ± 0.27 |
| Sun Pharmaceuticals | JKX5514A | 0.37 ± 0.04 |
| | HAC1612A | 0.41 ± 0.01 |
| Zydus Pharmaceuticals | P100084 | 1.32 ± 0.92 |

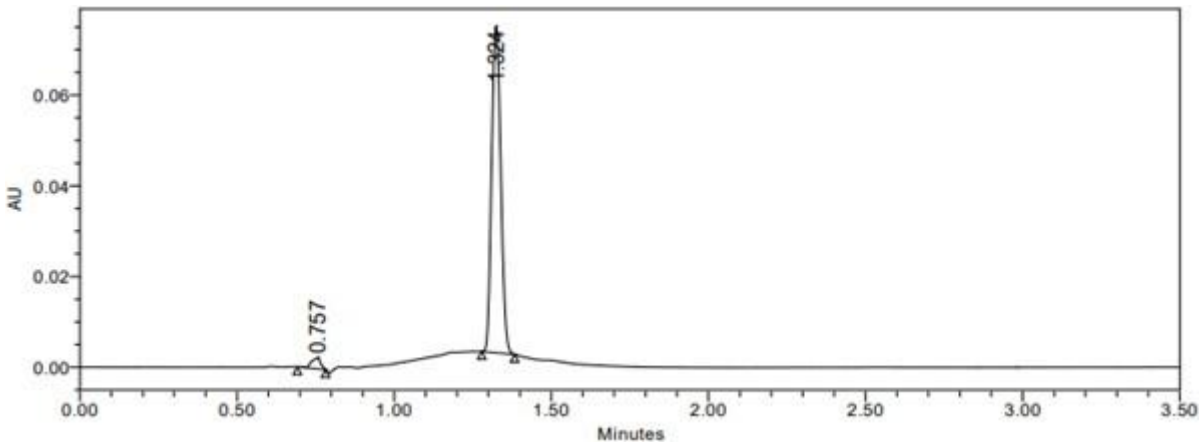


Figure C-0-11 Chromatographic identification of doxorubicin in a Doxil® formulation using an isocratic mobile phase of deionized water and methanol with 0.1% formic acid (Baxter Healthcare, batch no. MDZT300).

## Bibliography


1. Corner, G. W. & Allen, W. M. PHYSIOLOGY OF THE CORPUS LUTEUM.
2. Cable, J. K. & Grider, M. H. Physiology, Progesterone. in *StatPearls* (StatPearls Publishing, Treasure Island (FL), 2024).
3. Goletiani, N. V., Keith, D. R. & Gorsky, S. J. Progesterone: review of safety for clinical studies. *Exp Clin Psychopharmacol* **15**, 427–444 (2007).
4. González-Orozco, J. C. & Camacho-Arroyo, I. Progesterone Actions During Central Nervous System Development. *Front Neurosci* **13**, 503 (2019).
5. Prior, J. C. Progesterone for the prevention and treatment of osteoporosis in women. *Climacteric* **21**, 366–374 (2018).
6. Progesterone/RANKL Is a Major Regulatory Axis in the Human Breast | Science Translational Medicine. https://www.science.org/doi/10.1126/scitranslmed.3005654?url_ver=Z39.88-2003&rfr_id=ori:rid:crossref.org&rfr_dat=cr_pub%20%200pubmed.
7. Brisken, C. & Scabia, V. 90 YEARS OF PROGESTERONE: Progesterone receptor signaling in the normal breast and its implications for cancer. https://doi.org/10.1530/JME-20-0091 (2020) doi:10.1530/JME-20-0091.
8. Verhaegen, J. *et al.* Accuracy of single progesterone test to predict early pregnancy outcome in women with pain or bleeding: meta-analysis of cohort studies. https://doi.org/10.1136/bmj.e6077 (2012) doi:10.1136/bmj.e6077.

9. Nagy, B. *et al.* Key to Life: Physiological Role and Clinical Implications of Progesterone. *International Journal of Molecular Sciences* **22**, (2021).
10. Schumacher, M. *et al.* Progesterone synthesis in the nervous system: implications for myelination and myelin repair. *Front Neurosci* **6**, 10 (2012).
11. Meltzer-Brody, S. *et al.* Brexanolone injection in post-partum depression: two multicentre, double-blind, randomised, placebo-controlled, phase 3 trials. *Lancet* **392**, 1058–1070 (2018).
12. Rossouw, J. E. *et al.* Risks and benefits of estrogen plus progestin in healthy postmenopausal women: principal results From the Women's Health Initiative randomized controlled trial. *JAMA* **288**, 321–333 (2002).
13. Miller, V. M. *et al.* The Kronos Early Estrogen Prevention Study (KEEPS): what have we learned? *Menopause* **26**, 1071–1084 (2019).
14. Hodis, H. N. *et al.* Vascular Effects of Early versus Late Postmenopausal Treatment with Estradiol. *N Engl J Med* **374**, 1221–1231 (2016).
15. Manson, J. E. *et al.* Menopausal Hormone Therapy and Long-term All-Cause and Cause-Specific Mortality: The Women's Health Initiative Randomized Trials. *JAMA* **318**, 927–938 (2017).
16. Research, C. for D. E. and. FDA Approves Labeling Changes to Menopausal Hormone Therapy Products. *FDA* https://www.fda.gov/news-events/press-announcements/fda-approves-labeling-changes-menopausal-hormone-therapy-products (2026).
17. Penzias, A. S. Luteal phase support. *Fertil Steril* **77**, 318–323 (2002).
18. Cometti, B. Pharmaceutical and clinical development of a novel progesterone formulation. *Acta Obstetricia et Gynecologica Scandinavica* **94**, 28–37 (2015).

19. Hargrove, J. T., Maxson, W. S. & Colston Wentz, A. Absorption of oral progesterone is influenced by vehicle and particle size. *American Journal of Obstetrics and Gynecology* **161**, 948–951 (1989).
20. Penzias, A. S. Luteal phase support. *Fertil Steril* **77**, 318–323 (2002).
21. Erel, C. T. & Ozcivit Erkan, I. B. Oral versus vaginal micronized progesterone in menopausal hormone therapy. *Gynecological Endocrinology* **41**, 2592400 (2025).
22. De Ziegler, D., Bulletti, C., De Monstier, B. & Jääskeläinen, A.-S. The First Uterine Pass Effect. *Annals of the New York Academy of Sciences* **828**, 291–299 (1997).
23. Jalaliani, S., Davar, R., Akbarzadeh, F., Emami, F. & Eftekhar, M. Addition of intramuscular to vaginal progesterone for luteal phase support in fresh embryo transfer cycles: A cross-sectional study. *IJRM* 745–752 (2022) doi:10.18502/ijrm.v20i9.12064.
24. Patil, N., Maheshwari, R. & Wairkar, S. Advances in progesterone delivery systems: Still work in progress? *International Journal of Pharmaceutics* **643**, 123250 (2023).
25. Alekseev, N. P. Progesterone-Containing Gel Does Not Eliminate Postpartum Breast Engorgement? *Breastfeed Med* **12**, 122–123 (2017).
26. Stanczyk, F. Z. Treatment of postmenopausal women with topical progesterone creams and gels: are they effective? *Climacteric* **17**, 8–11 (2014).
27. McCoy, C. F. *et al.* Advances in drug-releasing vaginal rings. *Journal of Drug Delivery Science and Technology* **115**, 107813 (2026).
28. Temmerman, M. A new woman-controlled contraceptive vaginal ring: a global step forward. *The Lancet Global Health* **7**, e986–e987 (2019).
29. The World Health Organisation Task. A collaborative study of the progesterone intrauterine device (progestasert). *Contraception* **19**, 575–589 (1979).

30. Chaudhuri. *Practice Of Fertility Control: A Comprehensive Manual (7Th Edition)*. (Elsevier India, 2007).
31. Falcone, T. & Hurd, W. W. *Clinical Reproductive Medicine and Surgery*. (Elsevier Health Sciences, 2007).
32. Bickers, W. Progesterone; a comparison of intramuscular, oral and sublingual routes of administration. *J Clin Endocrinol Metab* **9**, 736–742 (1949).
33. Griesinger, G. *et al.* Network meta-analysis of progestogen administration routes for luteal phase support in fresh embryo transfer IVF cycles. *Reproductive BioMedicine Online* **52**, 105206 (2026).
34. Cook, M. T. & Brown, M. B. Polymeric gels for intravaginal drug delivery. *Journal of Controlled Release* **270**, 145–157 (2018).
35. Katz, D. F., Yuan, A. & Gao, Y. Vaginal Drug Distribution Modeling. *Adv Drug Deliv Rev* **92**, 2–13 (2015).
36. Lai, S. K., Wang, Y.-Y., Hida, K., Cone, R. & Hanes, J. Nanoparticles reveal that human cervicovaginal mucus is riddled with pores larger than viruses. *Proc Natl Acad Sci U S A* **107**, 598–603 (2010).
37. Ahmad, F., Alam, M., Khan, Z., Khar, R. & Ali, M. Development and in vitro evaluation of an acid buffering bioadhesive vaginal gel for mixed vaginal infections. *ACPH* **58**, 407–419 (2008).
38. Lupu, A., Gradinaru, L. M., Rusu, D. & Bercea, M. Self-Healing of Pluronic® F127 Hydrogels in the Presence of Various Polysaccharides. *Gels* **9**, 719 (2023).

39. Rossi, S. *et al.* Comparison of poloxamer- and chitosan-based thermally sensitive gels for the treatment of vaginal mucositis. *Drug Development and Industrial Pharmacy* **40**, 352–360 (2014).
40. Hani, U. & Shivakumar, H. G. Development of Miconazole nitrate Thermosensitive Bioadhesive Vaignal Gel for Vaginal Candidiasis.
41. Enggi, C. K. *et al.* Development of thermosensitive and mucoadhesive gels of cabotegravir for enhanced permeation and retention profiles in vaginal tissue: A proof of concept study. *International Journal of Pharmaceutics* **609**, 121182 (2021).
42. Permana, A. D. *et al.* Bioadhesive-Thermosensitive In Situ Vaginal Gel of the Gel Flake-Solid Dispersion of Itraconazole for Enhanced Antifungal Activity in the Treatment of Vaginal Candidiasis. *ACS Appl. Mater. Interfaces* **13**, 18128–18141 (2021).
43. Kang, J.-W., Davaa, E., Kim, Y.-T. & Park, J.-S. A new vaginal delivery system of amphotericin B: a dispersion of cationic liposomes in a thermosensitive gel. *Journal of Drug Targeting* **18**, 637–644 (2010).
44. Wang, L. *et al.* Development of a liposome microbicide formulation for vaginal delivery of octylglycerol for HIV prevention. *Drug Dev Ind Pharm* **38**, 995–1007 (2012).
45. Caron, M. *et al.* Protective properties of non-nucleoside reverse transcriptase inhibitor (MC1220) incorporated into liposome against intravaginal challenge of Rhesus macaques with RT-SHIV. *Virology* **405**, 225–233 (2010).
46. Malavia, N. *et al.* Liposomes for HIV prophylaxis. *Biomaterials* **32**, 8663–8668 (2011).
47. Pavelić, Ž., Škalko-Basnet, N. & Jalšenjak, I. Liposomes containing drugs for treatment of vaginal infections. *European Journal of Pharmaceutical Sciences* **8**, 345–351 (1999).

48. Hoang, T. *et al.* Development of a mucoinert progesterone nanosuspension for safer and more effective prevention of preterm birth. *Journal of Controlled Release* **295**, 74–86 (2019).
49. Valenta, C., Kast, C. E., Harich, I. & Bernkop-Schnürch, A. Development and in vitro evaluation of a mucoadhesive vaginal delivery system for progesterone. *Journal of Controlled Release* **77**, 323–332 (2001).
50. Callavid® technology | Calla Lily Clinical Care. *Calla Lily Clincal Care* https://www.callali.ly/en-gb/callavid.
51. Calla Lily Clinical Care Ltd. *First in Human Safety and Ease of Use Assessment of 400mg Progesterone Callavid in Women With Luteal Phase Insufficiency*. https://clinicaltrials.gov/study/NCT07136922 (2026).
52. 2024 U.S. Generic & Biosimilar Medicines Savings Report. *Association for Accessible Medicines* https://accessiblemeds.org/resources/reports/2024-savings-report/.
53. Bioavailability and Bioequivalence Studies Submitted in NDAs or INDs — General Considerations. (2014).
54. Hussaarts, L. *et al.* Equivalence of complex drug products: advances in and challenges for current regulatory frameworks. *Annals of the New York Academy of Sciences* **1407**, 39–49 (2017).
55. Lionberger, R. A. FDA Critical Path Initiatives: Opportunities for Generic Drug Development. *AAPS J* **10**, 103–109 (2008).
56. FDA CDER & Mahadevan, C. Draft Guidance on Doxorubicin hydrochloride. https://www.accessdata.fda.gov/drugsatfda_docs/psg/Doxorubicin%20Hydrochloride_draft_Injection%20injec%20lipo_RLD%2050718_RC09-18.pdf (2018).

57. FDA Draft Guidance on Progesterone. https://www.accessdata.fda.gov/drugsatfda_docs/psg/PSG_020701.pdf.

58. Barenholz, Y. (Chezy). Doxil® — The first FDA-approved nano-drug: Lessons learned. *Journal of Controlled Release* **160**, 117–134 (2012).

59. Jiang, W., Lionberger, R. & Yu, L. X. In vitro and in vivo characterizations of PEGylated liposomal doxorubicin. *Bioanalysis* **3**, 333–344 (2011).

60. Gabizon, A. *et al.* Prolonged Circulation Time and Enhanced Accumulation in Malignant Exudates of Doxorubicin Encapsulated in Polyethylene-glycol Coated Liposomes1. *Cancer Res* **54**, 987–992 (1994).

61. U.S. Food & Drug Administration. Doxil Package Insert. (2026).

62. Bulbake, U., Doppalapudi, S., Kommineni, N. & Khan, W. Liposomal Formulations in Clinical Use: An Updated Review. *Pharmaceutics* **9**, 12 (2017).

63. Jiang, W., Lionberger, R. & Yu, L. X. In Vitro and In Vivo Characterizations of Pegylated Liposomal Doxorubicin. *Bioanalysis* **3**, 333–344 (2011).

64. Berger, J. L. *et al.* Outcomes analysis of an alternative formulation of PEGylated liposomal doxorubicin in recurrent epithelial ovarian carcinoma during the drug shortage era. *Onco Targets Ther* **7**, 1409–1413 (2014).

65. Li, J. *et al.* Characterization of Crinone®: progesterone vaginal gel. *Int J Pharm* **684**, 126184 (2025).

66. Peters, S. A. E. Women's health: a new global agenda. *BMJ Global Health* **1**, e000080 (2016).

67. Coulson, J., Sharma, V. & Wen, H. Understanding the global dynamics of continuing unmet need for family planning and unintended pregnancy. *China Population and Development Studies* **7**, 1–14 (2023).
68. das Neves, J. & Ensign, L. Advances in drug delivery for women's health: A matter of gender equity. *Advanced Drug Delivery Reviews* **182**, 114132 (2022).
69. Di Renzo, G. C. Progesterone in normal and pathological pregnancy. *Hormone Molecular Biology and Clinical Investigation* **27**, 35–48 (2016).
70. Zierden, H. C. Enhanced drug delivery to the reproductive tract using nanomedicine reveals therapeutic options for prevention of preterm birth. *Science Translational Medicine* **13**, (2021).
71. Zierden, H. C. Avoiding a Sticky Situation: Bypassing the Mucus Barrier for Improved Local Drug Delivery. *Trends in Molecular Medicine* **27**, 436–450 (2021).
72. Child, T. Systematic review of the clinical efficacy of vaginal progesterone for luteal phase support in assisted reproductive technology cycles. *Reproductive Biomedicine Online* **36**, 630–645 (2018).
73. U.S. Food and Drug Administration. *Draft Guidance on Progesterone*. https://www.fda.gov/regulatoryinformation/search-fda-guidance-documents (2022).
74. Miranda, M. Topical bioequivalence: Experimental and regulatory considerations following formulation complexity. *International Journal of Pharmaceutics* **620**, 121705 (2022).
75. Miranda, M. Drilling down the bioequivalence assessment of topical antifungal products: Microstructure and release. *European Journal of Pharmaceutics and Biopharmaceutics* **185**, 94–106 (2023).

76. Rencber, S. Mucoadhesive in situ gel formulation for vaginal delivery of clotrimazole. *Pharmaceutical Development and Technology* **22**, 551–561 (2017).

77. da Silva, J. B. A mucosa-mimetic material for the mucoadhesion testing of thermogelling semi-solids. *International Journal of Pharmaceutics* **528**, 586–594 (2017).

78. Shah, V. P., Tsong, Y., Sathe, P. & Liu, J.-P. In Vitro Dissolution Profile Comparison—Statistics and Analysis of the Similarity Factor, f2. *Pharm Res* **15**, 889–896 (1998).

79. Elfakhri, K. H. Physicochemical and structural evaluation of microparticles in tretinoin topical gels. *International Journal of Pharmaceutics* **620**, 121748 (2022).

80. Sarkar, A. Polymorphism of Progesterone: Formation and stability. *Crystal Growth & Design* **14**, 4574–4582 (2014).

81. Pu, C. In Vitro-In Vivo Relationship of Amorphous Insoluble API in PLGA Microspheres. *Pharmaceutical Research* **34**, 2787–2797 (2017).

82. Yilmaz Usta, D. Evaluation of Emulgel and Nanostructured Lipid Carrier-Based Gel Formulations for Transdermal Administration of Ibuprofen. *AAPS PharmSciTech* **25**, 124 (2024).

83. Jones, D. S. Design and evaluation of mucoadhesive tetracycline formulation. *Journal of Controlled Release* **67**, 357–368 (2000).

84. Feng, X. Understanding syringeability and injectability of high molecular weight PEO solution. *International Journal of Pharmaceutics* **631**, 122486 (2023).

85. Campana-Seoane, M. Bioadhesive emulsions for progesterone delivery. *International Journal of Pharmaceutics* **477**, 495–505 (2014).

86. Chang, J. Y. Rheological evaluation of thermosensitive vaginal gels. *International Journal of Pharmaceutics* **241**, 155–163 (2002).

87. N'Guessan Gnaman, K. C. Vaginal gel containing Lactobacillus crispatus for prevention of gonorrhea. *International Journal of Pharmaceutics* **588**, 119733 (2020).

88. Chen, X. D. The Female Vaginal Microbiome in Health and Bacterial Vaginosis. *Frontiers in Cellular and Infection Microbiology* **11**, (2021).

89. Vander Borght, M. & Wyns, C. Fertility and infertility: Definition and epidemiology. *Clin Biochem* **62**, 2–10 (2018).

90. Brewster, M. E. & Loftsson, T. Cyclodextrins as pharmaceutical solubilizers. *Advanced Drug Delivery Reviews* **59**, 645–666 (2007).

91. Owen, D. H. & Katz, D. F. A vaginal fluid simulant. *Contraception* **59**, 91–95 (1999).

92. Connors, K. & Higuchi, T. Phase solubility techniques. *Adv. Anal. Chem. Instrum* **4**, 117–212 (1965).

93. Hernández-Sánchez, P. *et al.* Optimization of a method for preparing solid complexes of essential clove oil with β-cyclodextrins. *J Sci Food Agric* **97**, 420–426 (2017).

94. Cirri, M., Maestrelli, F., Mennini, N. & Mura, P. Influence of the preparation method on the physical–chemical properties of ketoprofen–cyclodextrin–phosphatidylcholine ternary systems. *Journal of Pharmaceutical and Biomedical Analysis* **50**, 690–694 (2009).

95. Cid-Samamed, A., Rakmai, J., Mejuto, J. C., Simal-Gandara, J. & Astray, G. Cyclodextrins inclusion complex: Preparation methods, analytical techniques and food industry applications. *Food Chemistry* **384**, 132467 (2022).

96. Lee, C., O'Day, P., Stouffer, D. G., Auchus, R. J. & Turcu, A. F. Artifactual elevations of 11β-hydroxyandrostenedione and 11-ketoandrostenedione in mass spectrometry assays. *J Steroid Biochem Mol Biol* **250**, 106717 (2025).

97. Schwarz, D. H., Engelke, A. & Wenz, G. Solubilizing steroidal drugs by β-cyclodextrin derivatives. *International Journal of Pharmaceutics* **531**, 559–567 (2017).

98. Solubility and Dissolution Rate of Progesterone-Cyclodextrin-Polymer Systems. *Drug Development and Industrial Pharmacy* https://www.tandfonline.com/doi/abs/10.1080/03639040600897093.

99. Zannou, E. A., Streng, W. H. & Stella, V. J. Osmotic properties of sulfobutylether and hydroxypropyl cyclodextrins. *Pharm Res* **18**, 1226–1231 (2001).

100. Másson, M., Loftsson, T., Másson, G. & Stefánsson, E. Cyclodextrins as permeation enhancers: some theoretical evaluations and in vitro testing. *Journal of Controlled Release* **59**, 107–118 (1999).

101. Sripetch, S., Prajapati, M. & Loftsson, T. Cyclodextrins and Drug Membrane Permeation: Thermodynamic Considerations. *Journal of Pharmaceutical Sciences* **111**, 2571–2580 (2022).

102. Lambert, D., O'Neill, C. & Padfield, P. Methyl-β-Cyclodextrin Increases Permeability of Caco-2 Cell Monolayers by Displacing Specific Claudins from Cholesterol Rich Domains Associated with Tight Junctions. https://dx.doi.org/10.1159/000107533.

103. Boulmedarat, L., Grossiord, J. L., Fattal, E. & Bochot, A. 甲基-β-环糊精和脂质体对卡波姆® 974P NF 凝胶流变学特性的影响. *International Journal of Pharmaceutics* **254**, 59–64 (2003).

104. Blanco-Fuente, H., Esteban-Fernández, B., Blanco-Méndez, J. & Otero-Espinar, F.-J. Use of β-Cyclodextrins to Prevent Modifications of the Properties of Carbopol Hydrogels Due to Carbopol–Drug Interactions. *Chemical and Pharmaceutical Bulletin* **50**, 40–46 (2002).

105. Miao, J., Willems, H. M. E. & Peters, B. M. Exogenous Reproductive Hormones nor Candida albicans Colonization Alter the Near Neutral Mouse Vaginal pH. *Infect Immun* **89**, e00550-20 (2021).

106. McCracken, J. M. *et al.* Animal models and alternatives in vaginal research: a comparative review. *Reprod Sci* **28**, 1759–1773 (2021).

107. Shapiro, R. L. *et al.* Hypotonic, gel-forming delivery system for vaginal drug administration. *Journal of Controlled Release* **371**, 101–110 (2024).

108. Is Wetter Better? An Evaluation of Over-the-Counter Personal Lubricants for Safety and Anti-HIV-1 Activity | PLOS One. https://journals.plos.org/plosone/article?id=10.1371/journal.pone.0048328.

109. Palmeira-de-Oliveira, R. *et al.* Women's preferences and acceptance for different drug delivery routes and products. *Advanced Drug Delivery Reviews* **182**, 114133 (2022).

110. Global Doxorubicin Market Trajectory & Analytics Report 2022-2026: Rising Incidence of Cancers & Development of Technologically Advanced Systems for Drug Delivery Driving Growth. *GlobeNewswire News Room* https://www.globenewswire.com/en/news-release/2022/05/25/2450132/28124/en/Global-Doxorubicin-Market-Trajectory-Analytics-Report-2022-2026-Rising-Incidence-of-Cancers-Development-of-Technologically-Advanced-Systems-for-Drug-Delivery-Driving-Growth.html (2022).

111. Ghosh, S. Liposomal Doxorubicin Market Outlook for 2024-2034. https://www.futuremarketinsights.com/reports/liposomal-doxorubicin-market (2024).

112. Alshaer, W. *et al.* Quality by Design Approach in Liposomal Formulations: Robust Product Development. *Molecules* **28**, 10 (2022).

113. Food and Drug Administration. 21 CFR 320.22 Criteria for waiver of evidence of in vivo bioavailability or bioequivalence. https://www.ecfr.gov/current/title-21/chapter-I/subchapter-D/part-320/subpart-B/section-320.22 (2002).

114. Food and Drug Administration, D. of H. and H. S. 21 CFR 320.24 -- Types of evidence to measure bioavailability or establish bioequivalence. https://www.ecfr.gov/current/title-21/part-320/section-320.24 (2002).

115. Yu, M. *et al.* Characterization of exparel bupivacaine multivesicular liposomes. *Int J Pharm* **639**, 122952 (2023).

116. Liu, Y. *et al.* Analytical method development and comparability study for AmBisome® and generic Amphotericin B liposomal products. *European Journal of Pharmaceutics and Biopharmaceutics* **157**, 241–249 (2020).

117. Food and Drug Administration. Orange Book: Approved Drug Products with Therapeutic Equivalence Evaluations. https://www.accessdata.fda.gov/scripts/cder/ob/search_product.cfm.

118. Mastronarde, D. N. SerialEM: A Program for Automated Tilt Series Acquisition on Tecnai Microscopes Using Prediction of Specimen Position. *Microsc Microanal* **9**, 1182–1183 (2003).

119. Mastronarde, D. N. Automated electron microscope tomography using robust prediction of specimen movements. *Journal of Structural Biology* **152**, 36–51 (2005).

120. Schindelin, J. *et al.* Fiji: an open-source platform for biological-image analysis. *Nat Methods* **9**, 676–682 (2012).

121. SIBYLS MailinSAXS HT-SAXS Instructions. https://sibyls.als.lbl.gov/htsaxs/instructions/htsaxs (2010).

122. Medicine, C. for V. Compilation of FDA Guidance and Resources for in vitro Dissolution Testing of Immediate Release Solid Oral Dosage Forms. *FDA* https://www.fda.gov/animal-veterinary/new-animal-drug-applications/compilation-fda-guidance-and-resources-in-vitro-dissolution-testing-immediate-release-solid-oral-dosage (2025).

123. Yuan, W. *et al.* Development of a Flow-Through USP-4 Apparatus Drug Release Assay to Evaluate Doxorubicin Liposomes. *AAPS J* **19**, 150–160 (2017).

124. Wu, Y. *et al.* Cryogenic Transmission Electron Microscopy (Cryo-TEM) Reveals Morphological Changes of Liposomal Doxorubicin during *In Vitro* Release. *Microsc Microanal* **23**, 1216–1217 (2017).

125. Murray, D. T., Shin, D. S., Classen, S., Brosey, C. A. & Hura, G. L. Visualizing and accessing correlated SAXS data sets with Similarity Maps and Simple Scattering web resources. *Methods Enzymol* **678**, 411–440 (2023).

126. Jiang, W., Lionberger, R. & Yu, L. X. In vitro and in vivo characterizations of PEGylated liposomal doxorubicin. *Bioanalysis* **3**, 333–344 (2011).

127. Maiti, K. *et al.* Comparison of Physicochemical Properties of Generic Doxorubicin HCl Liposome Injection with the Reference Listed Drug. *ACAMC* **18**, 597–609 (2018).

128. Souza, I. D. L., Saez, V. & Mansur, C. R. E. Lipid nanoparticles containing coenzyme Q10 for topical applications: An overview of their characterization. *Colloids and Surfaces B: Biointerfaces* **230**, 113491 (2023).

129. Bhattacharjee, S. DLS and zeta potential – What they are and what they are not? *Journal of Controlled Release* **235**, 337–351 (2016).

130. Smith, M. C., Crist, R. M., Clogston, J. D. & McNeil, S. E. Zeta potential: a case study of cationic, anionic, and neutral liposomes. *Anal Bioanal Chem* **409**, 5779–5787 (2017).

131. Outomuro, D., Grana, D. R., Azzato, F. & Milei, J. Adriamycin-induced myocardial toxicity: New solutions for an old problem? *International Journal of Cardiology* **117**, 6–15 (2007).